

AN ABSTRACT OF THE THESIS OF

Sarah M. Skinner for the degree of Master of Science in Applied Anthropology presented on June 18, 2018

Title: A Geometric Morphometric Analysis of Projectile Point Maintenance using Experimental Resharpener Techniques: An Examination of PFP1 Curation, Cooper's Ferry Site, Idaho

Abstract approved: _____

Loren G. Davis

The incorporation of experimental archaeology into the study of lithic technologies has provided archaeologists with a framework to understand past behaviors. The analysis of stone tools has the potential to reveal morphologic characteristics unique to the manufacture, use, and maintenance of stone tools. The implementation of controlled experiments to identify and describe the behaviors of the past has been influential in understanding the material evidence left behind in the archaeological record. The Cooper's Ferry Site in western Idaho has presented an opportunity to evaluate the curation of fourteen Western Stemmed Tradition (WST) projectile points discovered in a cache, Pit Feature P1 (PFP1). This cache pit has been described as having displayed distinct characteristics of use and resharpener before being interred in the ground (Davis et al. 2017), and this assumption will further be explored in this study. By introducing a series of resharpener experiments and geometric morphometric analyses, stages of resharpener will be identified and described as a comparative tool for stone tool curation.

©Copyright by Sarah M. Skinner
June 18, 2018
All Rights Reserved

A Geometric Morphometric Analysis of Projectile Point Maintenance using Experimental Resharpener Techniques: An Examination of PFP1 Curation, Cooper's Ferry Site, Idaho

by
Sarah M. Skinner

A THESIS

submitted to

Oregon State University

in partial fulfillment of
the requirements for the
degree of

Master of Science

Presented June 18, 2018
Commencement June 2019

Master of Science thesis of Sarah M. Skinner presented on June 18, 2018

APPROVED:

Major Professor, representing Applied Anthropology

Director of the School Language, Culture, and Society

Dean of the Graduate School

I understand that my thesis will become part of the permanent collection of Oregon State University libraries. My signature below authorizes release of my thesis to any reader upon request.

Sarah M. Skinner, Author

ACKNOWLEDGEMENTS

The completion of this research would not have been possible without the generous help and support of my friends and colleagues at Oregon State University and the Pacific Slope Archaeological Laboratory. I would like to thank Daniel Bean for his enthusiasm and unwavering assistance in working with me to generate the data and explore the novel measurements presented in this study. I would like to thank Dan Stueber for his expertise and insight surrounding experimental design and lithic analysis and spending countless hours' flintkapping and resharpening the stone tools used in this study. I would like to thank Alex Nyers for his help in using the 3D scanning technologies and his assistance in streamlining the 3D model preparation process. I would like to thank Dr. Loren Davis for his guidance and utmost support in this project and allowing me to work on this exciting research. I would finally like to thank David Sisson for his encouragement in pursuing graduate studies in archaeology and giving me the opportunity to be part of the Cooper's Ferry site since 2012. I appreciate everyone's willingness to help me on this project and I am happy to have worked with each of you to make it happen.

A final thanks to my committee members, Dr. Loren Davis, Dr. Leah Minc, Dr. Robert Kennedy, and Dr. Yvette Spitz for taking the time to review my thesis and offering your expertise on the topics presented in my research.

Table of Contents

	<u>Page</u>
Chapter 1: Introduction	1
1.1 Background	2
1.2 Research Goals and Hypotheses	6
1.3 Significance.....	7
Chapter 2: Literature Review	8
2.1 Experimental Archaeology	8
2.2 Lithic Curation	10
2.3 Lithic Tool Morphometry	12
2.4 Cooper’s Ferry Site (10IH73)	13
Chapter 3: Methods.....	16
3.1 WST Replication.....	16
3.2 Three-dimensional Models	27
3.3 GLiMR Measures.....	30
3.4 Analysis Preparation	36
Chapter 4: Results	37
4.1 Standard GLiMR Metrics	37
4.2 Slope Variation	50
4.3 Cross-Section Comparison.....	55
4.4 Blade Curvature	58
4.5 Inset Width.....	66
Chapter 5: PFP1 Results	68
5.1 Cooper’s Ferry PFP1 Comparison	68
5.2 Slope Images	71
5.3 Cross-section Comparison	74
5.4 Blade Curvature and Inset Width.....	79
Chapter 6: Discussion	82
6.1 Experimental Implications	82
6.2 PFP1 Implications	85
Chapter 7: Conclusion.....	88
7.1 Future Analysis	89

Table of Contents (Continued)

	<u>Page</u>
Bibliography	90
Appendix A.....	95
Appendix B.....	97
Appendix C.....	122

List of Figures

<u>Figure</u>	<u>Page</u>
Figure 1: Two-dimensional scans of PFP1	15
Figure 2: Experimental toolkit A.	19
Figure 3: Experimental toolkit B.	20
Figure 4: Paleoarchaic lithic reduction sequence.....	23
Figure 5: Hafting method.....	24
Figure 6: Unidirectional resharpening directions	25
Figure 7: Digital images of DS01-DS30.....	26
Figure 8: Example of a completed 3D digital model.....	29
Figure 9: InSet width	34
Figure 10: GLiMR analysis tools.....	35
Figure 11: Two-dimensional images of DS03	43
Figure 12: Length (mm) Results	44
Figure 13: Width (mm) Results	45
Figure 14: Max width Results.....	46
Figure 15: Thickness (mm) Results	47
Figure 16: Blade Volume (mm ³) Results.....	48
Figure 17: Comparison of haft length and area vs blade length	49
Figure 18: Surface TIN colored by slope.....	51
Figure 19: ArcGIS thickness output	52
Figure 20: Surface TIN colored by slope	53
Figure 21: Surface TIN colored by slope.....	54
Figure 22: Resharpening sequence directions.....	56
Figure 23: Midsection cross-sectional view	57
Figure 24: Blade Curve summary for the right blade of DS03.....	62
Figure 25: Blade Curve summary for the right blade of DS03.....	63
Figure 26: Curve summary of average right edge	64
Figure 27: Curve summary of average left edge.....	65
Figure 28: Slope results for PFP1 specimen 73-24940.....	72
Figure 29: Slope results for PFP1 specimen 73-24941.....	73
Figure 30: Slope results for PFP1 specimen 73-24942.....	73
Figure 31: Cross-section and thickness comparison.....	77
Figure 32: Cross-section and thickness comparison.....	78
Figure 33: Inset max width percentage.....	81
Figure 34: Z-Twist and S-Twist directions	83
Figure A.1: Experimental prismatic blade core	95
Figure A.2: Experimental resharpening images.....	96
Figure B.1: Two-dimensional scanned images DS01-DS30	97
Figure B.2: Outline overlay DS01-DS30.....	108
Figure B.3: Cross-Section comparison DS01-DS30.....	111
Figure C.1: PFP1 GLiMR analysis tool results	123

List of Tables

<u>Table</u>	<u>Page</u>
Table 1: Material Summary of Replicas	18
Table 2: Average Dimensional Attribute Descriptions.....	31
Table 3: Average Dimensional Attributes of Original WST PPT Replications.	39
Table 4: Average Dimensional Attributes for First PPT Resharpener.	39
Table 5: Average Dimensional Attributes for Second PPT Resharpener.	40
Table 6: Average Dimensional Attributes for Third PPT Resharpener.....	41
Table 7: Blade curvature of DS01-DS30	60
Table 8: Blade curvature of DS01-DS30	61
Table 9: Original Attributes for In-set Width	67
Table 10: First Resharpener Attributes for In-set Width	67
Table 11: Second Resharpener Attributes for In-set Width.....	67
Table 12: Third Resharpener Attributes for In-set Width.....	67
Table 13: Material Summary of PFP1 Points	69
Table 14: Average Dimensional Attributes of PFP1 Points	69
Table 15: Inset Width and Curve Data	79

Chapter 1: Introduction

The study of stone tools to further our understanding of the dynamic past has been a catalyst in expanding the innovative measures seen in lithic morphometric research during the past century. Archaeologists have commonly agreed that the analysis of stone tools has the potential to reveal evidence regarding the behaviors and concurrent actions of people who have lived in the past (Andrefsky 2005; Flenniken & Raymond 1986; Frison 1968; Shott 1996). Identifying these behaviors has given an opportunity to infer not only the function and design behind stone tools, but the technological variation and cultural transmission of ideas among populations. Archaeologists have measured these behaviors by relating the material patterns of known technological, economic, or social behavior to the patterns present in the archaeological record and amongst particular morphologic features of individual specimens. The relationship between observed phenomena and the material evidence is a key aspect of how archaeologists have built interpretations of the past and expanded lithic research.

In the field of lithic analysis, conducting experiments has provided an opportunity to simulate these behavioral patterns as evidence for comparison to material culture. The idea of curation is one behavioral pattern of interest, exploring how past humans make decisions about the production, use, maintenance, and discard of tools. Traditionally, tool curation – including concepts of re-use and resharpening - has been measured using calipers, limiting behavioral patterns into bounding box measurements. With the advent of new digital 3D scanning and geometric morphometric analysis methods, archaeologists have developed new ways to extract quantitative measures from stone tools, and in the process, establish novel approaches to the study of topics like tool curation. A unique opportunity to further morphometric research in tool curation

has presented itself in recent findings at the Cooper's Ferry Site in western Idaho. Excavations have revealed a pattern of stone tool caching associated with late Pleistocene-aged western stemmed tradition (WST) cultural occupation. In particular, the tools in PFP1 – interpreted as an equipment cache by the investigatory - have been described as bearing evidence of “having been used and resharpened prior to their burial” with the presence of pronounced “ears” along the blade-haft transition (Davis et al 2017:554). By drawing relationships between the geometric morphometry of PFP1 tools and the changes occurring within a stone tool retouch experiment, inferences towards curation and behavior can be made.

1.1 Background

The presence of lithic artifacts within the archaeological record has provided archaeologists with an invaluable analytical tool to understand prehistoric lifeways and cultural patterns. The significance of understanding stone tool technology as a chronological and behavioral marker did not come to fruition until the late 19th century. William H. Holmes (1894) was one of the first archaeologists to analyze lithic artifacts for their potential as chronological markers as well as understanding the processes of stone tool production and use (Andrefsky 2005). His work inspired the surge of archaeologists in the 20th century to explore artifact morphologic characteristics and replication techniques. Classification schemes were created to aid in artifact description and account for morphological variability seen both temporally and spatially. The incorporation of these schemes amongst lithic assemblages helped to facilitate comparison and was “a way of generating questions about the data” (Andrefsky 2005:61). These qualitative and quantitative descriptions set forth the analytical techniques used today in distinguishing typologies and stone tool use.

The introduction of flintknapping as a hobby and a tool for replication experiments during this time also greatly contributed to the understanding of stone tool production and use. Replication sought to explain archaeological phenomena through controlled methods of experimentations. Studies looking to explain the production sequence or *chaîne opératoire*, would conduct experiments producing flakes “with as much control as possible to model production behaviors utilized by stone tool producing populations” (Reti 2016:3). The results of these studies would provide potential answers to behavioral and technological expectations based on the conditions used during the experiment. Although experimental studies are unable to account for all variables occurring within a behavioral environment, the strict set of parameters used within a replication experiment allows for a known degree of lithic manufacture and variability to be controlled and understood (Andrefsky 2005). From this, inferences about a population’s behavior and lithic assemblage can be described.

With archaeological research focusing on experimentation and stone tool classification and identification, understanding an artifact’s use-life became important in explaining some of the variations seen amongst stone tool using populations. Binford (1973) used the term *curation* as a way of describing the series of events that led to an artifact being deposited within the archaeological record. Tool transport, maintenance, caching, and recycling were all factors that affected how an artifact appeared within its context, however the definition of curation at the time was too ambiguous. A strict definition was not conceived until Shott (1989) defined curation as “the degree of use or utility extracted, expressed as a relationship between how much utility a tool starts with – its maximum utility – and how much of that utility is realized before discard” (Shott 1996:267). The idea of actual use relative to an artifact’s maximum potential use became important in being able to measure how much maintenance a stone tool had undergone. For example, artifacts

that have not had significant amounts of resharpening have a low actual use relative to its maximum potential use, whereas artifacts that have undergone numerous resharpening phases have a high actual use relative to the maximum potential use (Andrefsky 2009). Being able to measure the degree of artifact curation through stone tool maintenance would greatly aid in understanding past behaviors, and if a population sought to exploit a tool even with a low potential use.

Current archaeological studies have relied on 2D measurements, qualitative descriptions, and intuition when analyzing lithic technologies. Artifact size and shape are often used as the primary designators of stone tool types (Shott 2007). However, this has resulted in the misclassification of stone tool types and typologies, due to differing interpretations of how lithic assemblages relate temporally and spatially with one another. The incorporation of basic measurements such as: maximum length, width, and thickness, have aided in typological classification; this approach, however, again limits variation into bounding box measurements. In addition, there remains a degree of irreproducibility and variation when using standard measurements and descriptors to infer form. Recent studies have sought to address this dilemma by furthering standard measurements away from calipers and incorporating additional two-dimensional attributes and new 2D and 3D measurement techniques into stone tool analyses (Ames 2010; Andrefsky 2006; Charlin & González-José 2012; Davis et al. 2015; Davis et al. 2017; Dogandzic et al. 2015; Serwatka & Reide 2016; and Shott & Seeman 2015). For example, expanding bounding box measurements to include: maximum shoulder width, neck width, blade length, and haft length have helped infer the shape of the artifact and differentiate between typologies more precisely (Ames et al. 2010). Further, dimensionless measurements of blade curvature, reentrants, and Procrustes landmark analyses have also allowed for shape to be more precisely defined (Davis et al. 2015, 2017).

By furthering two- and three-dimensional approaches, archaeologists can move beyond 2D limitations and begin to measure the more intricate surficial differences in form. However, to better understand measures of use and the degree of reduction and curation, a comparison is needed to an artifact's original form. In this instance, experimental studies are imperative to understanding stone tool curation; and which measures will help archaeologists identify between realized and maximum utility. In this regard, there is clearly an urgent need for experimental research, objective approaches, and alternative quantitative measurement techniques in the analysis of lithic technologies and curation. This study will implement experimental approaches in an effort to identify the behaviors associated with stone tool maintenance. Specifically, this study will conduct a series of resharpener events to illustrate use life of an artifact by establishing stages of artifact maintenance.

An advance in digital technologies during the past decade has given archaeologists an opportunity to explore the countless possibilities of 3D scanning technologies and analytical tools. Three-dimensional digitization has provided archaeologists the ability to create artifact replicas for data preservation, experimentation, and as teaching implements. With advancements in computer programming, the combination of 3D models and spatial analysis software, has given archaeologists a means to analyze data that would not have been feasible before the 21st century. In archaeological research, controlled replication experiments have generated important methodological analysis on lithic production techniques, however the products can now be better understood with alternative quantitative measurement techniques. This study will approach these alternative techniques by utilizing a geographic information systems-based lithic morphometric research (GLiMR) software to collect geometric morphometry data of a series of projectile points (Davis et al. 2015). The collection of these data will allow for the analysis of an artifacts 2D and

3D spatial data in characterizing specific attributes and measurable standards for artifact shape and type. In addition, this study will conduct a series of experimental resharpening events to illustrate use life of an artifact by establishing stages of artifact maintenance. Specifically, the countless possibilities of analytical tools will allow this research to identify attributes unique to resharpening episodes and provide inference into stone tool curation.

1.2 Research Goals and Hypotheses

The goal of this study is to evaluate the utility of 3D morphometric analyses to assess whether the PFP1 projectile points were made for internment in a pristine state or had already experienced use and retouch before internment in the cache. This will be accomplished by setting up a series of projectile point resharpening experiments that are subjected to 3D scanning and geometric morphometric measurements, the results of which can be organized into a comparative model that outlines the stages of projectile point resharpening. Additionally, the purpose of this study is to explore novel measurements unique to identifying evidence of retouch through the use of GLiMR, a software created to generate meaningful 2D and 3D spatial data. Finally, as a test case, these methods will be used to evaluate the hypotheses that the PFP1 cache represents a utilitarian equipment cache and not a special non-utilitarian ritual cache. The project has been divided into a series of phases from which to follow:

Phase 1: Using the David Laser Scanner, collect 3D spatial data on thirty experimental projectile points flint-knapped in the style of the Western Stemmed Tradition.

Phase 2: Establish a series of experiments, resharpening each point and collecting 3D spatial data for each of the reduction stages.

Phase 3: Using GLiMR, measure the slope and blade curvature for each stage of reduction, establishing an averaged sequence from which to measure other tools.

Phase 4: Collect 3D spatial data on fourteen projectile points from PFP1 at the Cooper's Ferry Site and identify where individual points might fall along the sequence established.

1.3 Significance

The significance of this study will be an enhanced ability to statistically capture data and attributes unique to the process of artifact maintenance and retouch. The incorporation of experimental resharpening will allow for tightly controlled variables and the ability to replicate the process used. As a form of corroborative experimentation, it will allow for previous results to be confirmed or new phenomena to be identified (P. Carr & A. Bradbury 2010). The results of this research will hopefully facilitate further research into artifact maintenance and generate comparable results to artifacts found within the archaeological record. To begin this comparison, the results of this study will be compared to projectile points from the Cooper's Ferry site to help further the culture history model of the Cooper's Ferry site in the lower Salmon River canyon. These points will be the focus of the fourth phase of this study, and the results will be used to illustrate the effectiveness of 3D morphometric data produced by the GLiMR software. By establishing how many stages of reduction these points have undergone, insight into the curation of the PFP1 cache at the Cooper's Ferry site can be better understood. Among the fourteen projectile points from Cooper's Ferry, several have displayed numerous visual characteristics of resharpening, however the variability between projectile points have yet to be understood. The use of GLiMR will allow for a statistical approach to these observations and provide a basis for further hypotheses to be made about the behavior behind stone tool maintenance of past peoples.

Chapter 2: Literature Review

2.1 Experimental Archaeology

In the mid-20th century, Experimental Archaeology and Ethnoarchaeology were introduced as a productive means to explain the relationship between behavioral phenomena and the modes of production of material culture. Lewis Binford (1967, 1981) was most influential in conducting ethnoarchaeological research by drawing relationships between current human behavior and the archaeological record. His use of analogies in combination with observable phenomena helped develop an explanation of the isolated “systematic variables which operated in the past” (Binford 1967:10). Although using similar theoretical frameworks, experimental archaeology diverged from ethnoarchaeology by focusing not just on ethnographic accounts, but looking at “the fabrication of material, behaviors, or both in order to observe one or more processes involved in the production, use, discard, deterioration, or recovery of material culture” (Skibo 1992:29). This has motivated archaeologists to conduct experiments and reconstruct technologies and man-made features based on the material evidence and assumptions on past behavior. The results produced in these controlled experiments have given insight and knowledge into cultural material and formation processes and provide a “firmer inferential footing” for readily describing and explaining past behavior (Skibo 1992:30).

Early approaches in flintknapping experimentation and analyses largely occurred between the 1940s and 1970s among expert flintknappers, notably including: François Bordes, Jacques Tixier, and Don Crabtree (Carr & Bradbury 2010). Controlled experimentation required “rigorous attention to research design and procedure”, developing a theoretical framework for material

expectation and comparison between studies (Marsh & Ferguson 2010:2). Experimental lithic research primarily focused on describing the technological aspect of projectile point shape, and the mode of production. Skibo (1994) has termed this focus on design and utilitarian function as “techno-function”. By identifying the sequence of activities or actions constituting an artifact's life history allows for behavioral inferences to be made. Without recorded accounts on stone tool manufacture and use amongst early people, experimental archaeology provides a unique opportunity to draw conclusions using replicable research. This application of multiple lines of evidence and redundant measures ends up painting a more accurate picture of reality (Magne 2001).

In attempts to find solutions to the variability seen in the archaeological record, flintknapping experiments resulted in three major types: technological, replicative, and highly controlled (Carr and Bradbury 2010). Technology experiments focused on *chaîne opératoire*, using debitage classifications to identify specific modes of production. Replication studies on the other hand used experimentation as a means to identify the production process and validate behavior and the specific techniques used by cultural groups (Flenniken 1984). Highly controlled experiments attempt to control for equifinality or variation, focusing on a single variable in order to explain the mechanics behind flake formation (Carr and Bradbury 2010). A combination of the above types of experimental studies would arguably provide a more accurate inference into the life history of lithic artifacts. The use of skilled knappers in replicative experiments would also aid in more accurate experiments as they can more accurately control for variables, using experience to produce flakes in a manner to model production behaviors. These factors in association with a distinct research design and expectations, would allow for reliable and consistent results that can be reproduced.

2.2 Lithic Curation

The use-life of lithic technologies has been explained as episodes or events and is organized into areas of artifact procurement, production, reduction, maintenance, and discard (Andrefsky 2009). Use-life begins when an artifact has been produced and ends when the artifact has been discarded. During this cycle, if the tool becomes dulled or broken from use, the artifact can undergo maintenance in the form of modification or resharpening, resulting in a transformation in which the tool resembles a more reduced shape than its previous form. This degree to which technology has been maintained for further use, has been coined by Lewis Binford (1979) as *technological curation*. In other examples, curation has been suggested to begin only during the maintenance or alteration of the stone tool. Specifically, the blade of a projectile point only begins its use-life once hafted, and curation begins at the first resharpening event (Andrefsky 2006). In another example, curation is understood to be the degree of use and the ratio of realized versus maximum utility (Shott 2015). Although there is no universal definition of the term, it can be generally agreed that curation encapsulates the behavior behind the selection, acquisition, and maintenance of stone tools (Smith 2015). Curation essentially represents the behavioral events that have shaped the final form of an artifact found in the archaeological record.

Archaeologists have sought to measure the degree of curation through studies of experimental stone tool use (Andrefsky 2006; Blades 2003; Flenniken & Raymond 1986; Kuhn 1990; Shott 2015; Towner and Warburton 1990). As tools undergo a systematic reduction, the shape will vary from its previous form. Shape types will differ based on the kinds and amounts of reduction experienced (Shott 2000). Modification typically occurs in two manners: resharpening and rejuvenation. Resharpening seeks to retouch an edge that was dulled through use while

rejuvenation refurbishes broken tools into functionally equivalent tools (Towner & Warburton 1990). The morphometric variations caused by this modification makes it difficult to truly distinguish between projectile point type typologies. In a study by Flenniken and Raymond (1986), the process of refitting a stem into the hafting element required additional retouch, changing the projectile point typology. In another study by Thomas (1981), The Monitor Valley typology sought to alleviate inconsistencies between Great Basin projectile point types by grouping quantitatively similar projectile points that display variation only as a result of modification, not varying types. These modifications, although identifiable based on the size, shape, and location of the flake scars removed, cause an alteration to the original shape making it difficult to accurately use strict quantitative typologies as temporal markers. The typology of a point ultimately represents the last mode or activity the tool was subjected to (Flenniken and Raymond 1986). The methods proposed in this research will measure the degree of change between consecutive resharpening events, creating a 3D snapshot of the form after each retouch event. By identifying the last mode of activity based on the modifications made to the blade, inferences about technique and behavior can be made.

Although this experimental study will not include an analysis of impact fracture and the refurbishing of broken points, the study will provide insight into retouch and maximizing blade efficiency. Projectile point morphology, mass, and the hafting element, have an impact on what portions of a projectile point are resharpened while seated in the hafting element. Andrefsky et al. (2006) have stated that hafted bifaces will experience retouch along the edges of the blade, whereas the hafted base will remain untouched. This is evident amongst the PFP1 projectile points that have retained “ears” along the shoulders, having been “bound with sinew at the upper limit of the hafting element” (Davis et al. 2017:550). It has been considered that resharpening a projectile point

within the haft element is more time and energy efficient (Towner and Warburton 1990) and allows the points to act as multitools rather than just for piercing (Andrefsky 2006). As a result of specialized use and resharpening along only dulled portions of a blade, asymmetry can result from one side being longer or shorter than the other (Andrefsky 2006). Irregularities in the size and shape of flakes, steepness of angles, volume loss, and blade curvature will help differentiate tools that have experienced curation; however, it can be difficult to distinguish one resharpening event from many. By creating a controlled experiment, behaviors and morphologic characteristics unique to the resharpening of the blade element can be identified and measured.

2.3 Lithic Tool Morphometry

Traditional analysis of stone tools has primarily focused on simple bounding box measurements, employing length, width, thickness, and shape as proxies for artifact form. Additional measurements such as thickness and blade angle add to the object's three-dimensional form; however, these "bounding box measurements are too generalized to reflect variation in artifact form needed to establish critical differences and similarities in stone tool manufacturing techniques" (Davis et al. 2017:537). The limitations of these measurements make it impossible to reconstruct the precise shape of the artifact, as the measurement values restrict the form to a rhombohedron-type shape. A more accurate and consistent representation of a projectile point's shape however, can be accomplished with 3D scanning technologies. The advantages of using digital 3D methods are that it minimizes user judgement and produces a digital model from which the morphometry can be measured using computer-based algorithms. Software that processes point cloud data can be used to read the XYZ information generated by the 3D scanner and extract distinct morphological features that may not have been recognizable to the naked eye.

Traditionally, the identification of key morphologic features has been conducted by archaeologists based on visually distinct features, however this will always be subjective. Recent studies have begun to explore alternative solutions to geometric morphometric shape analysis through the use of multivariate statistical analysis (Charlin & González-José 2012; Costa 2010; Serwatka & Riede 2016). In these studies, morphometric features are established by creating equidistant landmark points along a gridded outline of a projectile point, which allows for the comparison between variable projectile point shape and sizes. This however still deals with data in a relative 2D form, and the methods proposed in this study aim to expand these types of measures and explore the 3D form. Davis et al. (2015) have implemented a geometric morphometric analysis system that allows 3D digital data to be more readily generated, and morphologic features to be established objectively through software automation. Their GIS-based morphometric research approach, GLiMR, is capable of establishing landmark points along the surface and depicting technological features such as tips, blades, and hafting elements, without the need for manual adjustment. This study will utilize GLiMR to extract information such as blade curvature, slope, and basic measurements such as: length, width, and thickness to address the changes occurring after each episode of resharpening. This information is highly replicable and can be used to describe how a projectile point may have been made or maintained.

2.4 Projectile Points of PFP1

The Cooper's Ferry site located in the lower Salmon River canyon contains extensive intact cultural components of the WST spanning the late Pleistocene to early Holocene periods (Davis et al. 2017). The WST projectile points from the oldest components of the site date from 11,410-11,370 radiocarbon years (Davis et al. 2014). During excavations in 2012, a pit feature (PFP1) was

uncovered that yielded fourteen WST projectile points and very few other artifacts, likely representing a cache. Thirteen of the fourteen projectile points were found in situ, whereas the fourteenth was found in an auger during testing.

The WST has traditionally been characterized by shouldered or unshouldered stemmed projectile points occurring west of the Rocky Mountains (Bryan 1980; Davis et al. 2017). Among the fourteen projectile points from PFP1, all can be characterized as shouldered stemmed projectile points, with a total of nine having retained “ears” along the shoulder/haft juncture indicating periodic resharpening episodes (Figure 1). Davis et al. (2017) argue that the presence of these ears represent the unworked portion of the blade, due to sinew being bound onto the upper limit of the hafting element. This study will further explore the development of these ears by conducting a series of consecutive resharpening experiments of the same projectile point. As described in greater detail below, using a combination of controlled experimental resharpening, 3D scanning technologies, and geometric morphometric analysis of thirty projectile points, characteristics unique to resharpening behaviors can be identified. The results of which can be used to infer the curation of the fourteen WST projectile points from PFP1, and how they compare to the sequence of resharpenings conducted in this study. In general, the site has the potential to define the technological roles and behaviors of one of the earliest peoples of North America.

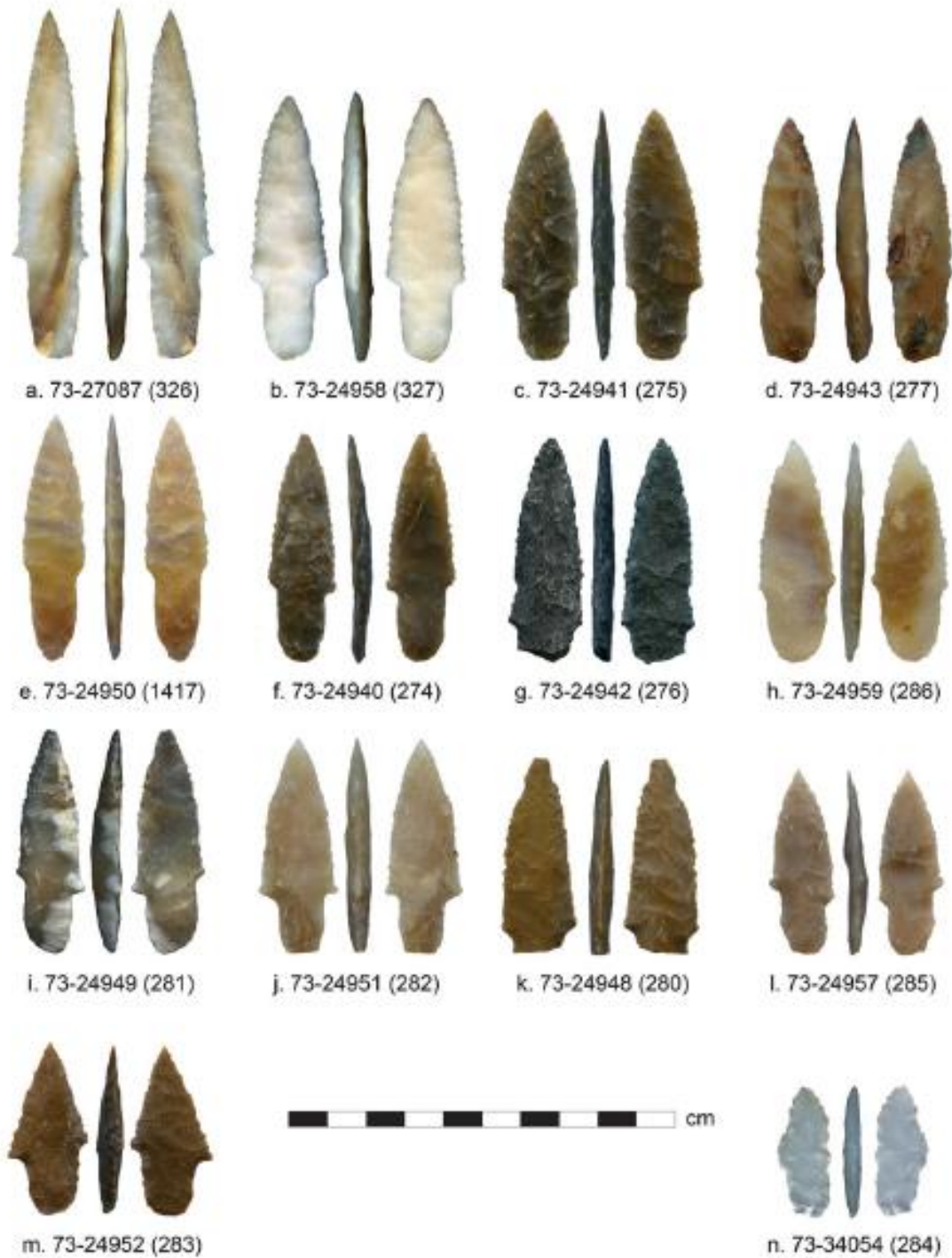


Figure 1: Digital images of the fourteen projectile points discovered in PFP1. Catalog numbers and GLiMR numbers (in parentheses) are shown at base of each artifact. Image and description from Davis et al. (2017:Figure 4).

Chapter 3: Methods

This chapter discusses the methods used to model the effects of resharpening and test the hypothesis that the fourteen projectile points from PFP1 represent a utilitarian cache, as opposed to a non-utilitarian ritual cache. By identifying whether the projectile points experienced use and resharpening, thirty projectile points were flintknapped in the style of the WST projectile points and scanned to create a 3D model for geometric morphometric analysis. Each of the projectile points was subjected to a total of three resharpening events and 3D scanned after each event. By creating a sequence of 3D models to represent the last mode of resharpening, geometric morphometric analyses were conducted to identify key morphologic changes to the blade. Both 2D and 3D measurements unique to identifying patterns of resharpening were used to assess how much resharpening the PFP1 projectile points experienced, if any. The methods outlined in this chapter illustrate the techniques and analysis tools used to evaluate and measure curation.

3.1 WST Replication

Experimental Design Considerations

The hafting method used for this analysis is from morphometric descriptions described by Davis et al. (2017) in a recent publication on fourteen WST projectile points from a pit feature at the Cooper's Ferry site. Davis et al. (2017) argued that the 14 points represent a flake-tool technology, rather than being made on cores, noting that the WST projectile points from PFP1 typically had the largest total cross-sectional area at the juncture between the haft and blade elements. This design is thought to have acted as a load-bearing buttress, causing impact force to be applied to the foreshaft, seated just below the haft collar. These results similarly follow suit

with Knecht's (1997) hypothesis that the design of most projectile points has shown the cross-sectional area at the base to be smaller than the cross-sectional area along the midsection (Knecht 1997:201). However, amongst the WST projectile points, the widest cross-sectional area is located below the midsection, just along the shoulder-haft transition. This characteristic, in association with the hypothesis that the PFP1 projectile points were made on macroflakes, was the premise of the size, shape, and mode of production for the experimental projectile points used in this study.

Experimental Methods

The experimental flintknapping process was conducted by an expert flintknapper and lithic specialist, Dan Stueber, who gained his 25 years of expertise in the manufacture and analysis of lithic technologies studying under Dr. John Fagan and Dr. Errett Callahan. His approach was strongly influenced by the Crabtree technique for stone tool reduction and maintenance using similar body movements in the wrist, arm, and shoulder during flintknapping. Lithic preference was given to the flintknapper (Stueber), who chose materials based on abundance and familiarity of the material type. In total, four very fine-grained materials were chosen for the study: dacite, obsidian, petrified wood, and cryptocrystalline silicate (CCS). Of the four materials, dacite and obsidian were the more prominent material type used for the study, making up 23 of the 30 replicated projectile points (Table 1). The tool kit consisted of an elk antler billet and two sandstone percussors, an antler tip mounted in a plum wood handle for pressure flaking, a sandstone for abrading and platform preparation, and a dried deer humerus for dulling the blade (Figure 2 & Figure 3).

Table 1: Material Summary of Replicas

Local ID	Material	Local ID	Material	Local ID	Material
DS01	Obsidian	DS11	Dacite	DS21	Petrified Wood
DS02	Obsidian	DS12	Dacite	DS22	Petrified Wood
DS03	Obsidian	DS13	Dacite	DS23	Dacite
DS04	Obsidian	DS14	Dacite	DS24	Dacite
DS05	Obsidian	DS15	Obsidian	DS25	Dacite
DS06	Dacite	DS16	Petrified Wood	DS26	Obsidian
DS07	Dacite	DS17	Dacite	DS27	Petrified Wood
DS08	Petrified Wood	DS18	Obsidian	DS28	Obsidian
DS09	Dacite	DS19	Dacite	DS29	Obsidian
DS10	Petrified Wood	DS20	Obsidian	DS30	CCS



Figure 2: Experimental Toolkit A. (a) Elk antler billet (b) Antler tip pressure flaker mounted in a plum wood handle.



Figure 3: Experimental Toolkit B. (a) Three sandstone percussors (b) Antler tip pressure flaker mounted in a plum wood handle.

Stone tool production occurred over a period of two months, where Stueber made thirty projectile point replicas in the style of the WST projectile points found in PFP1 at the Cooper's Ferry Site. A 3D print of the average WST projectile point from PFP1 (Davis et al. 2017) was used as a template for Stueber's replication work; however the blades were designed slightly larger than those seen in PFP1. Each of the projectile points were manufactured in roughly 40-60 minutes, following the reduction sequence outlined by Davis et al. (2012) (Figure 4). When creating each of the projectile points, flakes were removed around the edge of a nodule with percussion. Based on the hardness of the material, either a medium-sized hammerstone or a billet was used to generate a macroflake from the lithic nodule, ultimately creating a blade-core (Figure A.1). A small-sized hammerstone was then used to remove bifacial thinning flakes from the flake blank, until pressure flaking was necessary to refine the shape. An antler tip was used to pressure flake around the preform to create a stemmed projectile point with the desired width and thickness as compared to the 3D print. After each event, flake debris was collected for further analysis into the reduction technique used.

Before each resharpening episode, the projectile points were hafted into a modified version of a split foreshaft and secured using a waxed nylon cord as sinew. Since rehafting was necessary after each resharpening episode, additional adhesives such as pitch were not used for the study as it would adversely affect the 3D models. The hafting process involved securely fitting the stem into the split foreshaft and wrapping sinew onto the upper extent of the shoulder haft transition (Figure 5). Afterwards, the edge of the blade was dulled by "cutting" along a dried bone to simulate use. When needed, the blade was further dulled with the sandstone abrader for platform preparation (Figure A.2). The blade was then minimally resharpened to produce a sharp edge, removing as little material as possible to maximize use-life and tool expediency. Pressure flaking occurred

unidirectionally along one edge, removing material from the wrapped portion of the shoulder towards the tip of the blade. For most of the projectile points, pressure flakes were removed on opposing edges. Flake removal occurred unidirectionally along one edge, flipped 180 degrees about the x-axis, and removing flakes again on the other edge (Figure 6). In some cases, pressure flaking occurred unidirectionally on one edge and rotated 180 degrees about the y-axis, resulting in flake removals on one face rather than opposing faces (Figure 6). Only in certain circumstances where there were impurities in the stone or hinges from negative flake scars that the blade was resharpened from tip to base, or additional flakes were removed. This removal was in an effort to “maintain an effective cutting tool”, as seen in an experimental study conducted by Andrefsky (2008:88). These decisions were left to the discretion of the flintknapper and produced little discernable difference in flake size and shape. The final product resulted in a total of thirty WST-style projectile points with little variation in length and width (Figure 7).

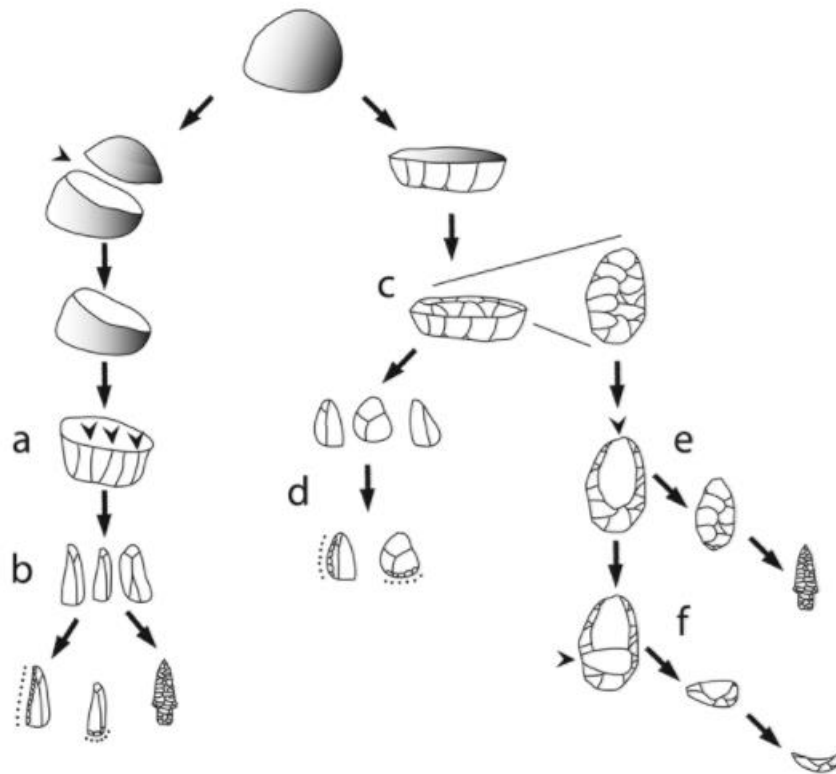


Figure 4: Paleoarchaic lithic reduction sequence from Davis et al. (2012:Figure 3.2). This experimental study used the (a – b) sequence, following the reduction sequence: nodule > core > flake blank > stemmed PPT.

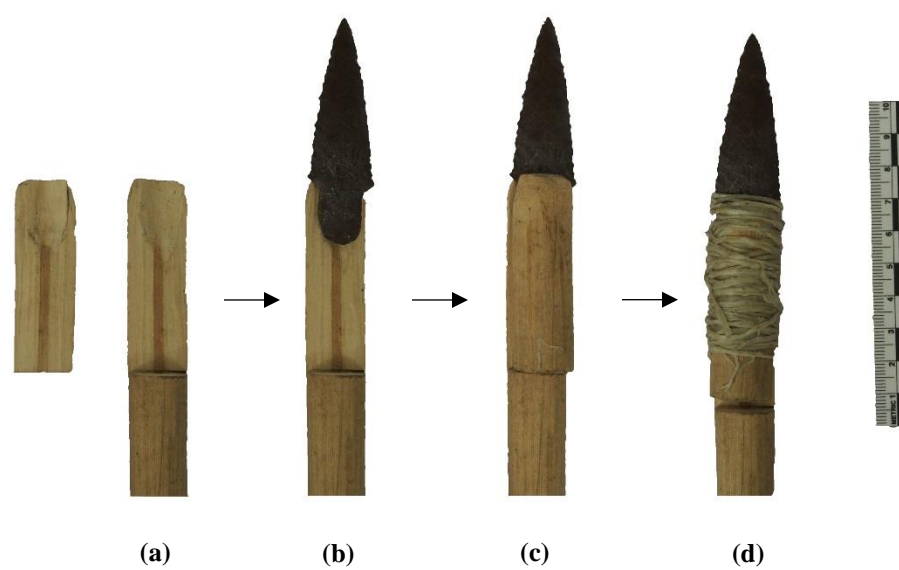


Figure 5: Hafting method used in the experimental study. (a) Split foreshaft components, (b) slot for stemmed point, (c) unsecured projectile point, and (d) waxed sinew onto the upper extent of the shoulder.

Flake scar orientation reveals resharpening pattern

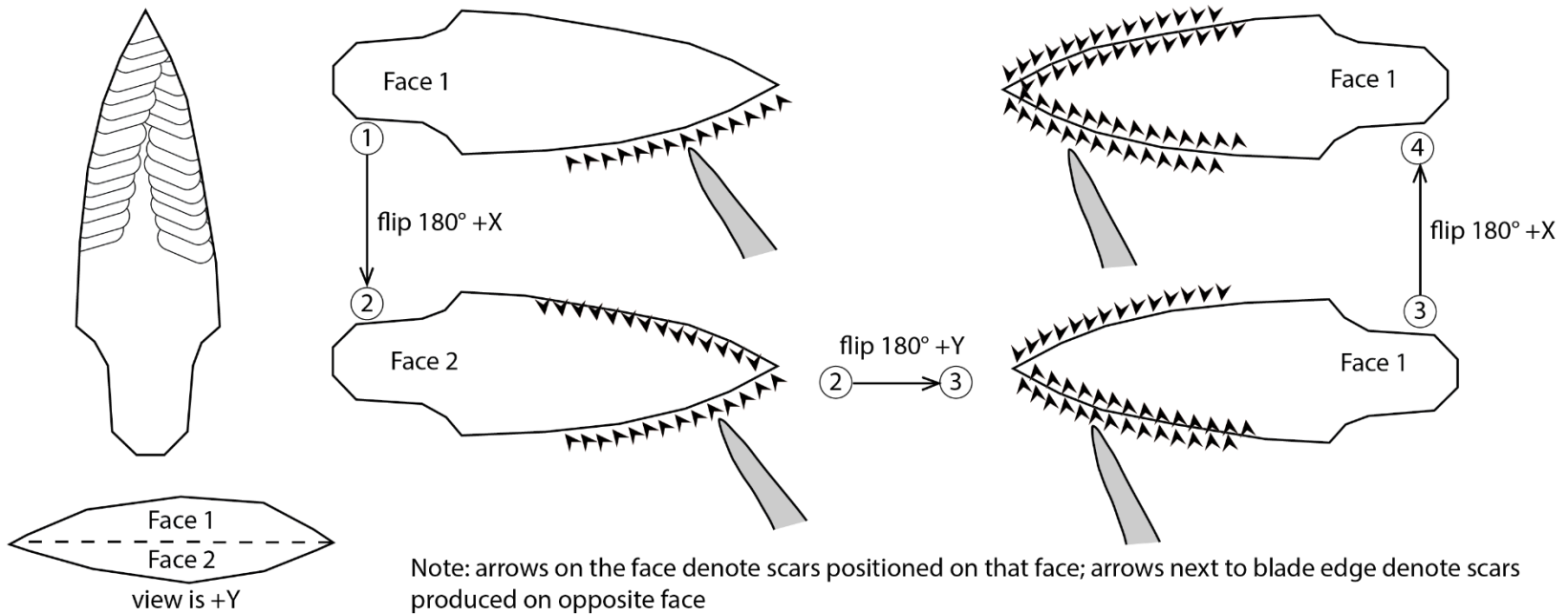


Figure 6: Unidirectional resharpening directions that experience three modes of resharpening: either flipped along the x-axis (1-2), flipped along the y-axis (2-3), or flipped along both the x- and y-axis (1-4). Image courtesy of L. Davis.

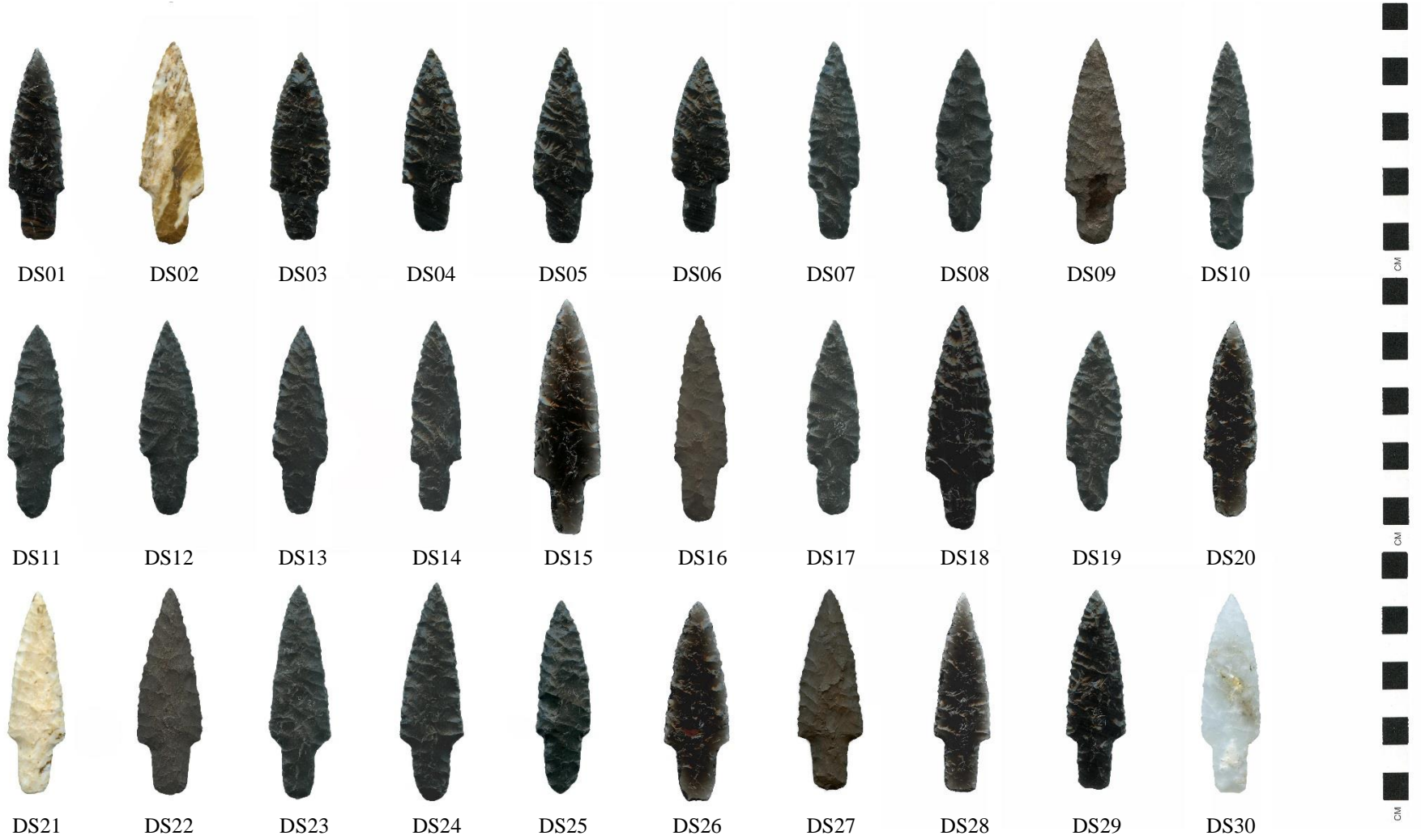


Figure 7: Digital images of the thirty replicated stemmed projectile points (DS01-DS30).

3.2 Three-dimensional Models

Three-dimensional digital models were created for each of the experimental WST projectile points, using a David SLS-2 scanning system. The scanner is an advanced structured light scanner that is capable of accurately scanning objects between the sizes of 30 mm to 500 mm at a precision of 0.05 mm. The scanning system is equipped with both a projector and monochrome camera, used to calibrate the system and provide texture to the object. The structured light scanning system is capable of projecting a series of stripes onto the object, and equipped with the camera, simultaneously record the distortion of the light patterns on the surface of the object (Wachowiak and Karas 2009). This is done by adjusting the angle of the camera with the projector and aligning the scanners within focus of a gridded backboard. The triangulation between the object and the projecting system creates three reference points that are used to compute the distance of any one point to the object surface. The object requires multiple overlapping scans at different angles in order to recreate the 3D surface. The high-resolution 3D models are comprised of thousands of spatial xyz data points that are used to align and reconstruct the object. For a medium-size projectile point like those featured in this study, a minimum of twenty scans were needed which were then fully aligned, smoothed, and fused together to create a 3D model from which accurate digital geometric morphometric measurements could be taken.

Before the projectile point can be scanned, the surface needed to be coated in a fine coat of white powder. Most raw material used in stone tool manufacture such as: obsidian, CCS, quartz, and quartzite, are very-fine grained and often have a glassy or reflective surface. Triangulation scanners that use sensors to capture light reflection to measure the artifacts surface have difficulty capturing surfaces with deep undercuts, reflective surfaces, or subsurface scattering (Wachowiak

& Karas 2009). In addition, translucent materials, very fine edges, or light-absorbing dark surfaces will be difficult to scan, making obsidian one of the more problematic materials to capture. The use of the Tinactin brand foot spray to coat the objects in a white talcum powder, allowed for many of these problems to be avoided as texture was not necessary to capture for this study. When scanning, the projectile point also needed to be captured in two separate scanning sequences. The projectile point base was placed in a foam block, with roughly 80% of the blade visible to the scanner. The top half of the projectile point was scanned a total of 10 times in 36-degree increments before reversing the orientation and repeating the process on the bottom half. Afterwards, each of the halves needed to be manually aligned with one another for a water-tight model to be created.

During the alignment process, time was spent removing obvious outlier point data in the form of “noise” from the dense cloud. Once the individual scans were aligned and fused together, a 3D representation of the artifact was created to within 0.07 mm accuracy of the original artifact. To make the data more manageable, each of the models were then exported with xyz point spacing between 0.80 to 1.20 mm to reduce the file size. The models were then reduced to 300,000 spatial points using the Quadric Edge Collapse Decimation tool within Meshlab, an open source program that allows for the processing and editing of three-dimensional meshes (Cignoni 2008). In addition, a low step Taubin smooth of “2” was applied to remove noise and avoid shrinkage and adversely affecting the curvature of the blade and flake scar depressions. Within Meshlab, the projectile points were then oriented along an xyz, axis with the length along the y-axis and width along the x-axis, based on the center of mass. For the resharpened projectile points, the models were alternatively oriented in the David Laser Scanner software to match the base orientation between consecutive resharpening episodes since the center of mass would have changed. The 3D models were then exported as .ply files and imported into MeshMixer to manually remove any additional

noise caused by the fusion process. These parameters allowed for a well-defined model to be produced with very little variation from the original form (Figure 8). In total, each of the thirty projectile points were fully scanned, aligned, and smoothed four times, resulting in approximately 150 hours of scanning work.

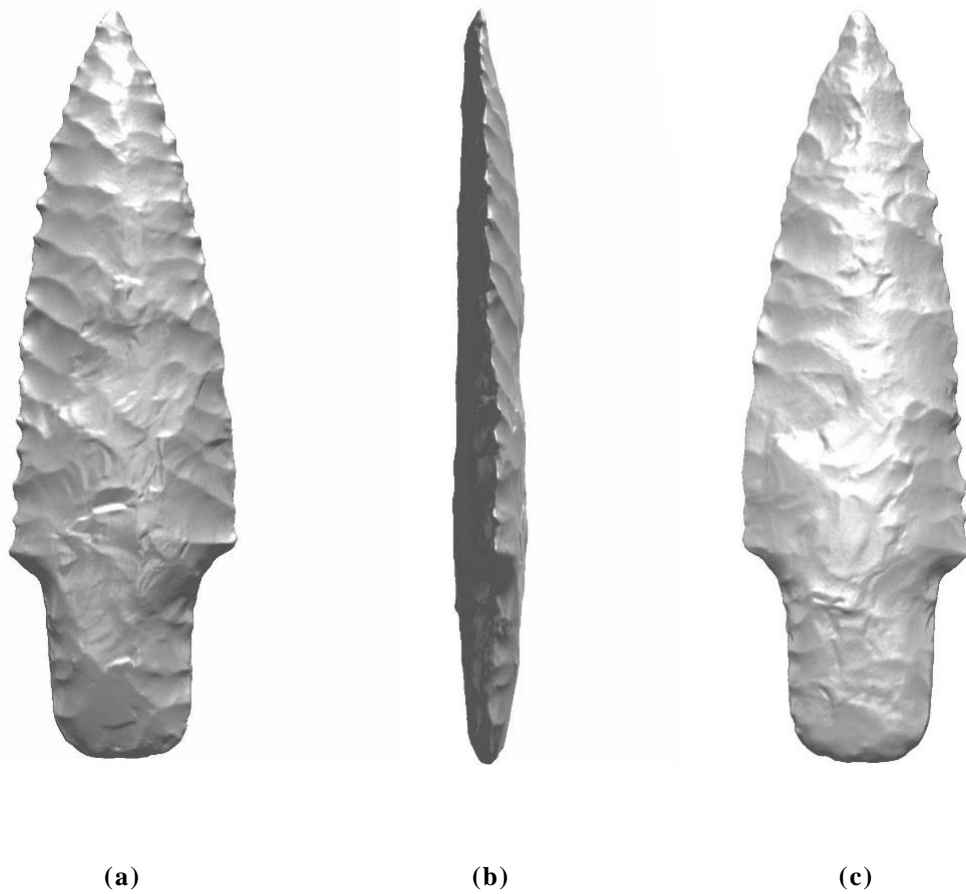


Figure 8: Example of a completed 3D digital model of DS01 representing (a) Face 1, (b) lateral cross-section, and (c) Face 2.

3.3 GLiMR Measures

Dimensional and Dimensionless Data

GLiMR is a python-based tool used in conjunction with the ArcGIS 10.4. This software was created by researchers in association with the Pacific Slope Archaeological Laboratory at Oregon State University (Davis et al. 2015). The software is automated and is capable of processing multiple models, generating a geodatabase for each and a numerical dataset within Microsoft Access. The data contains a multitude of dimensional and dimensionless data, such as: length, width, thickness, blade volume, haft volume, cross-sectional area, and reentrant angle (Davis et al. 2017). In total, GLiMR processes over 100 unique attributes, however only 24 of those attributes will be addressed in this study (Table 2). Before the models are ready for analysis, the aligned scans of the projectile point faces need to be separated due to the limited capabilities of 3D processing tools in ArcGIS. Specifically, ArcMap analyses are limited to 2.5D surficial data and require 3D models to be altered in such a way where only one z-value is present for each x-y location above “sea level”. By separating the projectile point models from edge to edge along an x-y axis direction, one face of the projectile point can be treated as the terrain of a stand-alone island. By reducing the models in this manner, a variety of analyses can be made in ArcGIS including: outline, topography, aspect, and slope (Davis et al., 2015).

When studying the geometric morphometry of an object, a series of points are established representing specific characteristics of an object. In the case of a projectile point, “landmark points are often placed at technological features such as tips, blades, and hafting elements” (Davis et al., 2015). The collection of thousands of individual points into a 3D point cloud, allows for a general shape to be defined and a surface to be created. By treating the points as a set of features or

polygons, significant information can be extracted from them. A polygon representing the “convex hull” can be established which represents “the smallest convex polygon that contains all spatial points” (Davis et al. 2015:202). The gaps in between the convex hull and the outermost edges of the projectile point are termed reentrants. The reentrants that appear on the sides of the blade, just above the haft collar are termed the lower blade reentrants, and this type of measurement will influence the novel technique “inset width” used in Phase 3 of the study and the dimensions may be an identifier for the stages of reduction.

Table 2: Average Dimensional Attribute Descriptions.

Attribute	Units	Definition
Length	mm	Distance from min y to max y
Width	mm	Distance from min x to max x
Thickness	mm	Distance from min z to max z
Max width	mm	Maximum distance from two adjacent edges along x
Blade length	mm	Distance from haft collar to max y
Blade max width	mm	Maximum distance from two adjacent blade edges along x
Blade width average	mm	Blade area / Blade length
Blade max thick	mm	Maximum distance from two adjacent blade faces along z
Blade max thick y	mm	Y coordinate where Blade max thick occurs
Haft Length	mm	Distance from haft collar to min y
Haft width average	mm	Haft Area / Haft Length
Haft max thick	mm	Maximum distance from two adjacent haft faces along z
Outline perimeter	mm	Length of bifacial edge outline
Hull perimeter	mm	Length of smallest bifacial convex hull
Area (xy)	mm ²	Area of outline along xy plane
Hull area	mm ²	Area of convex hull along xy plane
Blade area	mm ²	Area above haft collar along xy plane
Haft area	mm ²	Area below haft collar along xy plane
Area (xz) cross-section	mm ²	Maximum area of transverse cross-section
Volume	mm ³	Volume of entire PPT
Blade volume	cm ³	Volume above haft collar
Haft volume	cm ³	Volume below haft collar
Weight	gm	Measured weight of PPT
Density	gm/cm ³	Computer total Volume / Weight

Slope Measures

To perform geographic data analysis on each of the projectile point faces, GLiMR requires the use of the ArcPy site package to process the point cloud data within ArcGIS. Utilizing the 3D analyst license, a range of raster outputs can be created for the projectile point surficial data. These outputs provide topographic relief images which aid in identifying features and visual discrepancies between projectile points. Specifically, the display options of use in this research include: slope, thickness, and contour mapping. These three estimations help distinguish and compare flake scar morphologies and edge steepness over the courses of resharpening. The slope results will display these graphical summaries in an effort to better illustrate the morphologic change for each of the resharpening episodes.

The slopes of the projectile points were established using the “Slope (in_raster, {output_measurement}, {z_factor})” syntax. A graduated color ramp was applied with a manual classification interval of 2.5 degrees with contrasting colors representing the rate of change in z-values ranging from 0 – 90 degrees. In these slope outputs, the blue color spectrum represents slope variation between 0 – 20 degrees, the yellow spectrum from 20 – 35 degrees, and the red spectrum from 35 – 90 degrees. Although the mean slope values were not collected for this study, the spectrum change will provide a visual for projectile point resharpening along the edge of the blade.

Cross-Section Tool

The cross-section analysis tool is an interactive feature produced by the GLiMR software. The tool allows the user to visualize the cross-sectional orientation at any one point along the x- and y-axis. Manual adjustments can be made to superimpose two dissimilar projectile points onto one another. This involves shifting the xyz axis of one point to relatively match the two and three-

dimensional orientation of the original. The most recent update of the tool allows for at least five cross-sections to be viewed simultaneously in real-time. In this case all four resharpener episodes of one projectile point can be compared to one another in an interactive model.

The output interface generated by the GLiMR tool provides the user with four visualizations for the shape and size of the projectile points. All visualizations work in sync with one another, producing two images of the cross-sectional view along the y- and x-axis, and one image of the thickness slope, based on the cross-hair location along the outline (Figure 10). Each of the cross-sectional images used in this study focus on the midsection of the blade where location “0, 0” represents the center of mass for the original projectile point.

Blade Curvature

As part of the GLiMR summary, blade curvature graphs are generated for each of the two blade edges. The graphs assign both a linear fit line and a polynomial fit (or “poly fit”) line to the blade edge and performs a regression analysis. Along with producing a linear equation for slope-intercept, GLiMR calculates the R-squared value and residual for each linear and poly fit line. The R-squared value is a measure of how close the fitted line is to the outline data of the blade edge, and the residual measure indicates the difference between the observed and predicted lines. The higher the R-squared value, the higher amount of variability is explained in the model. The lower the residual value, the more accurate the predictions are for the regression.

Inset Width

The inset width is a novel measurement based upon the re-entrants discussed by Davis et al. (2015). The measurements look at the length of the “ears” along the shoulder of the blade, in comparison to the width of the projectile point. Re-entrants were not used in this study due to too

much variation between blade curvature and length of the blade. The presence or absence of serrated edges alter the convex hull and size of the reentrant, making it difficult to accurately compare between resharpened projectile points. The inset width bases the length of the ear on the previously calculated polyfit curve of the projectile point. The distance is measured from the point where the curve intercepts the most minimum y-value along the blade edge, to an adjacent point parallel to the y-intercept, representing the maximum shoulder width (Figure 9). This alteration to quantifying the size of the ear helps account for the variations along the blade edge, basing measurements off a smoothed curved line.

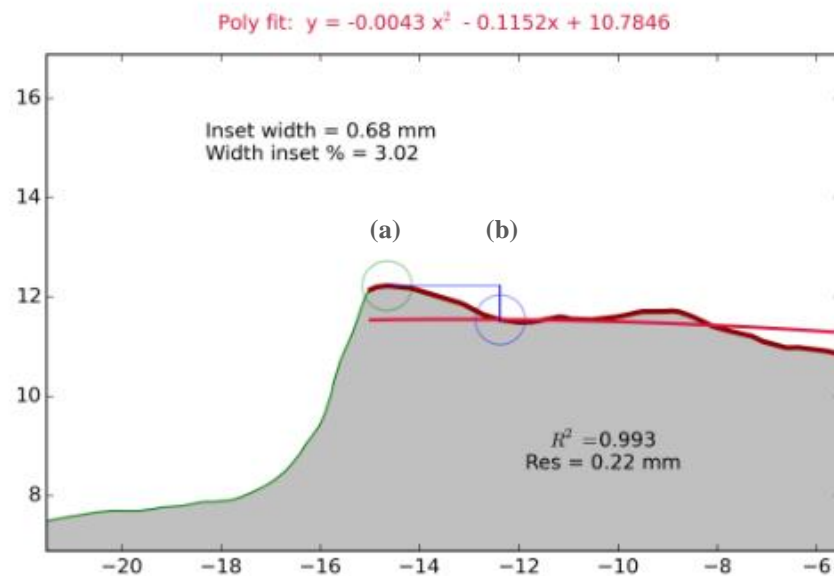


Figure 9: InSet width is a distance measurement from the y-value intersection between the blade curve and blade outline (a), to the y-value of maximum ear extent (b).

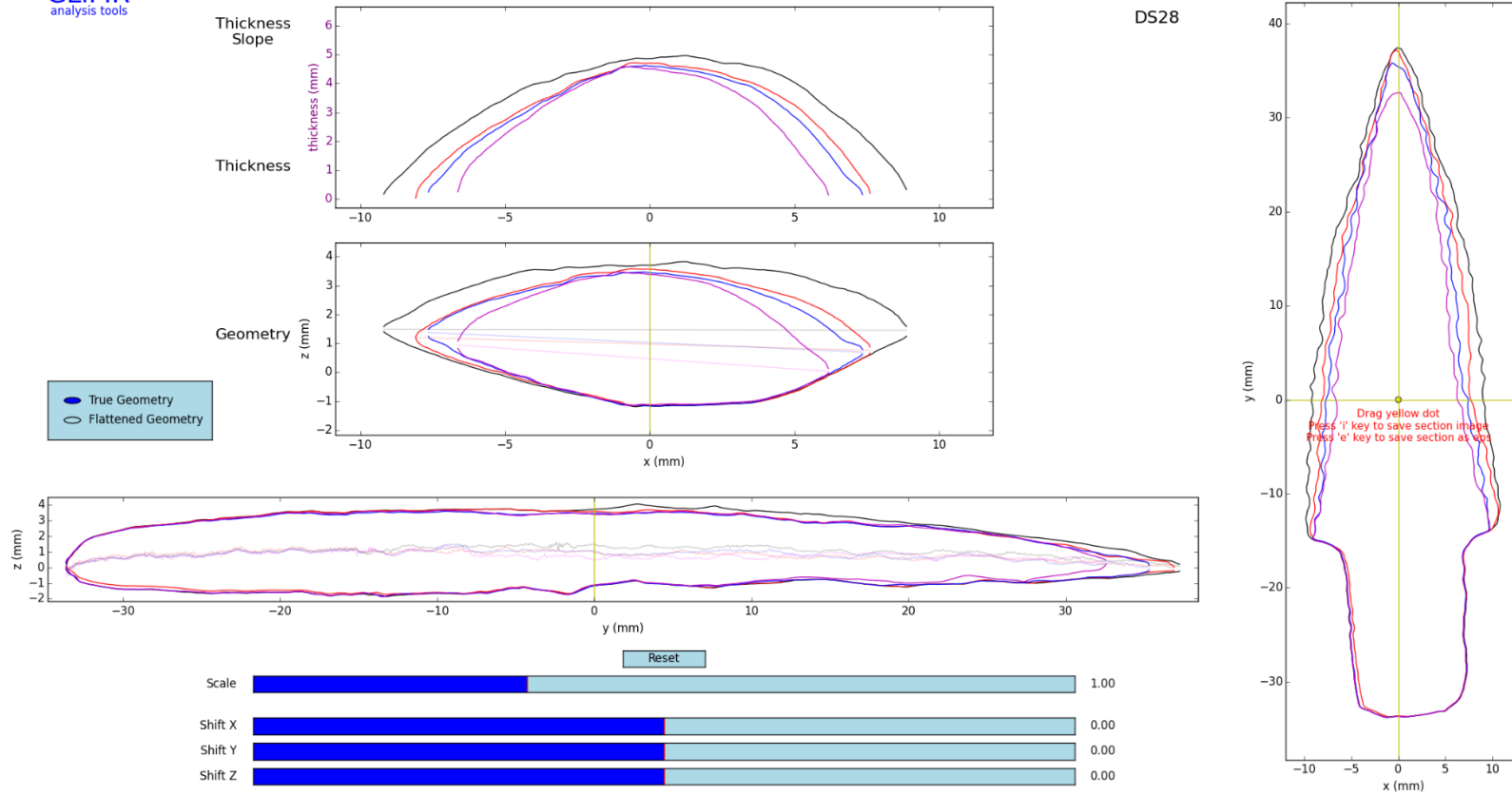


Figure 10: GLiMR analysis tools, interactive cross-sectional view for DS28.

3.4 Analysis Preparation

In order to make the data meaningful between multiples of the same projectile point that experienced resharpening, the following attributed had to be manually adjusted, although typically done through automation. First, as mentioned in subsection 3.2, the original projectile points were aligned along an xyz-plane in Meshlab based on the center of volume mass. However, with the resharpened point, the center of mass would have changed due to flake removal. In order for the projectile points to be aligned correctly in the GLiMR cross-sectional view, the projectile points needed to be manually aligned in the David software. Each of the four projectile points were uploaded into David and the blades removed, leaving only the bases. Since the haft elements were unchanged, all four bases were aligned with one another as if they were the same projectile point. After this alignment, duplicates of the four models were imported into David and re-aligned to their corresponding haft element. This allowed all four sequences to be accurately aligned to one another, based on the original's alignment. Second, the haft collars were re-adjusted in ArcMap from the widest portion of the blade-haft transition to below the shoulders of the blade. Individual haft collars were adjusted within a <0.1 mm accuracy of the original haft collar, which is below the standard error of the scanning system used. The purpose of this would alleviate volume loss discrepancies in the base as either part of resharpening or systematic error. These alterations differ from those used in the Davis et al. (2015) GLiMR summary article.

Chapter 4: Results

This chapter reviews the results of the measures discussed as part of the GLiMR methods in Chapter 3. These include: standard GLiMR metrics, slope, cross-sectional comparison, blade curvature, and inset width. Each of the categories provide replicable GLiMR measures that can be used to compare to the PFP1 projectile points. The incorporation of standard GLiMR metrics allow for the loss between each episode of resharpening to be described quantitatively. The slope results produce images depicting edge steepness and change along each face of the blade. The cross-sectional analysis tool illustrates flake removal patterns and areas of extensive retouch. The blade curvature results provide slope values and indicate change in the blade shape over consecutive resharpenings. Finally, the inset width data produce a summary of ear length and change after each resharpening event. The results of which will illustrate patterns of retouch and provide a basis for quantifying stone tool curation.

4.1 Standard GLiMR Metrics

As noted in subsection 3.3, GLiMR is capable of automatically calculating up to 100 standard measurements within minutes. Table 3 – 6 list 24 attributes that will be used as a basis for comparison between the three episodes of resharpening within this experimental study. Of those 24 attributes, length, width, thickness, and weight are the traditional measurements used for projectile point classification and comparison. The description of these attributes as absolute measures and as percentages, are used to illustrate the changes occurring within the experimental dataset. These measurements can be used to help in identify trends or patterns between stone tool types and curation and are be used as descriptors for observable features. Tables 3 – 6 list the

mean, standard deviation (SD), coefficient of variation (CV), minimum, maximum, and range of values for the experimental projectile points at each stage of resharpening. This section will review these attributes for each of the three consecutive resharpening events and compare the percent changes seen between them.

The original thirty replicated stemmed projectile points had measurement values ranging from 63.11 – 84.15 mm in length, 19.22 – 25.49 mm in width, 5.53 – 7.86 mm in thickness, 6.83 – 14.91 g in weight, and 3.00 – 5.51 mm³ in volume (Table 3). The CV for length, width, and thickness were fairly low, <0.10 or 10%, while weight and volume had higher CV values of 0.23 and 0.16, indicating greater degrees of variation. In addition to the overall length, width, thickness, and volume measurements, Table 3 also displays these measurements in association with only the blade and haft elements. For the overall mean length of 70.96 mm, the mean blade length was 52.58 mm and mean haft length was 18.38 mm, providing a stem to blade ratio of 1:4 with the haft making up 25.90% of the length, and the blade making up 74.10%.

The first resharpening episode (Table 4) had measurement values ranging from 62.69 – 80.76 mm in length, 18.28 – 25.18 mm in width, 5.42 – 7.97 mm in thickness, 6.18 – 14.15 g in weight, and 2.63– 5.15 mm³ in volume. The CV for length, width, and thickness were <0.1 and were higher for weight and volume with CV values of 0.24 and 0.17. The mean length was 69.42 mm with a mean blade length of 51.03 mm, making up 73.51% of the total length, and a mean haft length of 18.39 mm, making up 26.49% of the total length.

Table 3: Average Dimensional Attributes of Original WST PPT Replications.

Attribute	Units	Mean	SD	CV	Min	Max	Range
Length	mm	70.96	4.43	0.06	63.11	84.15	21.04
Width	mm	21.56	1.66	0.08	19.22	25.49	6.28
Thickness	mm	6.75	0.54	0.08	5.53	7.86	2.33
Max width	mm	21.38	1.71	0.08	19.00	25.43	6.43
Blade length	mm	52.58	4.00	0.08	45.05	64.52	19.47
Blade max width	mm	21.33	1.71	0.08	18.95	25.40	6.45
Blade width average	mm	15.31	1.04	0.07	13.67	17.93	4.26
Blade max thick	mm	6.75	0.54	0.08	5.53	7.86	2.33
Blade max thick y	mm	20.20	1.60	0.08	17.95	24.05	6.10
Haft Length	mm	18.38	1.07	0.06	17.00	20.68	3.68
Haft width average	mm	11.69	0.65	0.06	10.07	13.16	3.09
Haft max thick	mm	6.08	0.51	0.08	5.05	7.17	2.18
Outline perimeter	mm	159.71	9.44	0.06	143.80	188.88	45.08
Hull perimeter	mm	154.51	9.22	0.06	139.15	182.56	43.41
Area (xy)	mm ²	1021.83	113.90	0.11	859.45	1382.55	523.10
Hull area	mm ²	1086.74	123.94	0.11	924.80	1476.25	551.45
Blade area	mm ²	806.99	105.78	0.13	638.39	1154.19	515.80
Haft area	mm ²	214.84	16.87	0.08	171.17	259.32	88.16
Area (xz) cross-section	mm ²	92.98	11.59	0.12	75.27	120.95	45.68
Volume	mm ³	3.78	0.59	0.16	3.00	5.51	2.51
Blade volume	cm ³	2.97	0.54	0.18	2.28	4.57	2.29
Haft volume	cm ³	0.80	0.12	0.15	0.53	1.04	0.51
Weight	gm	9.14	2.07	0.23	6.83	14.91	8.08
Density	gm/cm ³	2.41	0.32	0.13	1.85	3.31	1.47

Table 4: Average Dimensional Attributes for First PPT Resharpener.

Attribute	Units	Mean	SD	CV	Min	Max	Range
Length	mm	69.42	4.67	0.07	62.69	80.76	18.07
Width	mm	20.49	1.77	0.09	18.28	25.18	6.90
Thickness	mm	6.63	0.56	0.08	5.42	7.97	2.55
Max width	mm	20.29	1.77	0.09	17.87	25.05	7.18
Blade length	mm	51.03	4.21	0.08	44.64	61.17	16.53
Blade max width	mm	20.24	1.77	0.09	17.80	25.00	7.20
Blade width average	mm	14.13	1.16	0.08	12.40	17.09	4.69
Blade max thick	mm	6.63	0.56	0.08	5.42	7.97	2.55
Blade max thick y	mm	18.73	1.73	0.09	15.35	22.90	7.55
Haft Length	mm	18.39	1.06	0.06	16.92	20.81	3.88
Haft width average	mm	11.67	0.61	0.05	10.08	12.77	2.70
Haft max thick	mm	6.06	0.52	0.09	5.01	7.05	2.05
Outline perimeter	mm	155.61	10.05	0.06	140.73	181.41	40.69
Hull perimeter	mm	150.74	9.22	0.06	137.23	175.20	37.96
Area (xy)	mm ²	937.61	110.55	0.12	859.45	1274.29	462.20
Hull area	mm ²	1000.23	122.18	0.12	857.05	1371.78	514.73
Blade area	mm ²	722.55	103.02	0.14	614.32	1043.91	429.60
Haft area	mm ²	214.50	16.51	0.08	170.53	251.93	81.40
Area (xz) cross-section	mm ²	85.87	11.75	0.14	71.38	119.82	48.44
Volume	mm ³	3.41	0.57	0.17	2.63	5.15	2.52
Blade volume	cm ³	2.61	0.51	0.20	2.02	4.25	2.23
Haft volume	cm ³	0.79	0.10	0.13	0.54	1.01	0.47
Weight	gm	8.37	2.04	0.24	6.18	14.15	7.97
Density	gm/cm ³	2.44	0.32	0.13	1.89	3.32	1.43

The second resharpening episode (Table 5) had measurement values ranging from 61.48 – 78.25 mm in length, 17.24 – 23.66 mm in width, 5.39 – 7.56 mm in thickness, 5.73 – 13.30 g in weight, and 2.44 – 4.48 mm³ in volume. The CV for length, width, and thickness were <0.1 and were higher for weight and volume with CV values of 0.25 and 0.17. The mean length was 68.17 mm with a mean blade length of 49.79 mm, making up 73.04% of the total length, and a mean haft length of 18.37 mm, making up 26.96% of the total length.

Table 5: Average Dimensional Attributes for Second PPT Resharpening.

Attribute	Units	Mean	SD	CV	Min	Max	Range
Length*	mm	68.17	4.30	0.06	61.48	78.25	16.76
Width	mm	19.45	1.51	0.08	17.24	23.66	6.41
Thickness	mm	6.52	0.52	0.08	5.39	7.56	2.17
Max width	mm	19.29	1.50	0.08	16.88	23.41	6.53
Blade length	mm	49.79	3.81	0.08	44.02	58.66	14.63
Blade max width	mm	19.24	1.50	0.08	16.85	23.35	6.50
Blade width average	mm	13.64	1.17	0.09	11.29	16.12	4.83
Blade max thick	mm	6.52	0.52	0.08	5.39	7.56	2.17
Blade max thick y	mm	17.52	1.77	0.10	14.65	21.60	6.95
Haft Length*	mm	18.37	1.06	0.06	17.00	20.62	3.62
Haft width average*	mm	11.69	0.60	0.05	10.12	12.83	2.70
Haft max thick*	mm	6.00	0.48	0.08	5.02	7.01	1.98
Outline perimeter*	mm	153.22	9.09	0.06	139.04	175.27	36.22
Hull perimeter*	mm	147.92	8.80	0.06	134.54	169.48	34.94
Area (xy)*	mm ²	876.23	101.33	0.12	759.38	1158.21	398.83
Hull area*	mm ²	938.53	108.67	0.12	806.50	1243.14	436.64
Blade area	mm ²	658.07	94.39	0.14	558.06	930.42	372.36
Haft area*	mm ²	214.71	15.72	0.07	172.76	250.87	78.12
Area (xz) cross-section*	mm ²	79.82	10.72	0.13	63.53	103.58	40.05
Volume*	mm ³	3.14	0.53	0.17	2.44	4.48	2.04
Blade volume	cm ³	2.35	0.49	0.21	1.74	3.66	1.92
Haft volume*	cm ³	0.78	0.08	0.11	0.58	0.99	0.41
Weight*	gm	7.71	1.96	0.25	5.73	13.30	7.57
Density*	gm/cm ³	2.44	0.31	0.13	1.90	3.34	1.44

*Excludes fragmentary specimen ID #10081

The third resharpening episode (Table 6) had measurement values ranging from 58.88 – 77.19 mm in length, 16.67 – 23.47 mm in width, 5.44 – 7.76 mm in thickness, 5.26 – 12.84 g in weight, and 2.26 – 4.43 mm³ in volume. The CV for length, width, and thickness were <0.1 and were higher for weight and volume with CV values of 0.27 and 0.18. The mean length was 66.43 mm with a mean blade length of 48.06 mm, making up 72.35% of the total length, and a mean haft length of 18.38 mm, making up 27.65% of the total length.

Table 6: Average Dimensional Attributes for Third PPT Resharpening.

Attribute	Units	Mean	SD	CV	Min	Max	Range
Length*	mm	66.43	4.61	0.07	58.88	77.19	18.31
Width	mm	19.32	1.52	0.08	16.67	23.47	6.80
Thickness	mm	6.48	0.56	0.09	5.44	7.76	2.32
Max width	mm	19.15	1.56	0.08	16.50	23.37	6.87
Blade length	mm	48.06	4.12	0.09	40.85	57.53	16.69
Blade max width	mm	18.93	1.99	0.11	12.05	23.30	11.25
Blade width average	mm	12.53	1.13	0.09	10.62	15.00	4.37
Blade max thick	mm	6.44	0.58	0.09	5.44	7.76	2.32
Blade max thick y	mm	16.67	2.30	0.14	10.10	20.45	10.35
Haft Length*	mm	18.38	1.08	0.06	16.93	20.71	3.78
Haft width average*	mm	11.73	0.62	0.05	10.11	12.90	2.79
Haft max thick*	mm	5.99	0.49	0.08	4.98	7.17	2.18
Outline perimeter*	mm	148.93	9.76	0.07	135.06	172.66	37.60
Hull perimeter*	mm	144.39	9.41	0.07	129.76	167.17	37.41
Area (xy)*	mm ²	822.35	98.85	0.12	701.42	1084.25	382.83
Hull area*	mm ²	884.87	106.40	0.12	758.19	1167.20	409.01
Blade area	mm ²	603.71	91.66	0.15	491.35	859.29	367.94
Haft area*	mm ²	215.60	16.75	0.08	171.18	251.94	80.76
Area (xz) cross-section*	mm ²	78.64	11.35	0.14	61.53	104.79	43.26
Volume*	mm ³	2.94	0.53	0.18	2.26	4.23	1.96
Blade volume	cm ³	2.12	0.55	0.26	0.74	3.42	2.68
Haft volume*	cm ³	0.77	0.09	0.12	0.58	0.99	0.41
Weight*	g	7.26	1.96	0.27	5.26	12.84	7.58
Density*	g/cm ³	2.45	0.30	0.12	1.89	3.25	1.36

* Excludes fragmentary specimen ID #10111

In comparison, each of the attributes, especially the maximum length, width, and weight experienced an overall decrease between each consecutive resharpening episode (Figure 11). Length experienced the greatest amount of loss (Figure 12), decreasing in mean value by 2.17% in the first resharpening, 1.80% in the second resharpening, and 2.55% in the last resharpening. Width experienced an inconsistent amount of loss (Figure 13), decreasing in mean value by 4.96% in the first resharpening, 5.08% in the second resharpening, and 0.77% in the third resharpening. This is likely due to the width normalizing at the ear, as evident in the lower placement of the maximum width relative to the base as the width shifts from the blade midsection to the shoulder over the courses of resharpening (Figure 14). Thickness experienced the least amount of loss (Figure 15), decreasing in mean value by 1.88% in the first resharpening, 1.66% in the second resharpening, and 0.61% in the third resharpening. As a result of these measurement decreases due to material loss along the blade, only the blade element experienced volume loss of 28.62% (Figure 16) while the haft element remained relatively the same, having a loss of 3.75%.

With the haft element remaining fairly consistent over the courses of resharpening, it makes it a valuable constant from which to measure. Figure 17 illustrates the ratios between the haft measures and blade measures for each resharpening event. The scatterplots have a noticeable trend, decreasing in value as the projectile point experiences resharpening. The haft area versus the blade area is the most distinctive in terms of the trend, as the individual resharpening groups can easily be clustered on the graph. The haft length versus blade length is the least distinctive in terms of identifying a trend between the resharpening events. Plotting the haft area versus the blade area is the most useful comparative tool to plot the patterns of the change in lengths between each resharpening episode.

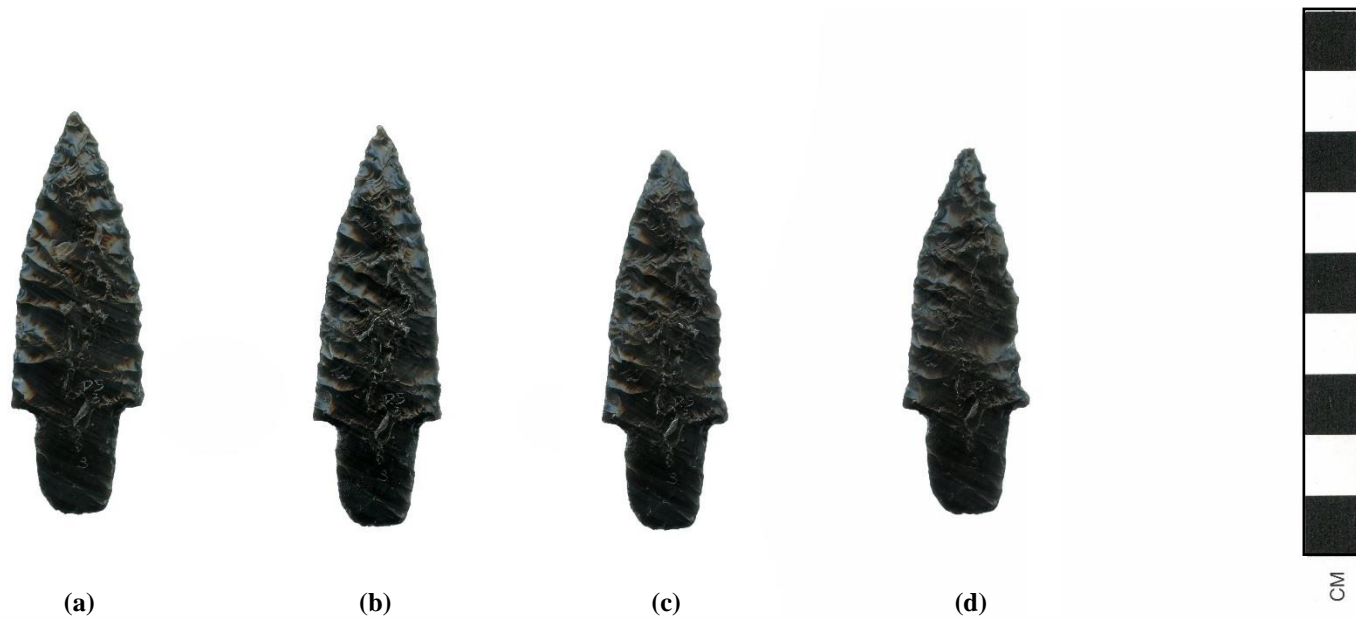


Figure 11: Two-dimensional images of DS03, (a) Original, (b) First Resharpening, (c) Second Resharpening, and (d) Third Resharpening.

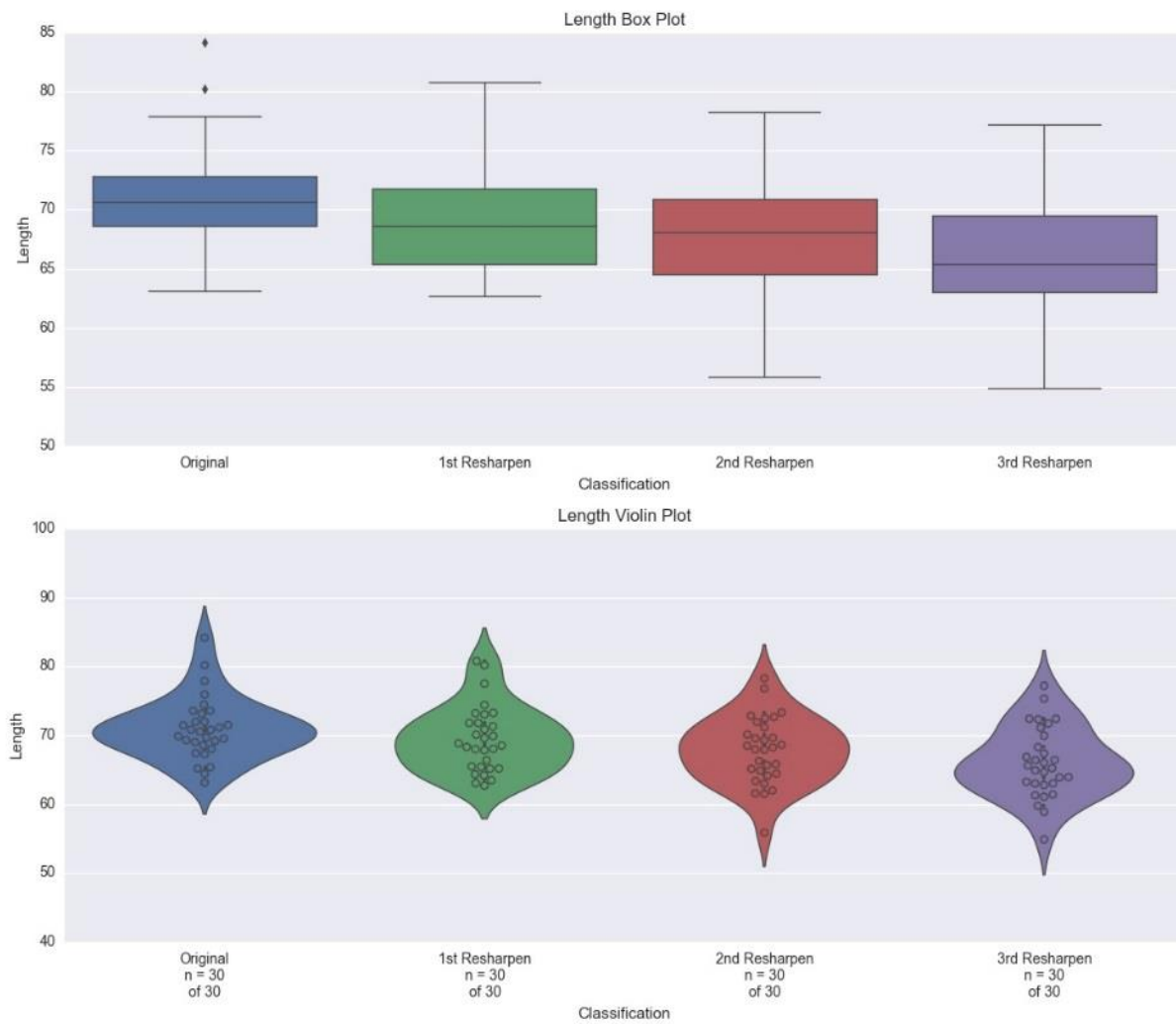


Figure 12: Length (mm) of projectile points after each resharpening event.

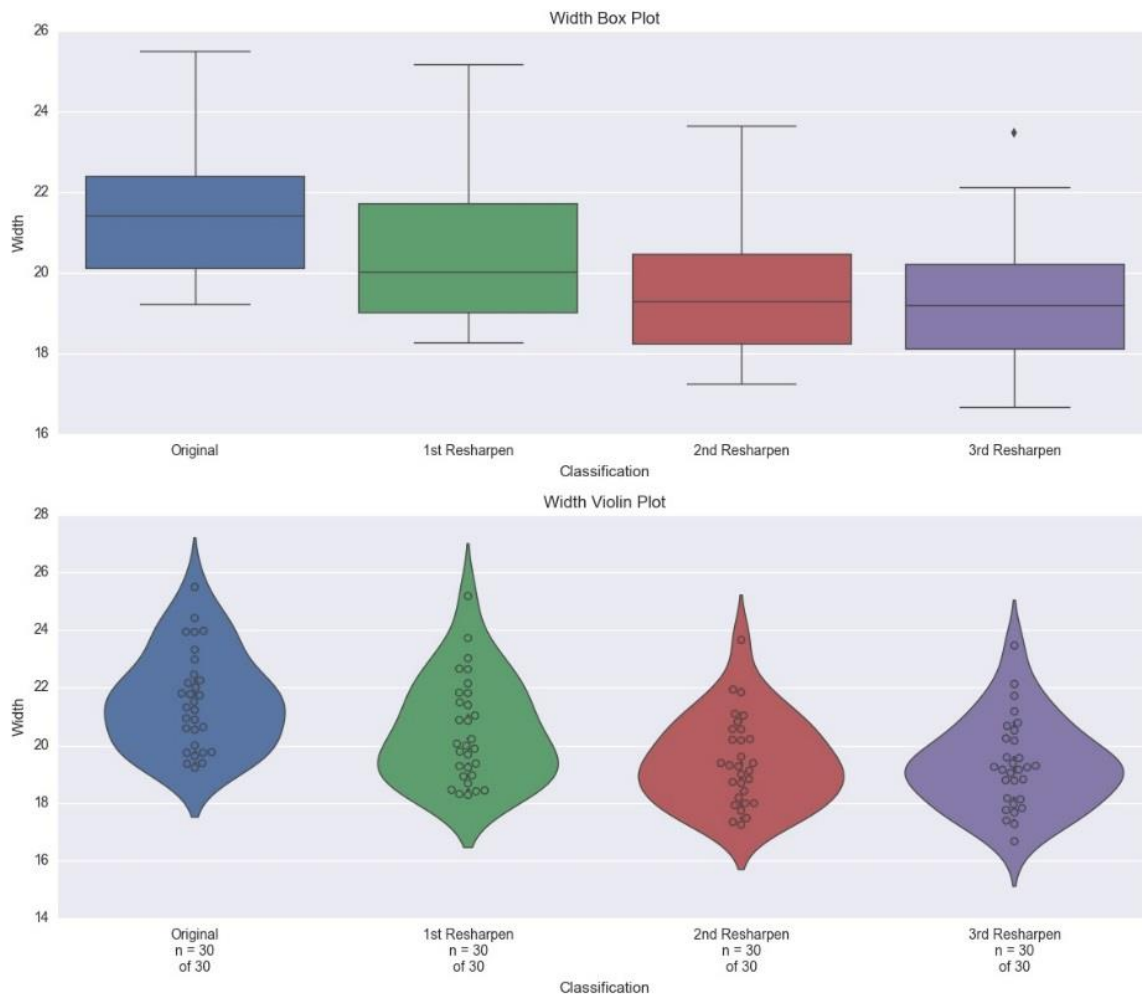


Figure 13: Width (mm) of projectile points after each resharpening event.

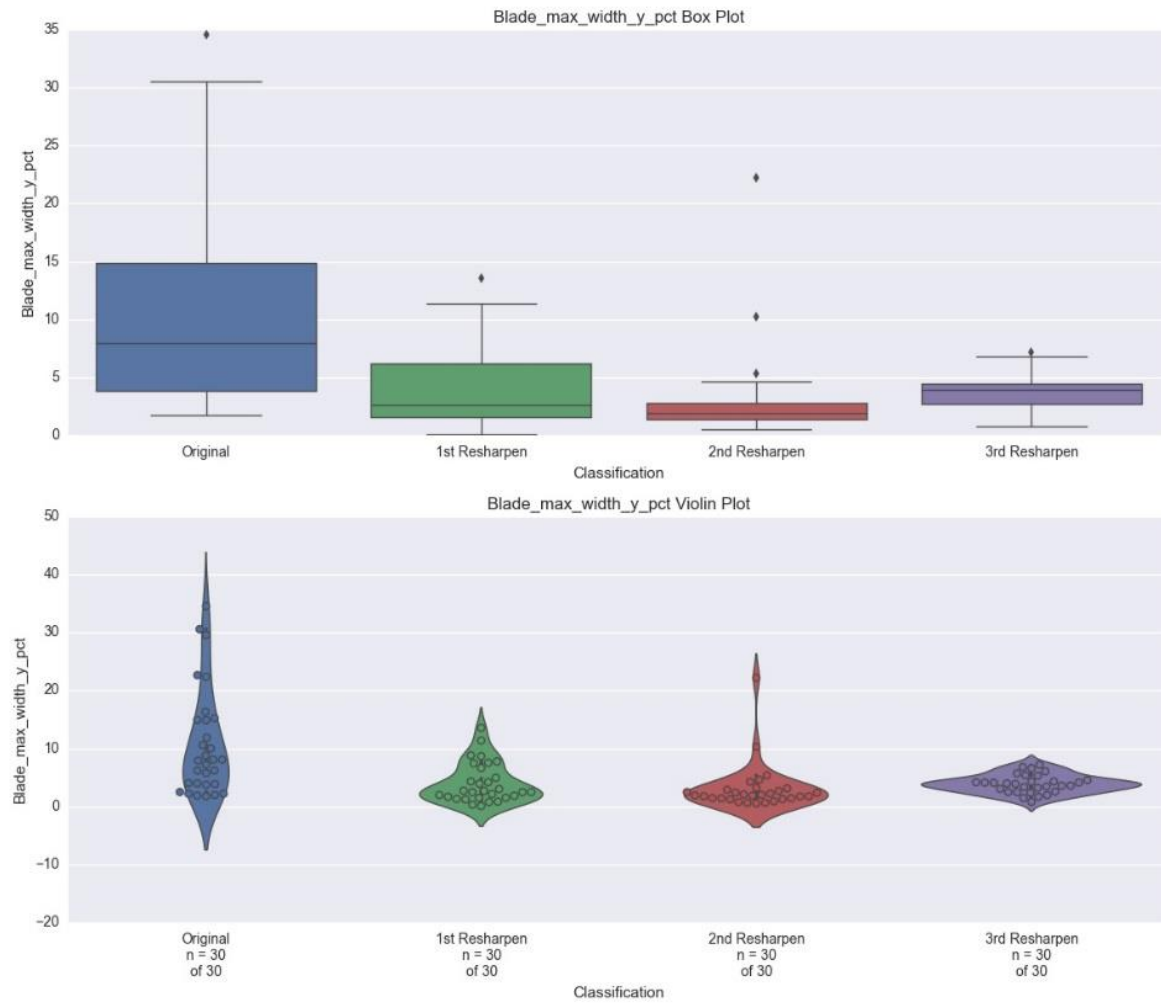


Figure 14: Max width location as a percentage of total projectile point length after each resharpening event.

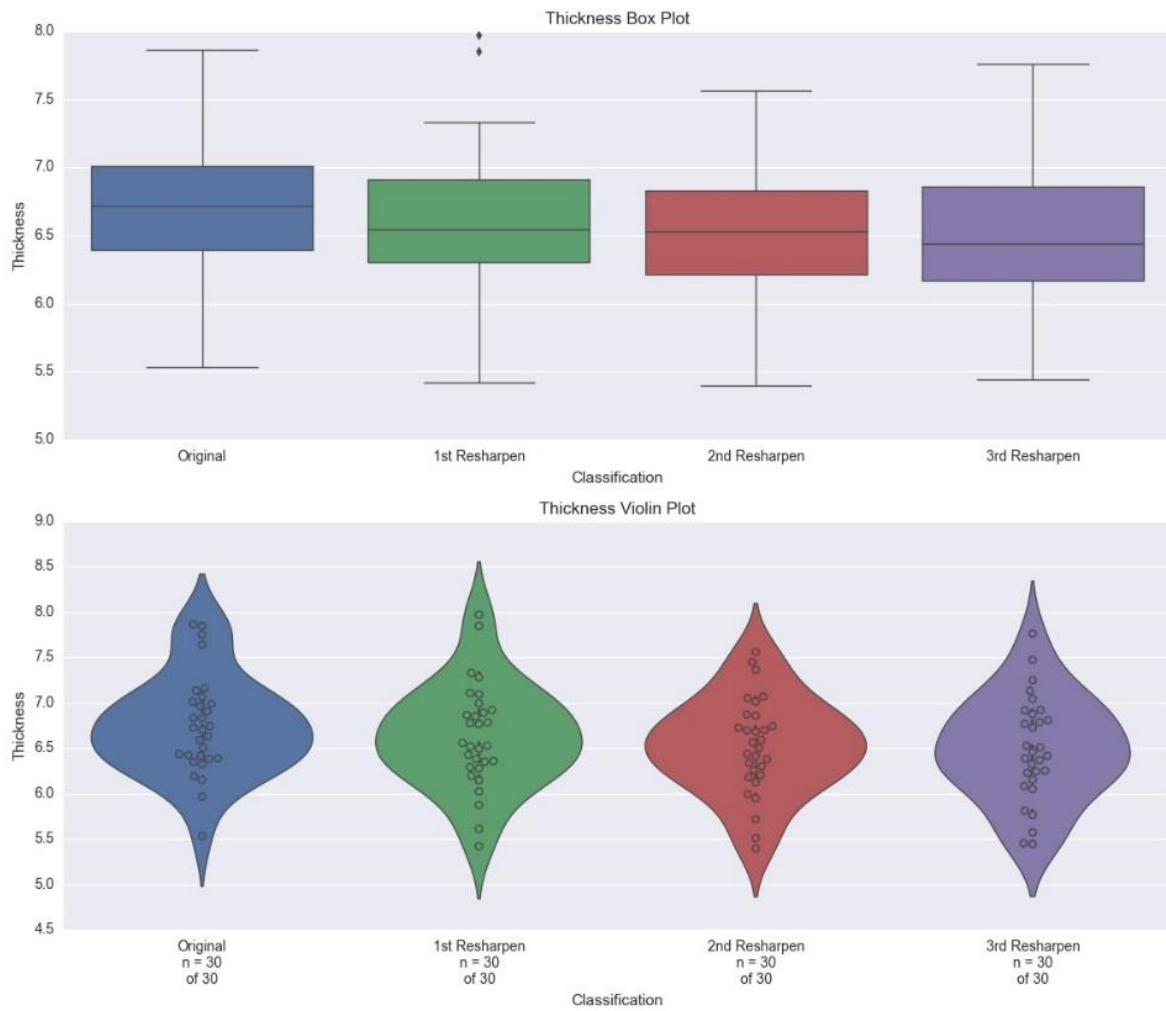


Figure 15: Thickness (mm) of projectile points after each resharpening event.

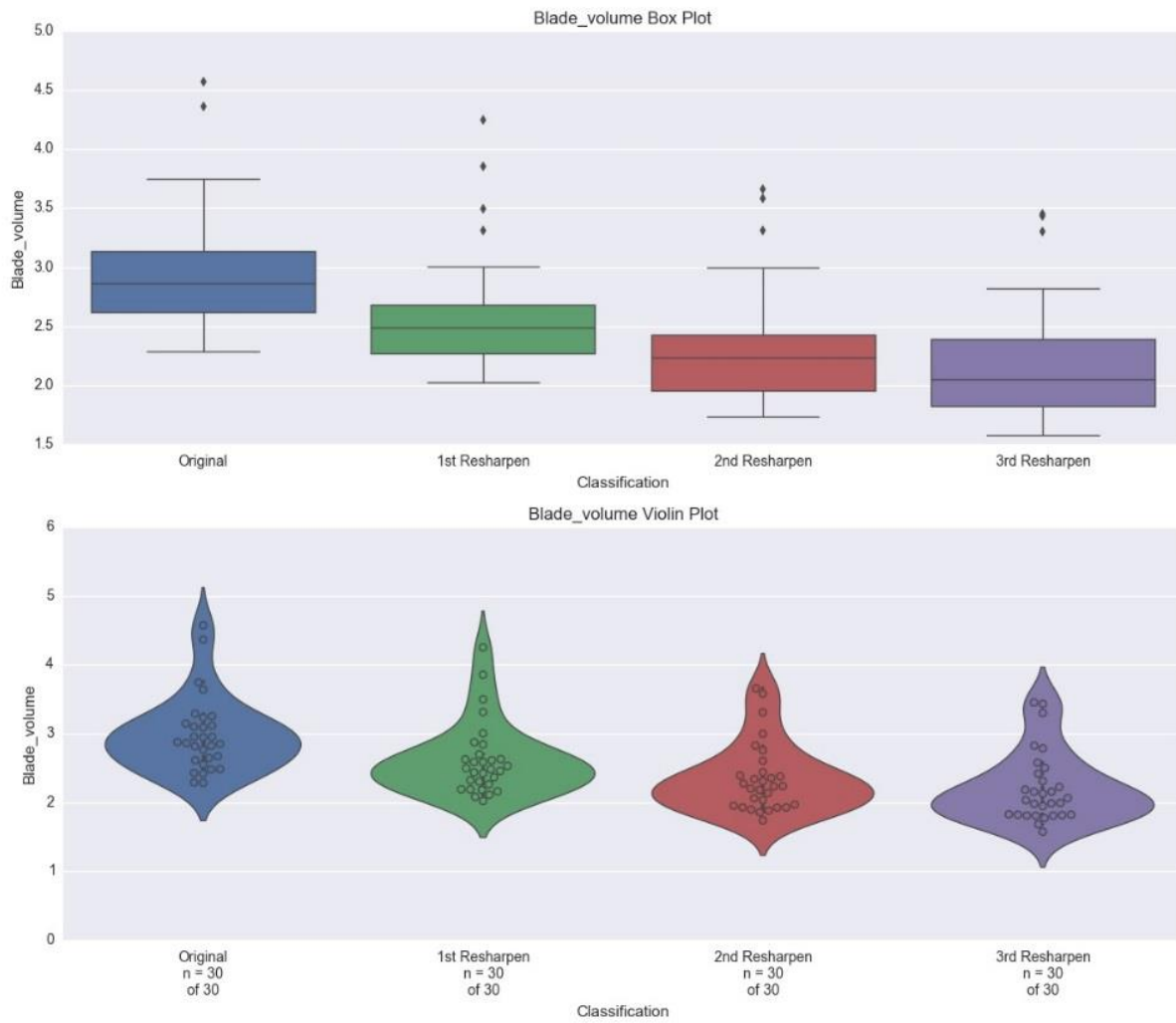


Figure 16: Blade Volume (mm^3) of projectile points for each resharpening event.

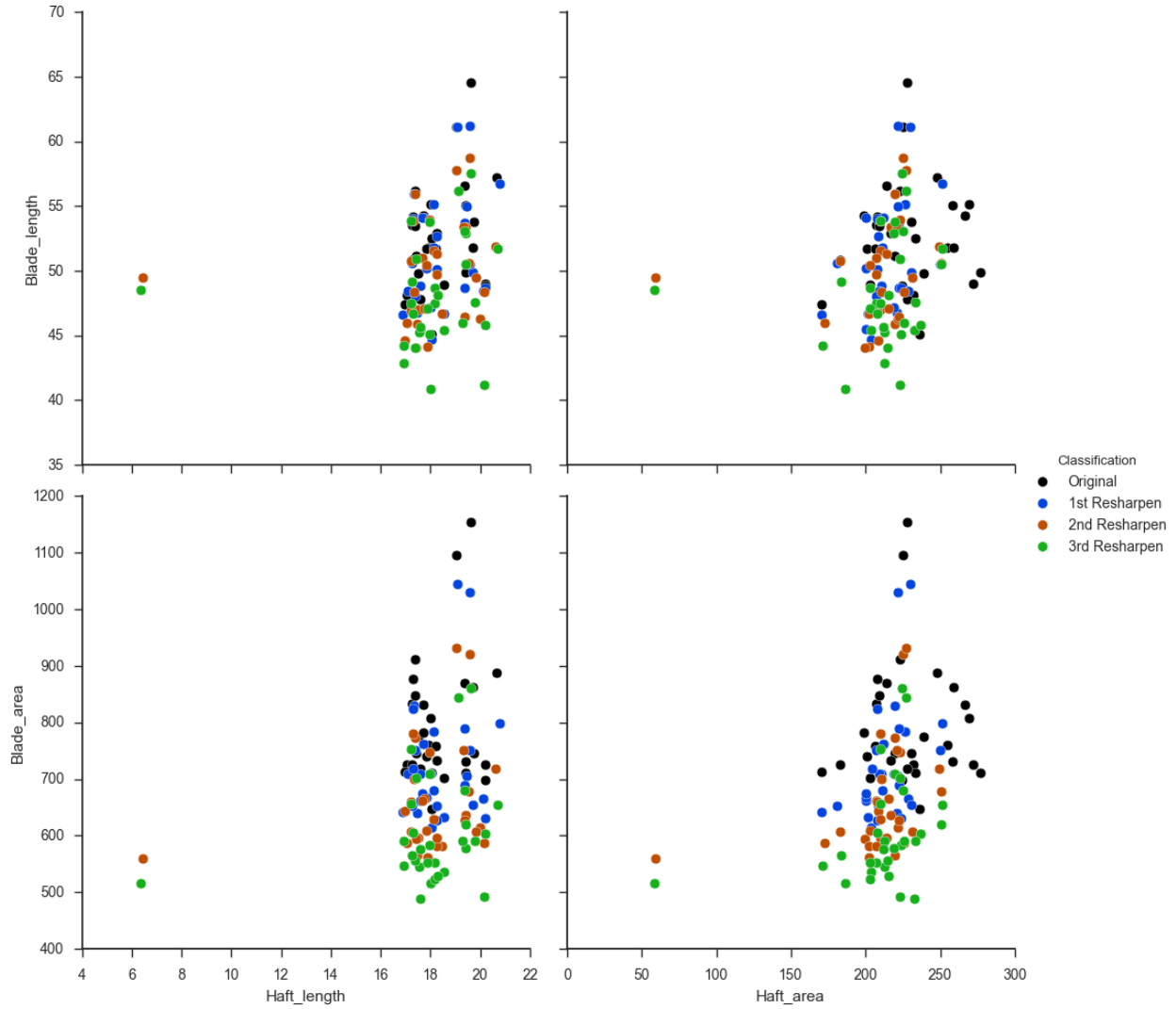


Figure 17: Comparison of haft length and area, against blade length and area, for each resharpening event.

4.2 Slope Variation

A slope image output was created for each of the projectile point resharpening events and is accessible as a geodatabase online in the Oregon State University ScholarsArchive. The following section reviews the mean slope change of only one of the projectile points, chosen based on a more uniform slope change that did not demonstrate preferential resharpening on one side of the blade. In Figure 18, Face 1 of the original projectile point had a mean slope of 32.75 degrees increasing to 33.32 degrees in the first resharpening, 34.07 degrees in the second resharpening, and 34.94 degrees in the third resharpening. Similarly, Face 2 of the original projectile point had a mean slope of 19.65 degrees increasing to 20.44 degrees in the first resharpening, decreasing to 20.12 degrees in the second resharpening, and increasing to 22.57 degrees in the third resharpening. Overall, as the projectile points undergo consecutive resharpenings, the mean slope of the entire point increases as a result of flake removal along the edge of the blade, and a reduction in thickness near the center of mass. Figure 19 illustrates the reduction in thickness as the projectile point becomes more convex and less planar along the midsection. This phenomenon will be better illustrated in the cross-sectional view results in subsection 4.3.

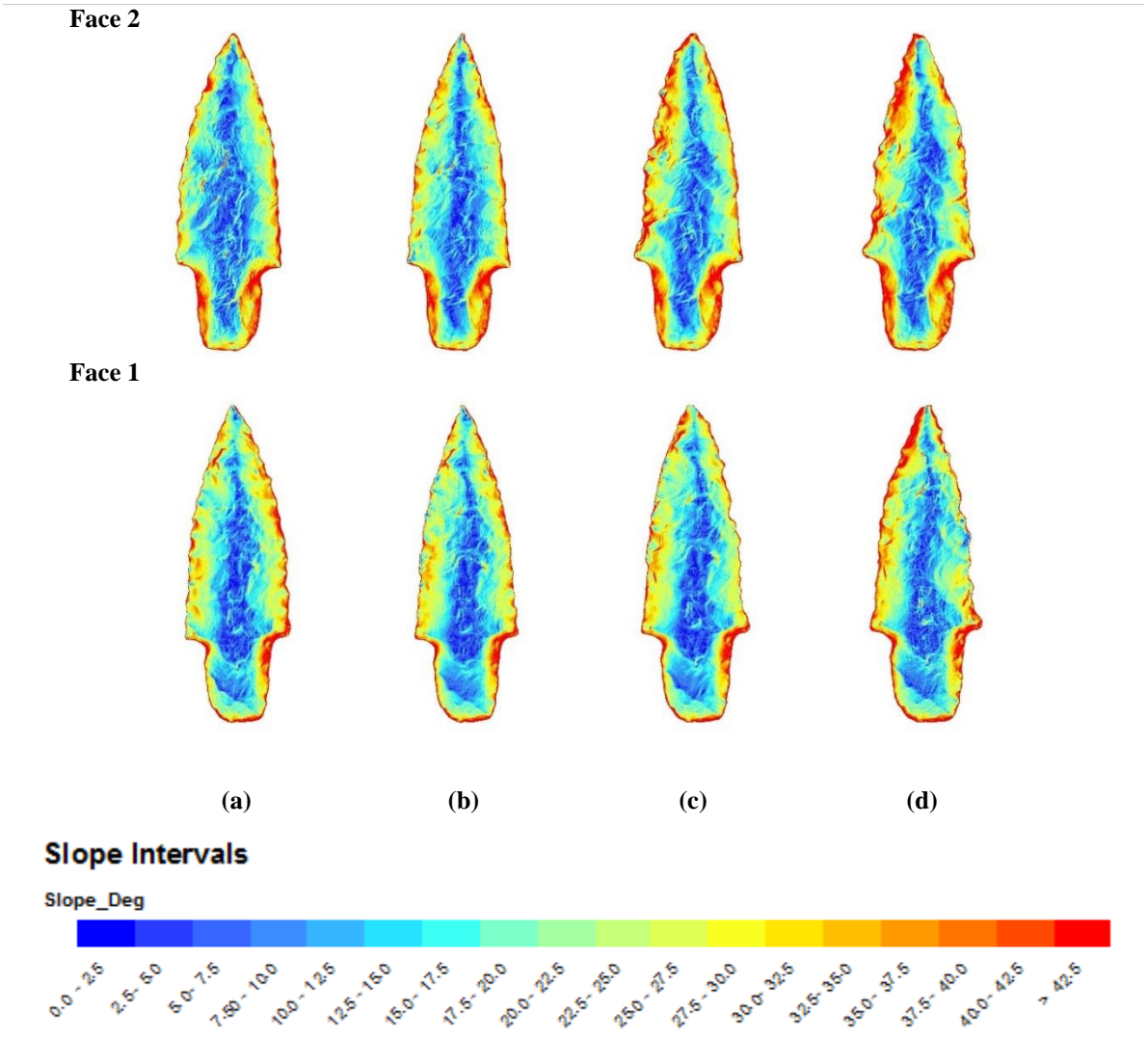


Figure 18: Surface TIN colored by slope (a) Original, (b) First Resharpener, (c) Second Resharpener, (d) Third Resharpener.

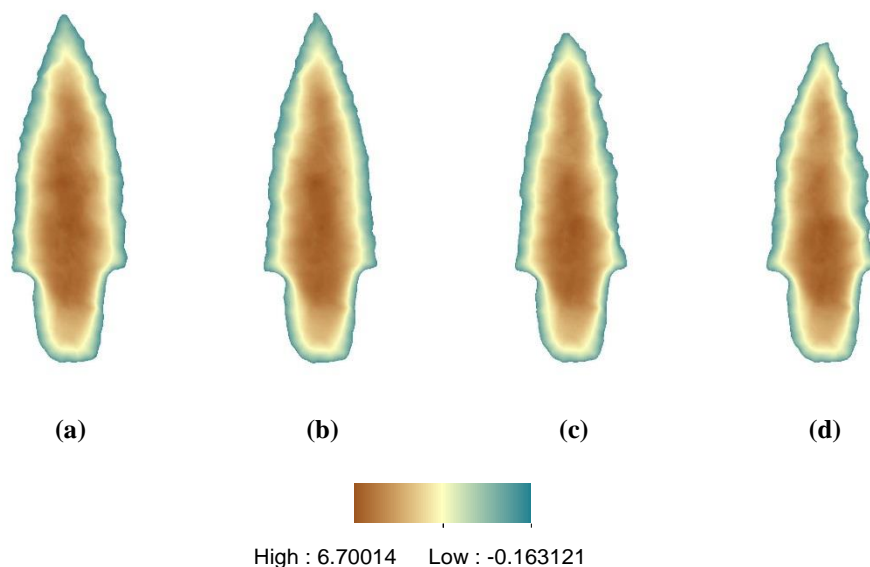


Figure 19: ArcGIS thickness output (0-6.7 mm). (a) Original, (b) First Resharpening, (c) Second Resharpening, (d) Third Resharpening.

The mean slope values for each resharpening episode, although not an accurate representation of edge steepness, is a useful concept for illustrating the overall change in ratio between steep and planar portions of the blade, regardless of the resharpening method. This will become important when comparing blades that experience differing resharpening methods and the amount of resharpening. Figure 20 and Figure 21 are two examples of points that had preferential resharpening in one direction and on one edge of the blade. In this case, the slope of the left or right blade are steeper than the opposing side, making it difficult to compare between dissimilar resharpened projectile points. Identifying these dissimilarities provide a basis to begin further investigation into morphologic change and variation caused by continuous use and retouch of the blade.

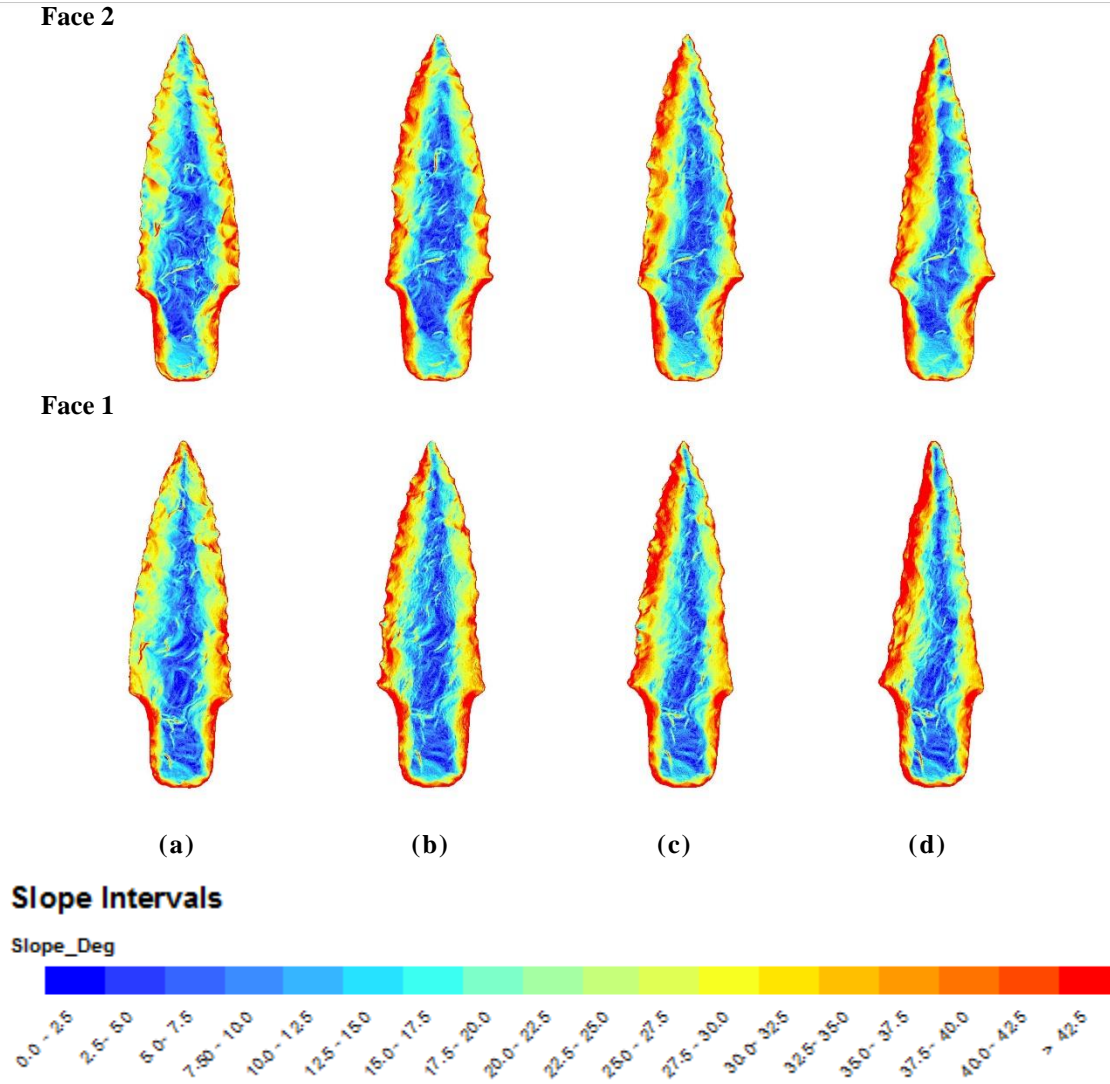


Figure 20: Surface TIN colored by slope illustrating resharpening preference on the left. (a) Original, (b) First Resharpening, (c) Second Resharpening, (d) Third Resharpening.

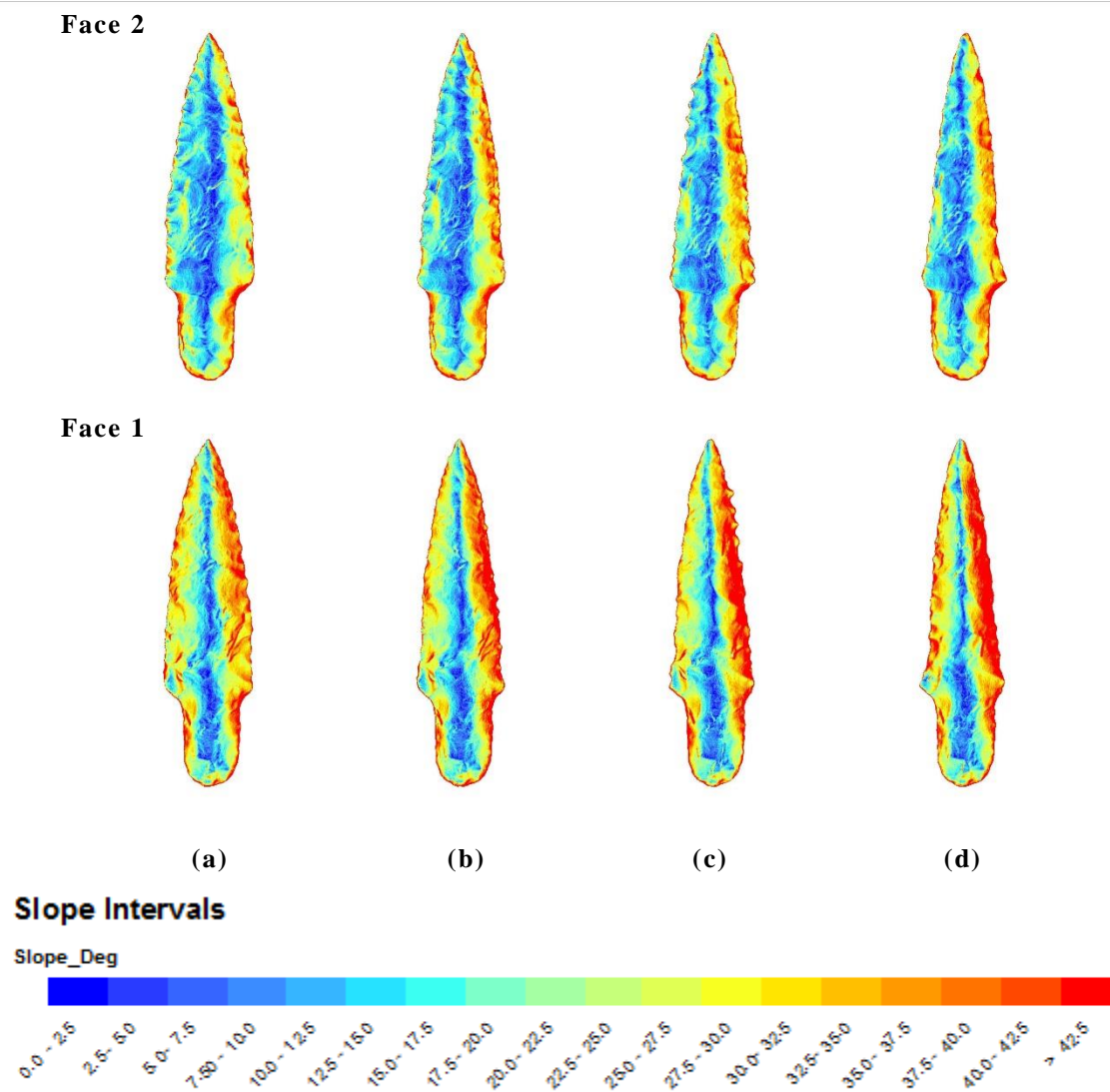


Figure 21: Surface TIN colored by slope illustrating resharpening preference on the right. (a) Original, (b) First Resharpening, (c) Second Resharpening, (d) Third Resharpening.

4.3 Cross-Section Comparison

The following section provides snapshots of the GLiMR cross-sectional analysis tool as a method of comparison for each of the resharpening episodes. When comparing the cross-sectional view of the midsection between each of the thirty projectile points (Figure B.3), it is evident that each have been resharpened in a distinctively different manner. The cross-sections either show flake removal along the same face, or along two alternate edges (Figure 22). With projectile points exhibiting resharpening of alternate edges, the blade takes on a spiral form and is no longer parallel to the x-axis, as seen with the original. With projectile points exhibiting resharpening primarily along one face of the blade, the blade remains parallel to the x-axis and typically deviates in convexity from the original form, becoming either more biconvex or planoconvex.

In this study, there are three types of flake removal directions that are evident when looking at the projectile points in cross-section. Figure 23(a) is an example of one of the projectile points that experienced flake removal primarily on the left side of the blade. In contrast Figure 23(b), is an example which experienced flake removal primarily along the right side of the blade. Both are examples of retouch occurring on both opposing faces and opposing edges. Figure 23(c) on the other hand experienced flake removal along opposing edges however only along one face. When using GLiMR to view the cross-sections of the resharpening episodes, the resharpening method can be inferred without ever knowing the resharpening method. In each of the figures, the red outline indicates the first resharpening episode, the blue line indicates the second resharpening episode, and the purple line indicates the third resharpening episode. Figure 23(a) shows flake removal along the left face for alternate sides for the first, second, and third resharpenings, however during the last resharpening, the left edge experiences a small amount of volume loss on the

opposite face. Since this is resharpening, whereas alternate edges were resharpened during the first two resharpening episodes. These analyses can continue for each of the resharpening events by only interpreting the cross-sectional views. By comparing the orientation of other projectile points to the experimental ones, inferences can be made on how the projectile point may have been resharpened.

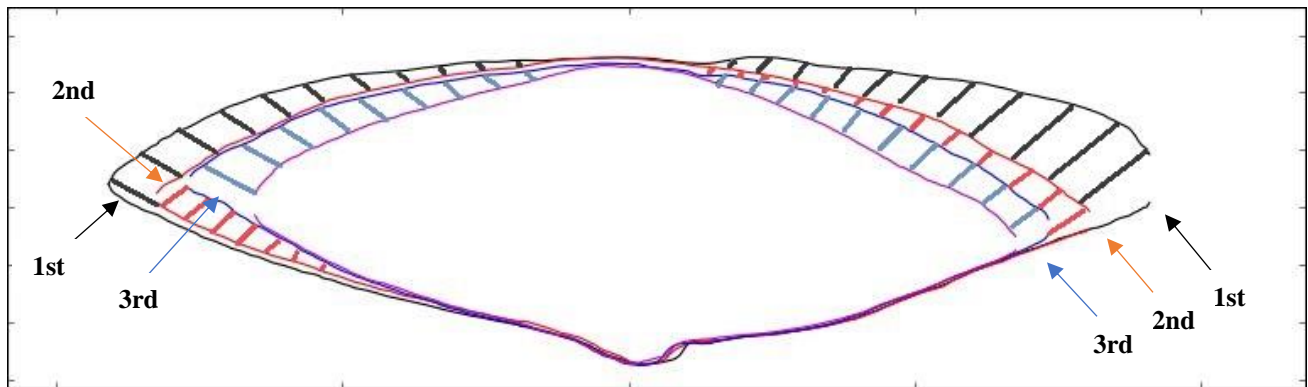


Figure 22: Resharpening sequence directions. Black represents the first resharpening, red the second resharpening, and blue the third resharpening. Arrows indicate the direction of the pressure flaker, and the lines indicate the material removed.

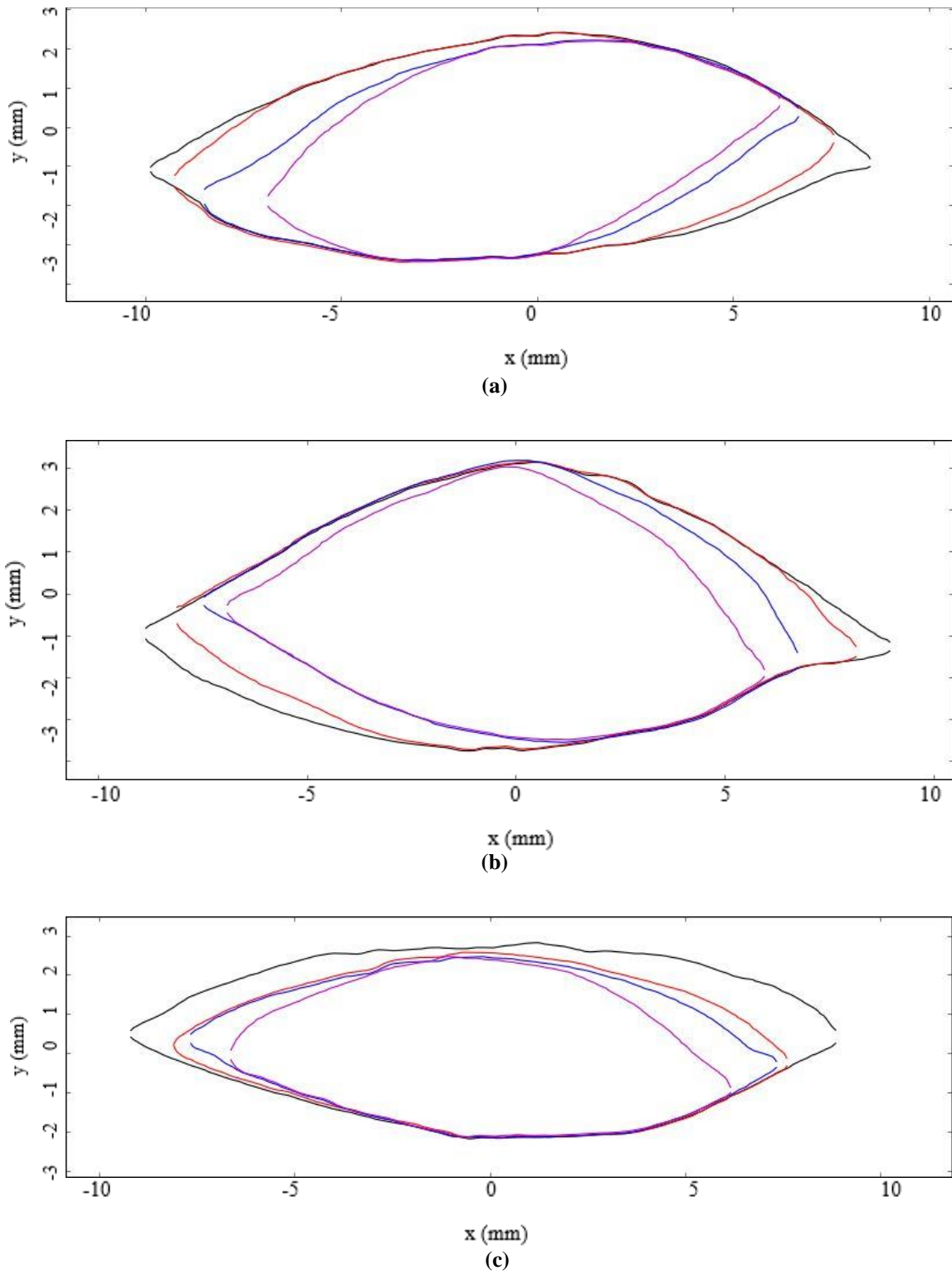


Figure 23: Midsection cross-sectional view of reshaping events. (a) DS01, (b) DS09, and (c) DS28.

4.4 Blade Curvature

The following section will review the results of the regression analysis for one of the projectile points, and the results for each DS group can be found in Table 7 and Table 8. Figure 24 displays the curve summaries of the original and first resharpening events for the right blade of projectile point DS03. The linear fit line of the original projectile point has a slope “m” value of 0.2253, and a residual variance of 1.00 mm. The linear fit line of the second resharpening has a slope “m” value of 0.2227, and a residual variance of 0.88 mm. The polyfit equation applies a fitted curve to the blade edge and minimizes the residual variance to 0.20 mm for the original projectile point, and 0.18 mm to the first resharpening event. The polyfit line of the original projectile point has a curve “a” of 0.0067, and for the first resharpening a curve of 0.0057, representing a decrease in convexity.

Figure 25 displays the curve summaries of the second and third resharpening events for the right blade of projectile point DS03. The linear fit line of the second resharpening has a slope “m” value of 0.2093, and a residual variance of 0.74 mm. The linear fit line of the third resharpening has a slope “m” value of 0.2049, and a residual variance of 0.57 mm. The polyfit line again decreases the residual variance to 0.40 mm for the second resharpening event, and 0.31 mm to the third resharpening event. The polyfit line of the second resharpening has a curve “a” value of 0.0052, and for the third resharpening a curve of 0.0041, again a decrease in convexity of the blade.

Overall, DS3 experiences a linear slope decrease between the three resharpening episodes by 0.0204, and a residual variance decrease of 0.43 mm. The polyfit line on the other hand has a smaller decrease between the three episodes of resharpening by 0.0026 and does not have a constant decrease in residuals, deviating between 0.40 mm and 0.18 mm regardless of resharpening

episode. Although the curvature does not provide an identifiable trend between each of the resharpening groups (Figure 26-27), the lower residual variance reflects the accuracy of the polyfit line to the curve of the blade edge. The application of this data provides information about the uniformity of the blade between the episodes of resharpening, however, it is difficult to compare across multiple projectile points. The linear and poly fit lines are dependent on the maximum width of the blade and the blade length, making it difficult to compare minor slope and curve variations between dissimilar blade lengths and widths. The poly fit line better addresses the change in blade curvature for one projectile point by applying a stricter line along the blade edge with little residual variance, however the curve “a” produces too small of a number to compare among populations. The curve however will be important when discussing the new measurement parameter for blade resharpening in subsection 4.5.

Table 7: Blade curvature coefficient of the right blade of DS01-DS30

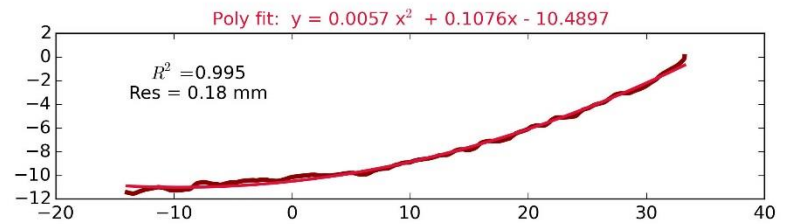
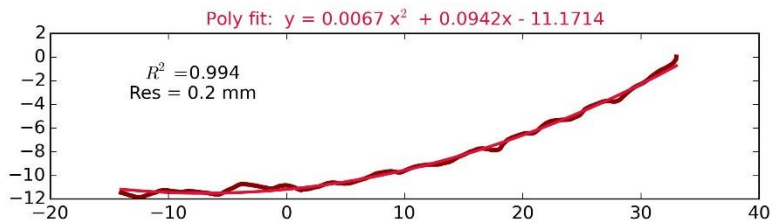
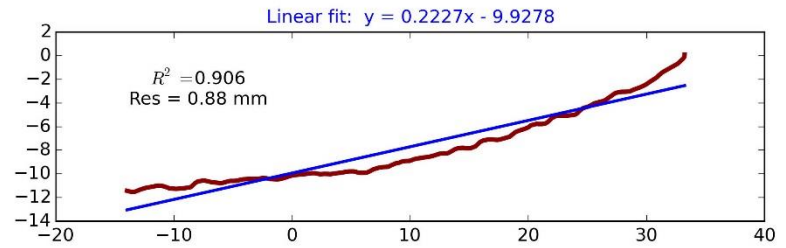
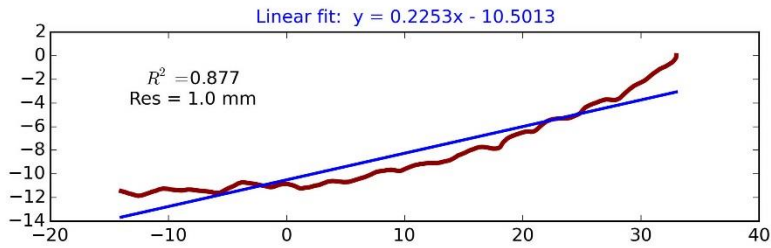
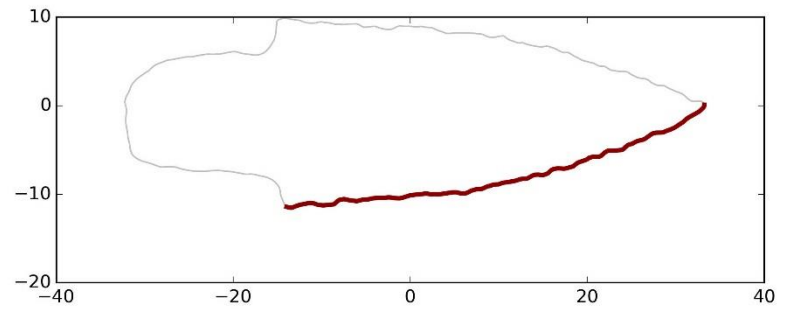
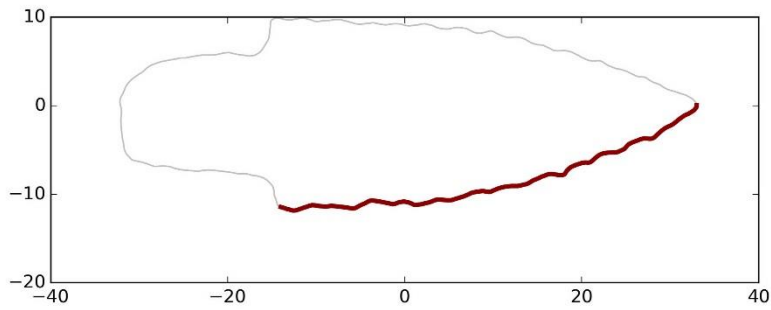
Local ID	0	1	2	3
DS01	0.0047	0.0051	0.0044	0.0016
DS02	0.0068	0.0067	0.0057	0.0041
DS03	0.0068	0.0057	0.0052	0.0041
DS04	0.0048	0.0061	0.0054	0.0044
DS05	0.0080	0.0064	0.0052	0.0045
DS06	0.0052	0.0039	0.0038	0.0041
DS07	0.0070	0.0060	0.0049	0.0043
DS08	0.0044	0.0035	0.0032	0.0027
DS09	0.0039	0.0029	0.0024	0.0017
DS10	0.0041	0.0040	0.0040	0.0040
DS11	0.0054	0.0050	0.0050	0.0051
DS12	0.0055	0.0049	0.0050	0.0036
DS13	0.0056	0.0045	0.0035	0.0023
DS14	0.0060	0.0049	0.0042	0.0038
DS15	0.0036	0.0032	0.0038	0.0033
DS16	0.0033	0.0033	0.0034	0.0034
DS17	0.0056	0.0041	0.0037	0.0032
DS18	0.0039	0.0033	0.0037	0.0027
DS19	0.0074	0.0061	0.0052	0.0045
DS20	0.0054	0.0045	0.0039	0.0032
DS21	0.0033	0.0027	0.0019	0.0016
DS22	0.0032	0.0032	0.0027	0.0033
DS23	0.0033	0.0039	0.0034	0.0027
DS24	0.0040	0.0029	0.0033	0.0031
DS25	0.0065	0.0056	0.0039	0.0059
DS26	0.0042	0.0030	0.0025	0.0015
DS27	0.0038	0.0034	0.0028	0.0025
DS28	0.0035	0.0022	0.0016	0.0001
DS29	0.0047	0.0062	0.0057	0.0045
DS30	0.0060	0.0077	0.0075	0.0071
Mean	0.0050	0.0045	0.0040	0.0034

Note: Resharpening episodes are delineated as “0”, “1”, “2”, and “3”. A linear blade receives a value of 0.00.

Table 8: Blade curvature coefficient of the left blade of DS01-DS30

Local ID	0	1	2	3
DS01	-0.0046	-0.0051	-0.0031	-0.0007
DS02	-0.0067	-0.0044	-0.0029	-0.0025
DS03	-0.0055	-0.0051	-0.0055	-0.0068
DS04	-0.0042	-0.0050	-0.0049	-0.0042
DS05	-0.0064	-0.0052	-0.0039	-0.0024
DS06	-0.0051	-0.0045	-0.0043	-0.0038
DS07	-0.0075	-0.0080	-0.0063	-0.0055
DS08	-0.0034	-0.0028	-0.0027	-0.0024
DS09	-0.0039	-0.0032	-0.0026	-0.0019
DS10	-0.0029	-0.0023	-0.0022	-0.0020
DS11	-0.0061	-0.0046	-0.0048	-0.0040
DS12	-0.0062	-0.0063	-0.0054	-0.0046
DS13	-0.0046	-0.0040	-0.0028	-0.0019
DS14	-0.0046	-0.0038	-0.0026	-0.0022
DS15	-0.0040	-0.0040	-0.0036	-0.0031
DS16	-0.0042	-0.0046	-0.0035	-0.0032
DS17	-0.0048	-0.0044	-0.0034	-0.0030
DS18	-0.0036	-0.0032	-0.0026	-0.0024
DS19	-0.0076	-0.0063	-0.0054	-0.0048
DS20	-0.0054	-0.0024	-0.0022	-0.0010
DS21	-0.0040	-0.0028	-0.0021	-0.0023
DS22	-0.0042	-0.0036	-0.0042	-0.0033
DS23	-0.0035	-0.0038	-0.0033	-0.0024
DS24	-0.0024	-0.0019	-0.0027	-0.0010
DS25	-0.0048	-0.0038	-0.0036	-0.0041
DS26	-0.0043	-0.0028	-0.0031	-0.0022
DS27	-0.0047	-0.0043	-0.0037	-0.0032
DS28	-0.0040	-0.0030	-0.0026	-0.0015
DS29	-0.0045	-0.0062	-0.0052	-0.0044
DS30	-0.0058	-0.0070	-0.0062	-0.0061
Mean	-0.0048	-0.0043	-0.0037	-0.0031

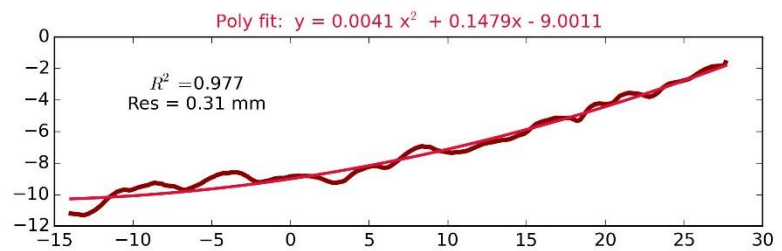
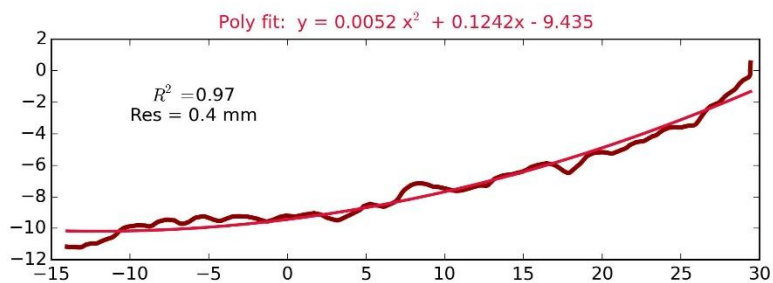
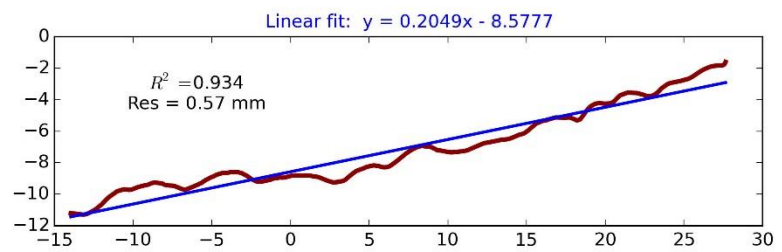
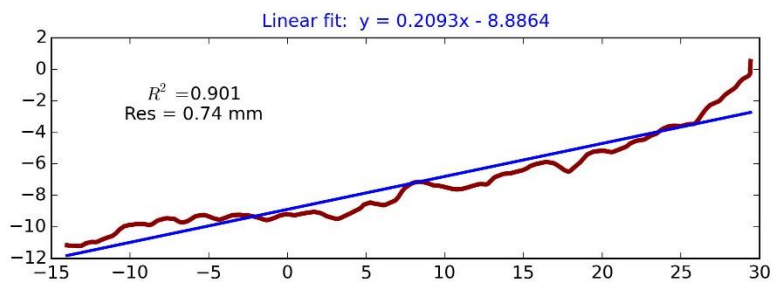
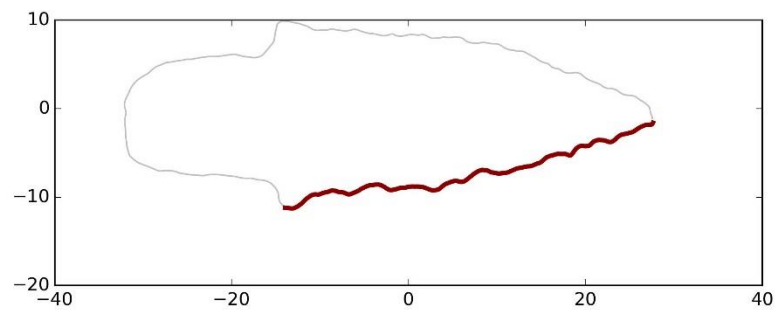
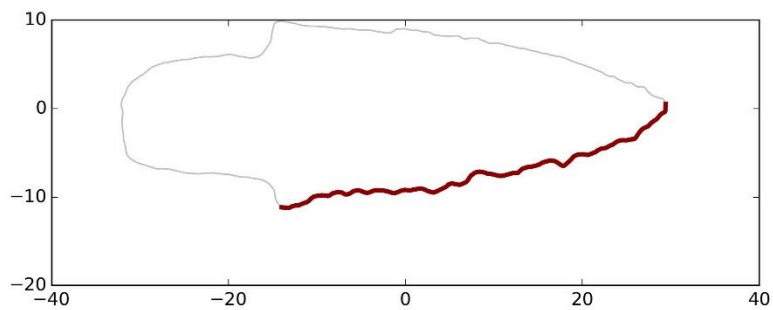
Note: Resharpener episodes are delineated as “0”, “1”, “2”, and “3”. A linear blade receives a value of 0.00.



(a)

(b)

Figure 24: Blade Curve summary for the right blade of DS03, (a) Original, and (b) First Resharpening.



(a)

(b)

Figure 25: Blade Curve summary for the right blade of DS03, (a) Second Resharpening, and (b) Third Resharpening.

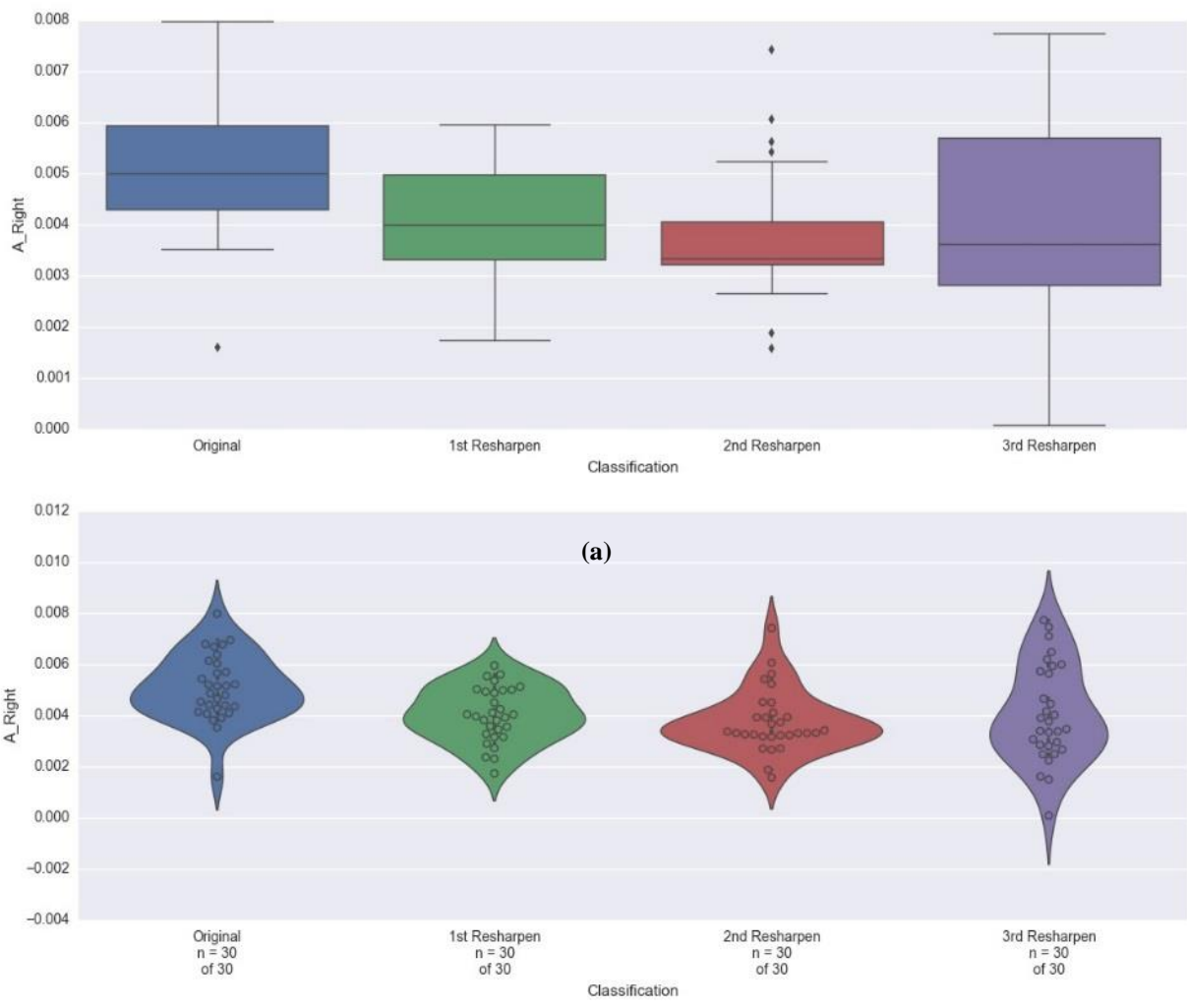


Figure 26: Curve summary of the right edge for each resharpening episode. As values approach “0” the curvature of the blade becomes linear.

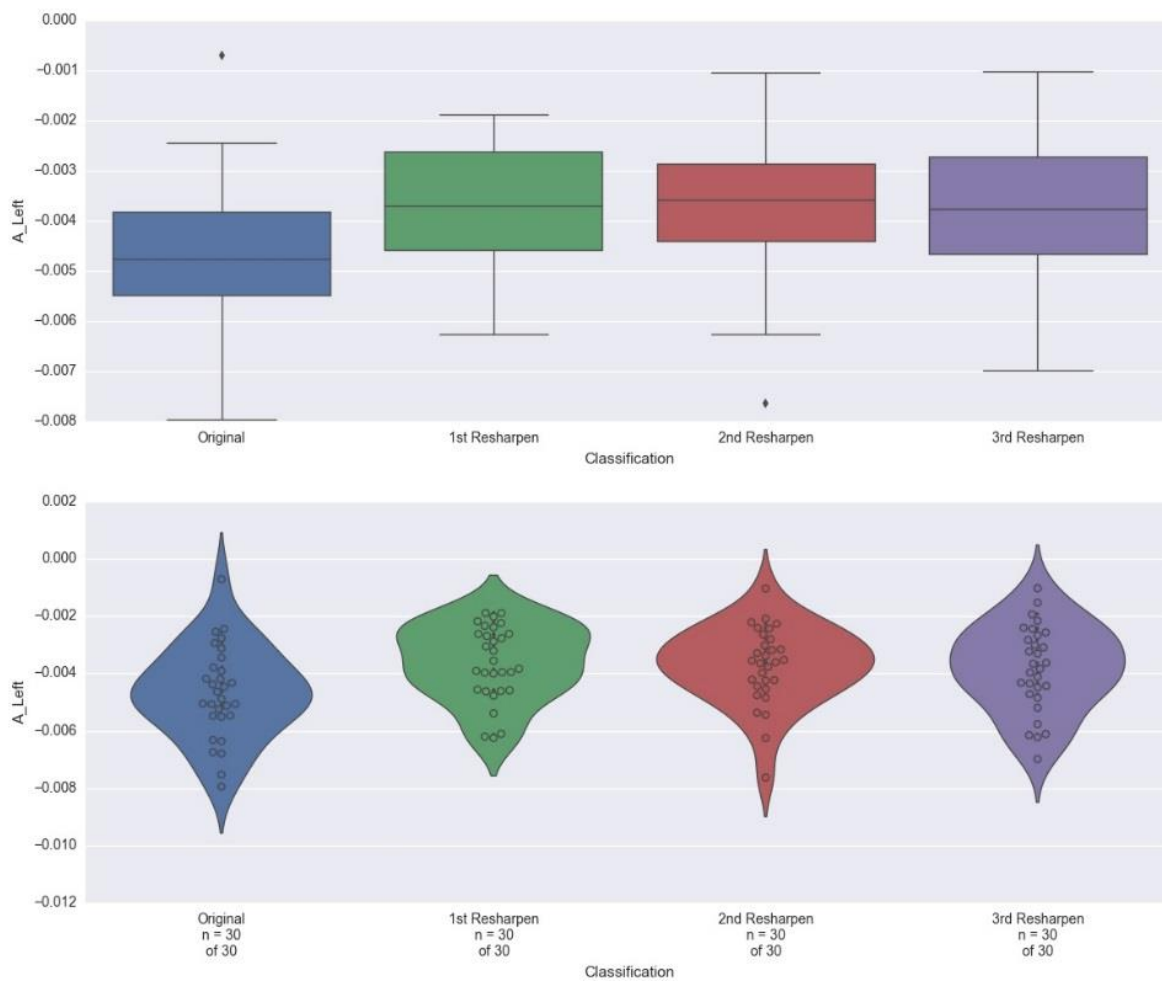


Figure 27: Curve summary of the left edge for each resharpening episode. As values approach “0” the curvature of the blade becomes linear.

4.5 Inset Width

The original replicated thirty projectile points (Table 9), had a mean inset width measurement of 0.27 mm and an inset width percentage of 1.24% of the maximum width. The range was 0.87 mm and the CV value was 0.94. The high CV value was likely due to the presence of inset widths measuring 0.00 mm which is an indication of there being no ears before the first resharpening event. This high CV also translated to the width percentage, with a CV value of 0.95. The first resharpening episode (Table 10) had a mean inset width measurement of 0.45 mm and an inset width percentage of 2.24% of the maximum width. The range was 1.24 mm and the CV value was 0.65. The second resharpening episode (Table 11) had a mean inset width measurement of 0.55 mm and an inset width percentage of 2.88% of the maximum width. The range was 1.07 mm and the CV value was 0.58. The third resharpening episode (Table 12) had a mean inset width measurement of 0.87 mm and an in-set width percentage of 4.55% of the maximum width. The range was 1.60 mm and the CV value was 0.36. Overall, there was an increase in inset width measurement of 0.60 mm and an increase in in-set width percentage of 3.31%, averaging a rough 0.60 – 1.00% increase between each resharpening event. The CV value greatly decreases between each episode of resharpening, likely due to the normalizing of numbers as the ear width becomes prominent.

Table 9: Original Attributes for In-set Width

Attribute	Units	Mean	SD	CV	Min	Max	Range
In-set Width	mm	0.27	0.25	0.94	0.00	0.87	0.87
In-set of Max Width	(%)	1.24	1.18	0.95	0.00	4.03	4.03

Table 10: First Resharpener Attributes for In-set Width

Attribute	Units	Mean	SD	CV	Min	Max	Range
In-set Width	mm	0.45	0.29	0.65	0.00	1.24	1.24
In-set of Max Width	(%)	2.24	1.42	0.63	0.00	5.90	5.90

Table 11: Second Resharpener Attributes for In-set Width

Attribute	Units	Mean	SD	CV	Min	Max	Range
In-set Width	mm	0.55	0.32	0.58	0.00	1.07	1.07
In-set of Max Width	(%)	2.88	1.66	0.58	0.00	5.93	5.93

Table 12: Third Resharpener Attributes for In-set Width

Attribute	Units	Mean	SD	CV	Min	Max	Range
In-set Width	mm	0.87	0.31	0.36	0.00	1.60	1.60
In-set of Max Width	(%)	4.55	1.66	0.37	0.00	8.14	8.14

Chapter 5: PFP1 Results

5.1 Cooper's Ferry PFP1 Comparison

In a recent study by Davis et al. (2017), metrics for blade curvature, reentrants, and slope were used as evidence to suggest WST modes of production and maintenance. The incorporation of similar methodologies in this study provides a basis to begin comparison between experimental and authentic specimens, in attempts to shed light on WST technological and behavioral patterns. The following section will review GLiMR data from PFP1, in comparison to the resharpening experiment established in this research, to test the hypothesis that PFP1 represent a utilitarian equipment cache by way of assessing if you occurred before internment in the cache. This data will hopefully act as a model for the morphometric outcomes and behavioral implications of resharpening.

Standard GLiMR Metrics

The fourteen projectile points from PFP1 were used as the basis for the technological design of the experimental projectile points used in this study. Only twelve of the fourteen projectile points were reviewed in this comparison due to the blade length of artifacts 73-24952 and 73-34054 being too small for a meaningful comparison. Table 13 illustrates the two types of materials observed amongst the PFP1 collection. The following data presented in Table 14 was previously collected by Davis and colleagues (2017) and will be compared to the metrics gathered in the WST replication experiment.

Table 13: Material Summary of PFP1 Points
Table information adapted from Davis et al. (2017: Table 1).

Catalog ID	Material	Catalog ID	Material	Catalog ID	Material
73-24940	CCS	73-24948	CCS	73-24957	CCS
73-24941	CCS	73-24949	CCS	73-24958	CCS
73-24942	FGV	73-24950	CCS	73-24959	CCS
73-24943	CCS	73-24951	CCS	73-27087	CCS

Note: Excludes specimens 73-24952 and 73-34054

Table 14: Average Dimensional Attributes of PFP1 Points
Table from Davis et al. (2017: Table 2).

Attribute	Units	Mean	SD	CV	Min	Max	Range
Length	mm	59.24	6.16	0.10	47.10	67.68	20.58
Width	mm	18.61	1.40	0.08	16.58	20.20	3.62
Thickness	mm	6.10	1.30	0.21	4.20	8.64	4.45
Max width	mm	18.14	1.61	0.09	16.05	20.10	4.05
Blade length	mm	42.50	9.69	0.23	27.10	62.31	35.21
Blade max width	mm	18.81	1.38	0.07	16.35	20.55	4.20
Blade width average	mm	12.83	1.01	0.08	11.48	14.54	3.06
Blade max thick	mm	5.94	1.29	0.22	4.20	8.64	4.45
Blade max thick y	mm	17.31	1.18	0.07	15.30	19.25	3.95
Haft Length	mm	20.07	5.02	0.25	9.86	26.26	16.41
Haft width average	mm	12.24	0.89	0.07	10.58	13.47	2.88
Haft max thick	mm	5.51	1.07	0.19	4.20	7.69	3.49
Outline perimeter	mm	134.53	12.53	0.09	109.16	153.07	43.91
Hull perimeter	mm	129.77	12.25	0.09	104.88	146.93	42.05
Area (xy)	mm ²	742.01	120.02	0.16	515.29	910.68	395.39
Hull area	mm ²	789.52	125.56	0.16	553.86	978.11	424.25
Blade area	mm ²	547.86	138.42	0.25	323.12	763.97	440.85
Haft area	mm ²	244.53	58.39	0.24	120.76	311.87	191.12
Area (xz) cross-section	mm ²	69.05	16.30	0.24	47.97	93.64	45.67
Volume	mm ³	2.44	0.70	0.29	1.34	3.56	2.21
Blade volume	cm ³	1.81	0.57	0.32	0.96	2.50	1.54
Haft volume	cm ³	0.78	0.28	0.36	0.43	1.37	0.95
Weight	g	6.41	1.74	0.27	3.58	9.05	5.47
Density	g/cm ³	2.64	0.05	0.02	2.54	2.72	0.18

Note: Fragmentary and outlier specimens excluded

The average PFP1 projectile points (Table 14) had measurement values ranging from 47.10 – 67.68 mm in length, 16.58 – 20.20 mm in width, 4.20 – 8.64 mm in thickness, 3.58 – 9.05 g in weight, and 1.34 – 3.56 mm³ in volume. The CV for length and width were <0.10 and were higher

for thickness, weight, and volume with CV values between 0.20 and 0.30. The mean length was 59.24 mm with a mean blade length of 42.50 mm, making up 67.92% of the total length, and a mean haft length of 20.07 mm, making up 32.08% of the total length.

Compared to the experimental dataset all values except for the haft size dimensions were slightly below those of the third resharpening event. Compared to the last resharpening, the mean length varied by 10.82%, the mean width varied by 3.67%, and the mean thickness varied by 5.86%. Although the mean absolute value of thickness did not vary greatly from the experimental projectile points, the higher CV of 0.21 indicates a greater degree of variability between specimens. The mean volume of the PFP1 projectile points differed by 17.01%, with the blade volumes differing by 14.62% and the haft volume differing by only 1.28%. Overall, the dimensions of the PFP1 projectile points were on average smaller than the last resharpening event of the experimental projectile points. The size of haft element is mostly consistent for the experimental projectile points, however varies more greatly in length for the PFP1 projectile points. This haft length variance is evident amongst specimens 73-27087 and 73-24950 which may have caused the high CV value of 0.25 for haft length. The higher variation seen with the PFP1 projectile points is a result of averaging the absolute values together, however the percentages presented above shows how much greater the dimensions were of the experimental points compared to that of the mean cast created for reference.

5.2 Slope Images

The following slope data was obtained from GLiMR analyses conducted in the Davis et al. (2017) paper on the PFP1 cache. Only three of the PFP1 projectile points will be assessed more in depth in this study, chosen based on their distinct variation from one another in cross-section. This is to minimize the number of projectile points discussed in this chapter, and to choose projectile points that would represent the morphology styles found in the cache. This section will review the slope images and discuss the edge steepness to create an initial evaluation of the amount of resharpening. The slope will be used to compare to the cross-section analysis data to further assess patterns of flake removal.

Specimen 73-24940 (Figure 28): The colored slope data for Face 1 of specimen 73-24940 shows a steeper edge angle along the right side of the blade. The presence of the red angular lines adjacent to the edge is indicative of hinges, which could suggest secondary flake removal. In the experimental study, most hinges formed as a result of impurities in the rock and flakes fracturing short of the midline. Face 2 on the other hand is more planar, which indicates having been made on a flake. The minimal flake removal along the edge would suggest if flake removal occurred, it would have been removed from Face 1.

Specimen 73-24941 (Figure 29): The colored slope data for Face 1 and Face 2 of specimen 73-24941 is fairly symmetrical, with Face 1 having the steeper edges. In comparison to 73-24940, the edges are not as steep, but flake removal may have occurred more on the left edge of the blade based on a higher rugosity near the tip. Face 2 is also more planar and may suggest that it was made on a flake, however an analysis of the cross-section would confirm this.

Specimen 73-24942 (Figure 30): The colored slope data for Face 1 of specimen 73-24942 shows a steeper edge angle along the left side of the blade. Face 2 on the other hand is again more planar, which could suggest preferential resharpening on the opposite face. Compared with the other two PFP1 projectile points, this one shows steeper edge anglers nearer to the tip of the blade. This projectile point also had a higher rugosity than the other projectile points, suggesting a more coarse-grained material as seen with DS09, DS16, and DS27 in the experimental study.

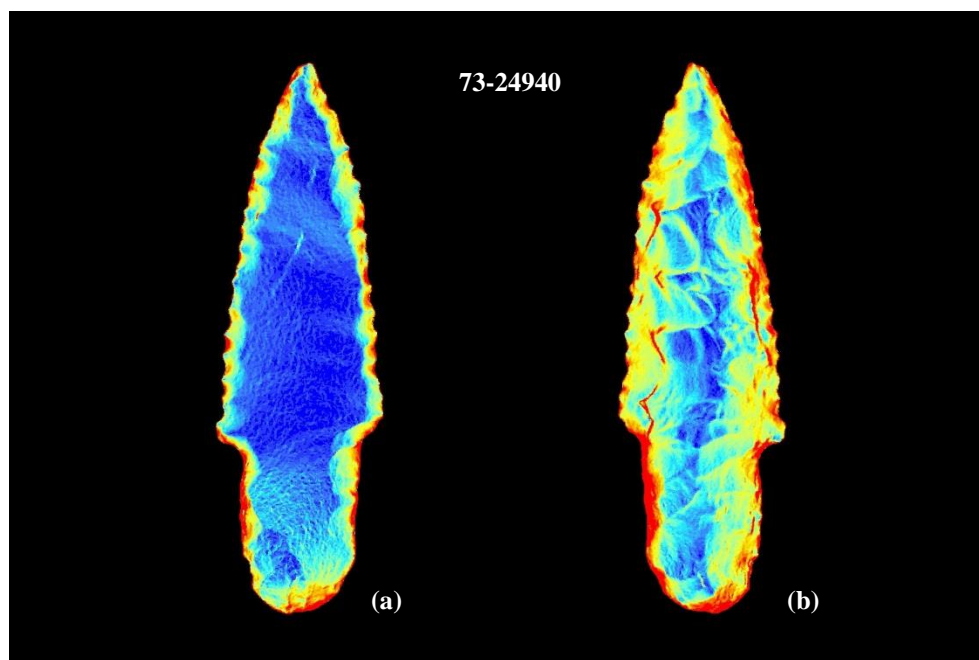


Figure 28: Surface TIN colored by slope results for PFP1 specimen 73-24940 (a) Face 2, and (b) Face 1.

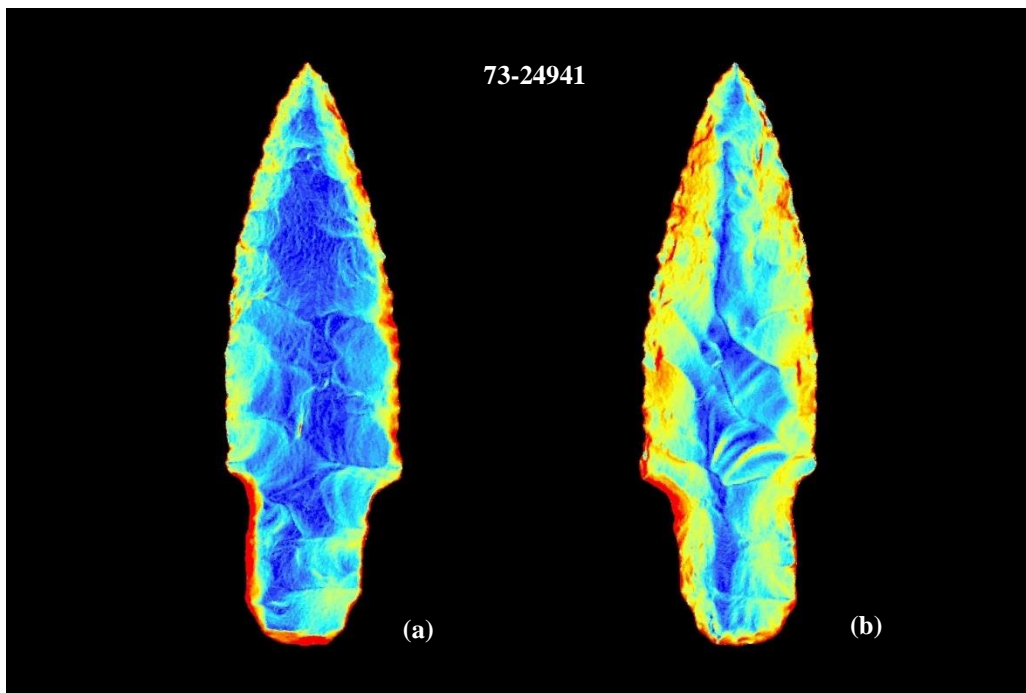


Figure 29: Surface TIN colored by slope results for PFP1 specimen 73-24941 (a) Face 2, and (b) Face 1.

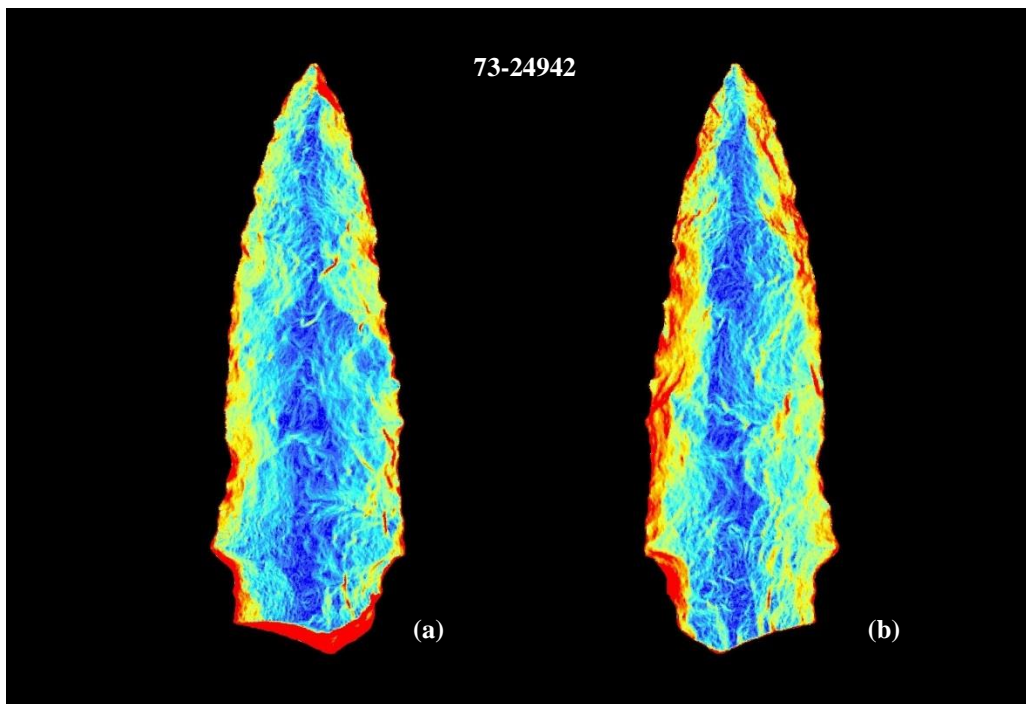


Figure 30: Surface TIN colored by slope results for PFP1 specimen 73-24942 (a) Face 2, and (b) Face 1.

5.3 Cross-section Comparison

Previous GLiMR data of the PFP1 projectile points were used to compare the cross-section images to the experimental ones. Using the newly updated GLiMR interactive analysis tool, each of the twelve PFP1 projectile points were compared between the resharpening groups DS01-DS30. Those with similar cross-sectional orientations were identified and the best fit example was chosen to be displayed in the following section. Figure 31 and Figure 32 display the specific catalog number and corresponding DS number used for comparison. Both the cross-sectional view and thickness comparison are listed within each figure, however a full image summary of the GLiMR analysis tool is viewable in Figure C.1. The comparison between the experimental group and the PFP1 specimens provide an interpretive framework for projectile point resharpening.

Specimen 73-24940 (Figure 31 (a)): The cross-sectional view of this projectile point was difficult to match to any one example in the experimental study. The PFP1 projectile point was noticeably plano-convex, having been made on a flake with unequal upper and lower volumes. Only one face of the blade had extensive retouch due to the concavity of the opposite face which exhibited only minimal flake removal. Based on this visual interpretation, the cross-section was compared to DS12 which experienced flake removal primarily on one face over the courses of resharpening. For DS12, the face that exhibited resharpening resulted in a shift in the midline to the right due to flake removal on the left extending over the initial midline during the second resharpening event. Alternatively, the shorter flake removals during the first and third resharpening stopped short of the midline, creating a steeper slope. The off-center midline of the PFP1 projectile point could indicate a similar resharpening technique or having been made on a macroblade with an already off-center ridgeline.

Specimen 73-24941 (Figure 31(b)): The cross-sectional view of this projectile point was matched with DS07 due to very similar thickness and biconvex nature of the blade. Both exhibit midlines near the center of the blade with gently sloping edges. The first episode of resharpening for DS07 experiences flake removal on the upper face of the blade with flake removal on the right extending near the thickest portion of the blade. Similarly, the second episode of resharpening experiences flake removal on the lower face maintaining a biconvex cross-section. Only during the third resharpening are flakes removed from alternate edges of the blade, making the cross-section less symmetrical. The steepness of the edges of 73-24940 as compared to the second episode of resharpening for DS07 may indicate similar resharpening on one face of the blade with flakes stopping short of the midline. This steepness as compared to DS07 is also noticeable in the thickness plot comparison. The steep slope on the left may indicate more abrupt flake removal, whereas the gentle sloping on the right indicates longer flake removal extending towards the midline. When resharpening occurs primarily on one face of the blade, it becomes difficult to delineate between unresharpened projectile points as it maintains a symmetrical cross-section.

Specimen 73-24942 (Figure 32): The cross-sectional view of this projectile point was matched with DS09 due to the asymmetrical nature of the blade. This type of cross-section is most indicative of projectile point resharpening due to the occurrence of two off-center midlines that are adjacent to one another. Flake removal extending onto the midline, truncates the edge of the projectile point and shifts the midline off-center, as seen with experimental projectile point DS12. The third resharpening event attempts to correct the asymmetry of the blade by only removing flake along one face, instead of alternate edges. Specimen 73-24942 has a similar midline shift as DS09, however the edges where flake removal occurred are not as steep. This could be the result

of flake removals extending past the midline, creating a more gentle slope. In this instance, a slope comparison would not aid in describing how much resharpening the blade would have experienced.

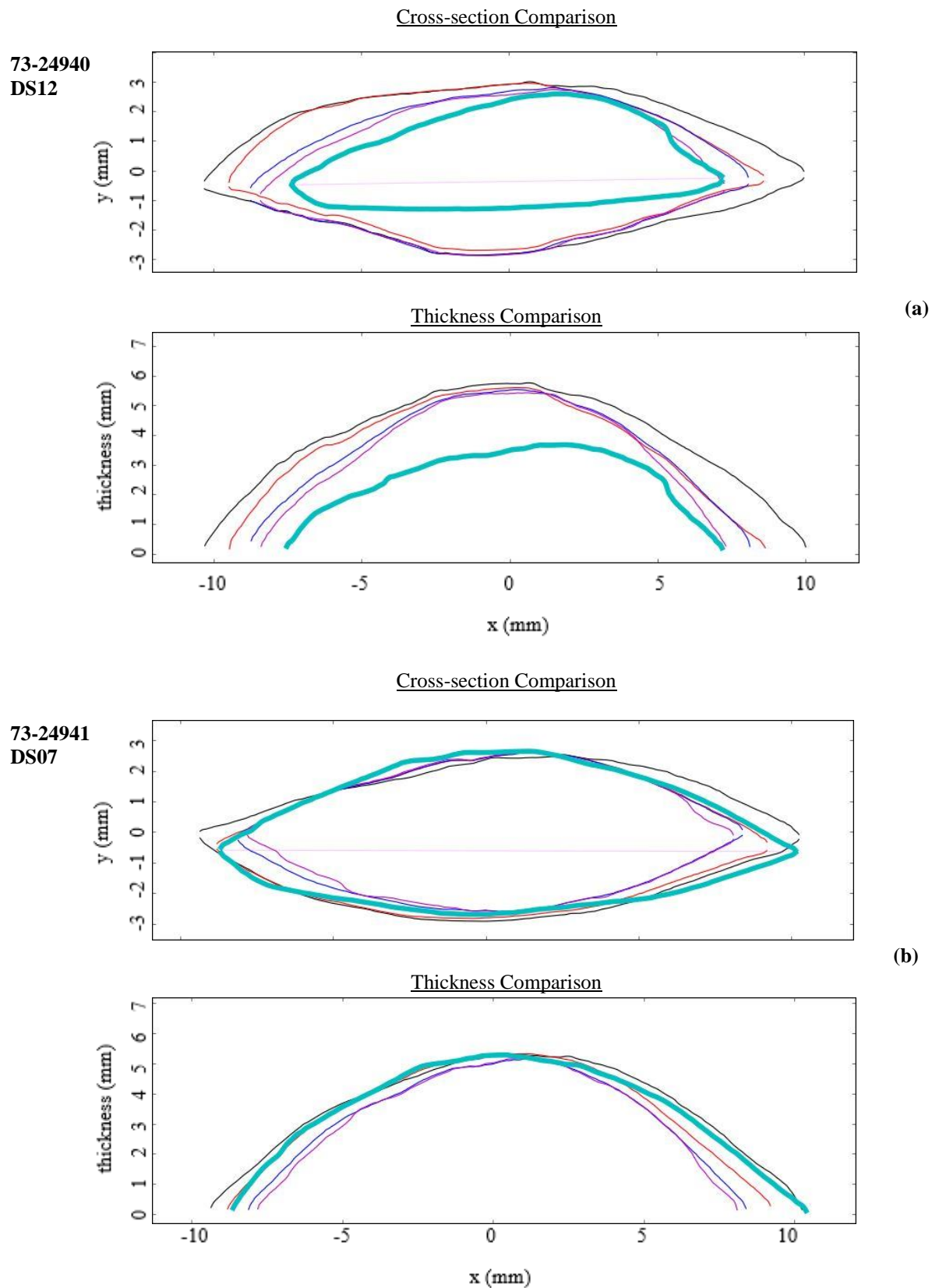


Figure 31: Cross-section and thickness comparison between PFP1 projectile points 73-24940 and 73-24941, and best fit DS group.

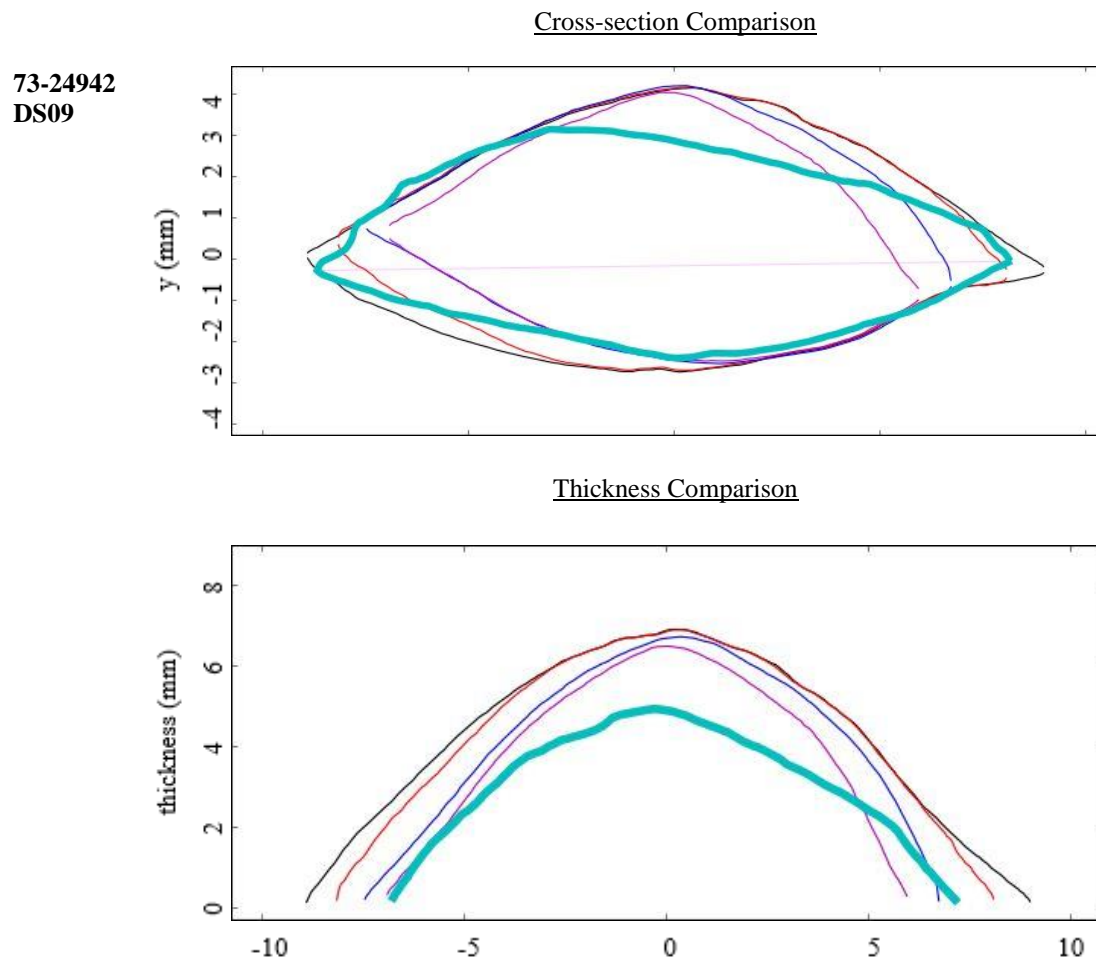


Figure 32: Cross-section and thickness comparison between PFD projectile point 73-24942, and best fit DS group.

5.4 Blade Curvature and Inset Width

The following table (Table 15) lists the curvature and in-set width results of the PFP1 projectile points in comparison to the mean results of the experimental projectile points. Overall the majority of the curve values for the left and right blade were > 0.0050 , which is more than the blade curve average for the original experimental projectile points. One PFP1 projectile point had a curve value below the average curve value for the third resharpening event. Only three of the twelve PFP1 projectile points were within the experimental curve value range, likely indicating a technological variation in design, or the breaking of tips and subsequent refurbishing of the distal end of the blade.

Table 15: Inset Width and Curve Data for the Experimental and PFP1 Projectile Points

Specimen	In-set Width (mm)	In-set Max Width (%)	Left Curve	Right Curve
Mean Original	0.27	1.24	-0.0048	0.0050
Mean First Resharpening	0.45	2.21	-0.0043	0.0045
Mean Second Resharpening	0.55	2.88	-0.0037	0.0040
Mean Third Resharpening	0.87	4.55	-0.0031	0.0034
73-24940	0.65	3.77	-0.0060	0.0060
73-24941	0.36	1.82	-0.0063	0.0069
73-24942	0.66	3.43	-0.0043	0.0050
73-24943	0.56	3.09	-0.0069	0.0062
73-24948	0.79	4.06	-0.0066	0.0038
73-24949	0.99	5.88	-0.0055	0.0060
73-24950	0.40	2.43	-0.0065	0.0064
73-24951	0.71	3.54	-0.0053	0.0072
73-24957	0.70	4.35	-0.0094	0.0099
73-24958	0.61	3.07	-0.0047	0.0041
73-24959	0.62	3.24	-0.0072	0.0051
73-27087	1.37	7.06	-0.0018	0.0021

Note: Excludes PFP1 specimens 73-24952 and 73-34054

The in-set width values for the PFP1 projectile points ranged from 0.36 – 1.37 mm and the inset percent of maximum width ranged from 1.82 – 1.06%. The mean in-set width values for the resharpening episodes similarly ranged from 0.27 – 0.87 mm and had an in-set width percentages ranging from 1.24 – 4.55%. Excluding the one outlier 73-27087, the mean PFP1 projectile point had an in-set width of 0.64 mm and max width percent of 3.52%. This would place the projectile point resharpenings between experimental resharpening episodes two and three. However, projectile points 73-24941 and 73-24950 had no identifiable inset width on one edge of the blade indicating very minimal resharpening, or preferential resharpening on the other edge.

Based on the results for each of the PFP1 projectile point, there is little variance between predicted and expected values of inset width and percentage as compared to the mean values produced in the experimental study. Figure 33 plots a trendline against the mean inset max width percent of each resharpening event. The PFP1 projectile points were then manually plotted against the trendline to evaluate the stage of resharpening. Based on this graph, two PFP1 projectile points fall below the second stage of resharpening, eight PFP1 projectile points fall between the second and third stages of resharpening, and two PFP1 projectile points exceed the experimental dataset and plot above the third stage of resharpening. Additional experimental stages would be necessary to accurately evaluate the stage of resharpening for PFP1 projectile points 73-27087 and 73-24949.

The in-set maximum width percent has proven to be the most useful measure as it explained for variances in blade size and the size of the ear. PFP1 projectile points 73-24951 and 73-24957 are good examples of projectile points that have similar inset width values of 0.71 and 0.70 mm and different inset percentages of 3.54 and 4.35%. This difference is important in understanding that although both projectile points have similar ear widths, based on the overall blade width they do not represent the same resharpening event. Projectile point 73-24951 may have experienced

two episodes of resharpener in comparison to the experimental study, whereas 73-24957 may have experienced three episodes of resharpener. This holds true for both projectile points when compared to individual cross-sections of DS29 and DS10 (Figure C.1). The ears proportion to the blade width is more crucial in identifying the stage of reduction than comparing the general sizes to one another. Using multiple lines of evidence will help illustrate and suggest the stages of reduction occurring for projectile points.

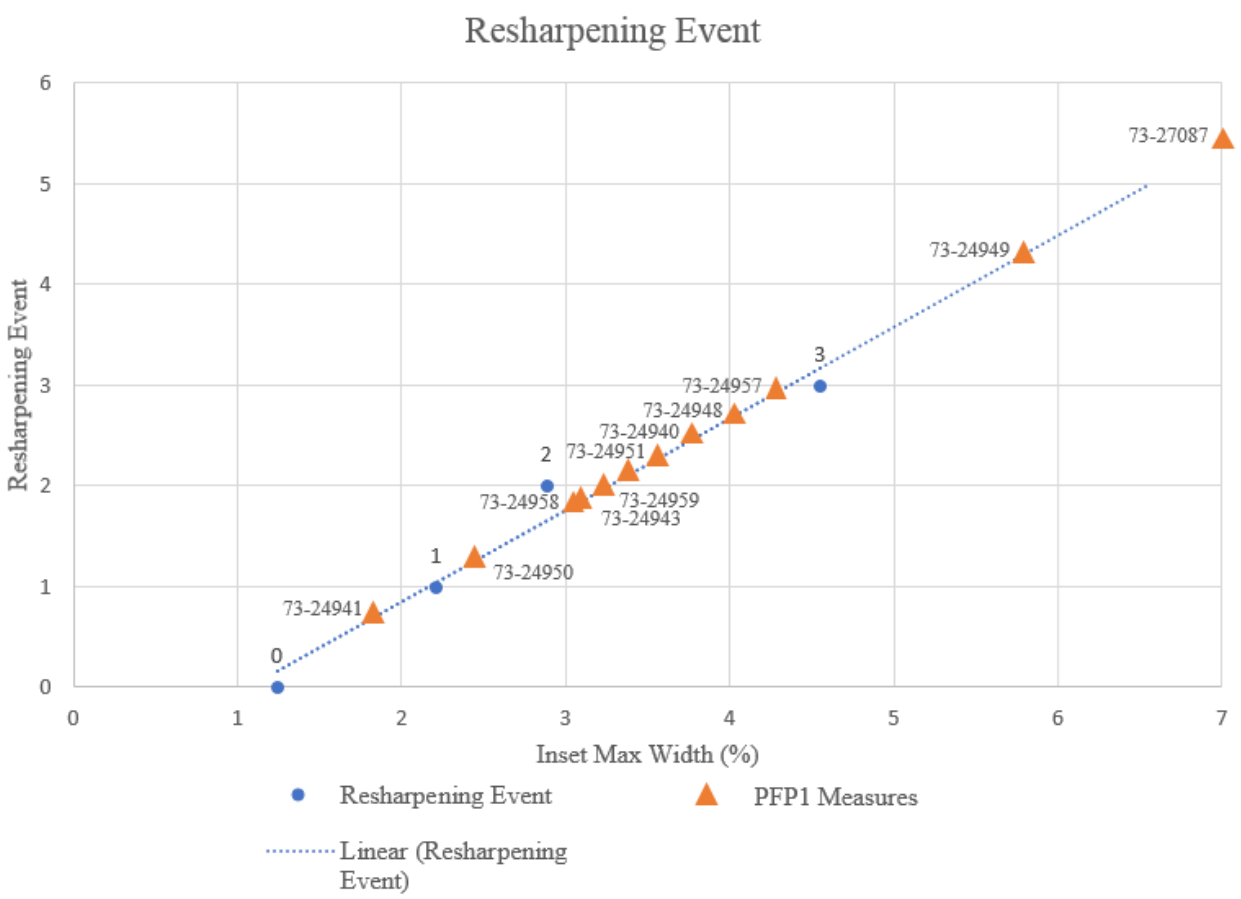


Figure 33: Inset max width percentage of the average experimental resharpener events and manually plotted PFP1 projectile point resharpenerings.

Chapter 6: Discussion

6.1 Experimental Implications

Analysis of the experimental data produced results that can be used to interpret stone tool maintenance behaviors and the larger issue of technological curation. Most notable of those analyses were changes in the cross-section, curvature, and inset width of the ears. This section will discuss these features as potential models of comparison for future research into stone tool maintenance. The use of three-dimensional models has allowed the collection of this data in a stream-lined process, and the ability to capture stages of the experimental process and the geometric morphometric outcomes of specific behavioral actions of maintenance. Experimental variability will also be discussed to address research design problems and facilitate future morphometric studies in stone tool curation.

The cross-section comparison has been a useful tool for stone tool maintenance comparison as it provides a basis for resharpening and/or manufacturing techniques. The nature of reduction and change of symmetry in cross-sectional view has been noted before in archaeological research (Frison 1968; Kuhn 1990; and Nance 1971). Figure 34 demonstrates a novel model to interpret the type of removal patterns seen with resharpening. The two structural types used in the model are traditionally used to describe the patterns associated with cordage and weaving directions. In the model, the terms “Z” twist and “S” twist have instead been applied to the resharpening direction, where a Z-twist would result from flake removal occurring on the right side of the blade, and the S-twist would result in flake removal occurring on the left side of the blade. This form of retouch depicted in Figure 35 has been previously coined by Nance (1971) as *alternate retouch*, and would

be a behavioral result of resharpening one edge of the blade in one direction, flipping the projectile point to the alternate face, and resharpening again in the same direction. This is in contrast to resharpening only one face of a projectile point, where the flintknapper would have had to resharpen one edge of the blade in one direction, and rotating the projectile point 180 degrees instead of flipping to the alternate face. Both a Z-twist and S-twist resharpening direction occurred during the experimental study as an unintended result to make the projectile points blade uniform. For a more precise study of projectile point morphologic change, the resharpening location will need to be better controlled and recorded. As for behavioral implications, this study illustrates the outcome when the method is used is random not pre-determined.

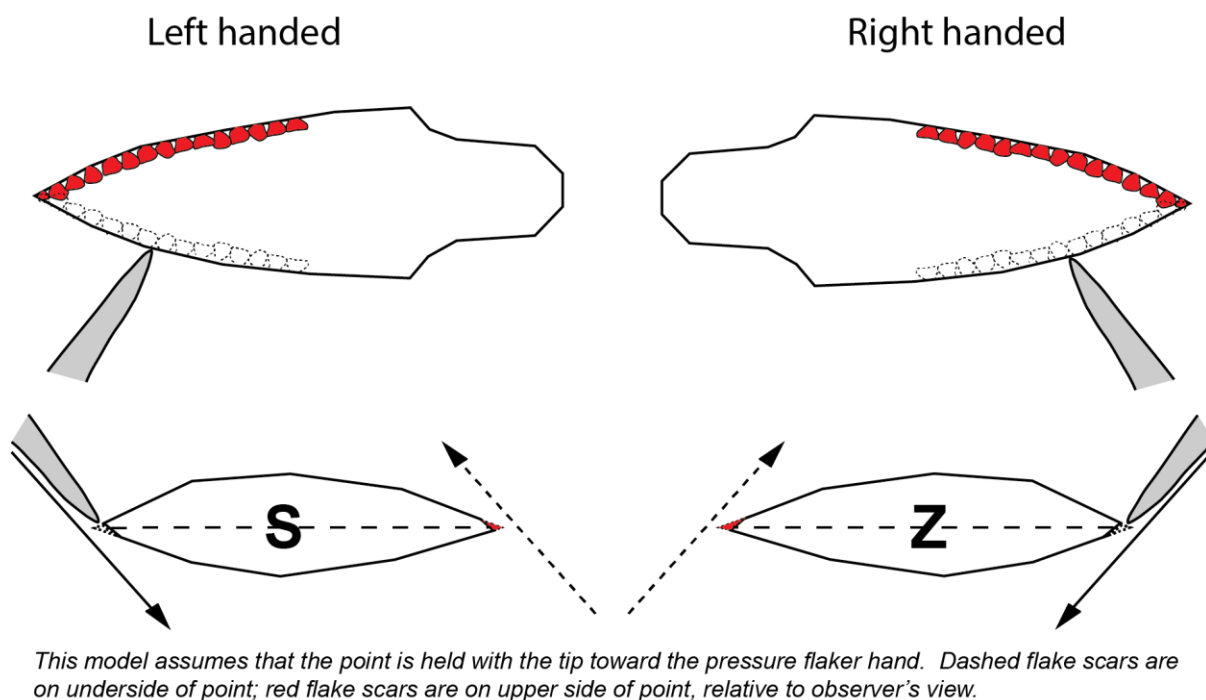


Figure 34: Z-Twist and S-Twist directions as applied to projectile point cross-sections. Image courtesy of L. Davis.

The direction of projectile point resharpening also helps in understanding the handedness of the individual resharpening the point. In the case of this experimental study, the flintknapper (Stueber), is right handed and thus the direction the projectile point was held can be inferred based on the slope and cross-section images. In Figure 20 the occurrence of flake removal on the left side of the face suggests that the projectile point was resharpened pointing downwards in the left hand, or the projectile point was resharpening pointing upwards in the right hand. In Figure 21 the occurrence of flake removal on the right side of the face suggests that the projectile point was resharpened pointing upwards in the left hand, or the projectile point was resharpened pointing downwards in the right hand. The first example would result in an S-twist cross-section, whereas the second example would result in a Z-twist cross-section (Figure 34). The combination of these data helps infer the direction of flake removal and the handedness of the individual. If specific flintknapping preferences are identifiable amongst a sampled population, this could help understand a specific technological behaviour of a cultural group or individual.

The design of this experiment was an exploratory study in maintenance behavior and did not control for all the variables of flintknapping manufacture and maintenance. The results of this allowed the research to isolate the effects of minor actions and explore the resultant changes in projectile point morphology. Future studies can be more tightly controlled, paying more rigorous attention to detail and procedure to isolate certain sets of variables. The results of this research will hopefully aid in future experimental designs, providing a basis to begin isolating certain variables and quantifying those results. Using multiple lines of evidence would be “more accurate indicators of reduction realities than any single line of evidence” (Magne 2001:23), which illustrates the effectiveness of corroborative experimental archaeology and the furthering of this research.

6.2 PFP1 Implications

After reviewing the results of the PFP1 projectile points analyzed in this study, we can infer that each of the projectile points has undergone at least one stage of resharpening. This supports the hypothesis that the PFP1 projectile points represent a utilitarian cache, having experienced use and resharpening before being interred in the ground. The inset width measurement and cross-sectional view were the most supportive measures in confirming this hypothesis. The results have shown that the PFP1 projectile points were extensively retouched, based on the majority of projectile points falling between the second and third stages of resharpening. The cross-section analysis has additionally verified resharpening in either a Z- or S-twist fashion, beyond the initial manufacture of the blade. In terms of behavior, the cross-section analysis tool used on three of the PFP1 projectile points have provided a glimpse into the WST cultural component and types of techniques that may have been used at the site. The occurrence of both Z- and S-twist resharpening of the PFP1 assemblage may indicate a single flintknapper as seen in the experimental study, or multiple flintknappers with different preferential resharpening methods. Further research into flake removal patterns and size may help indicate one individual from many, which may allow for the *مني* of flintknappers to be determined for a single assemblage.

In addition, the results of the PFP1 and experimental GLiMR data can be used to support previous research in measuring the rate of curation and maximum utility. Lithic studies have addressed quantifying curation by measuring the degree of change (Davis 1998; Flenniken & Raymond 1986; Iovita 2011; Shott 2015) and this research will further these methods by implementing novel measurements to understanding material loss and curation rate. Incorporating cross-section analysis of twist direction, blade curvature, slope, and inset width, these measures

will help facilitate discussion on resharpening techniques and the amount of utility and retouch occurring on individual specimens. This will help further our understanding of the variation we see in the archaeological record. Given that the controlled experiment produced measureable outcomes and can be used to infer the actions that occurred in the past, it provides a potential base measurement to compare with other stemmed projectile points. Projectile points that were hafted in a similar fashion with sinew reaching the upper extent of the shoulder and retaining ears can be compared to this study and the inset width measured. Further research can control for more variables by accounting for broken and refurbished points, to better assess the degree of curation.

This research also plays an important role in furthering the culture history model of the Cooper's Ferry Site, specifically when understanding resource acquisition and availability. "The manner in which lithic tools and debitage are designed, produced, recycled, and discarded is intimately linked to forager land-use practices, which in turn are often associated with environmental and resource exploitation strategies" (Andrefsky 2005:4). The occupation of a specific site locality is dependent on a variety of factors that include: resource availability, population size, and lithic raw material sources. Lithic raw material can be acquired through primary or secondary source acquisition or trade networks. Depending on the number of lithic resources within a site's vicinity, resource availability influences the behavior behind tool modification and resource exploitation. It has been argued that the more access a group has to a raw material source, the less the tools are modified, and the more production there are of newer tools (Smith, 2015). At the Cooper's Ferry site, a recent geochemical sourcing study on 400 CCS samples has placed known CCS sources within 20 km of Coopers Ferry (Davis & Nyers 2014). This close proximity of raw material counters the argument that the tools would experience less modification due to a higher abundance of resource material availability. The PFP1 assemblage

experienced multiple resharpening events, and were continually maintained for further use rather than discarded. However, how much modification a tool undergoes before it is discarded is not just reliant on location, but also on behavior. It is difficult to describe the relationship between lithic artifact retouch and human behavior because technology is highly influenced by factors such as raw material availability, adaptive practices, and environment constraints (Andrefsky, 2010). The more we understand about these variables, the better we can make interpretations about behavior. Identifying between curated assemblages and expedient tools will help further these mobility models and the role a site has within its environmental and geographic context. The incorporation of experimental work and focusing on the behaviors of individual site localities will help generate the information desired for these greater research questions.

Chapter 7: Conclusion

The analyses discussed in this experimental study are an example of the dynamic range of possibilities of two- and three-dimensional spatial data. Explaining observable phenomena through experimentation and data exploration has the potential to further our knowledge of the dynamic past. In addition, being able to map the stages of artifact procurement, manufacture, maintenance, and discard helps further our understanding of an artifact's placement in the static present. The use of experimental design in archaeological research has influenced archaeologists to explore why artifacts appear the way they do in the archaeological record. This experimental study has introduced a controlled scenario with measurable outcomes that have been used to explain morphometric changes as a result of curation. Specific actions of a flintknapper leave identifiable traces that if understood, can be used to reconstruct past behaviors. The incorporation of three-dimensional models has helped facilitate these analyses and open the door to understand variations of artifact forms across populations, requiring analytical tools that were not feasible before the 21st century.

The collection of geometric morphometric data of projectile points using computer-based methodologies have been essential in understanding a projectile point's use-life and maintenance. Comparison with an archaeological sample, has allowed this study to move past experimentation and interpret the function of these artifacts and their behavioral implications. The PFP1 projectile point assemblage has provided a unique opportunity to compare experimental data with a collection of projectile points deposited in one occurrence. Traditional measurements have also been useful for identifying trends and patterns between the stone tool varieties, however there remains a degree of error and irreproducibility that can be controlled with novel techniques and

software. Incorporation of replicable experimentation and analyses will help standardize lithic research and allow for greater populations to be analyzed and understood.

7.1 Future Analysis

The use of GLiMR has provided a modern approach to explain observable phenomena that has been impractical to record by hand. The automated capabilities of the software allow for additional analyses to be explored with accuracy and efficiency. Future work can utilize the results of this study to conduct additional experiments with more tightly controlled variables. Three-dimensional digitization has the ability to capture data patterns that can be mapped through replicable experimentation. By identifying these trends and occurrences of specific attributes, behavior can be more tightly controlled and understood. Expanding our knowledge and collection of two- and three-dimensional data will provide limitless possibilities for artifact analysis and comparison.

Bibliography

- Ames, Kenneth M. (2010). Dart and Arrow Points on the Columbian Plateau of Western North America. *American Antiquity*, 75(2):287-325.
- Andrefsky, Jr., W. (2005). *Lithics: Macroscopic Approaches to Analysis*. Cambridge University Press, 2nd edition.
- Andrefsky, Jr., W. (2006). Experimental and Archaeological Verification of an Index of Retouch for Hafted Bifaces. *American Antiquity*, 71(4):743-757.
- Binford, Lewis R. (1967). Smudge Pits and Hide Smoking: The Use of Analogy in Archaeological Reasoning. *American Antiquity*, 32(1):1-12.
- Binford, Lewis R. (1979). Organization and Formation Processes: Looking at Curated Technologies. *Journal of Anthropological Research*, 35(3):255-273.
- Blades, Brooke S. (2003). End Scraper Reduction and Hunter-Gatherer Mobility. *American Antiquity*, 68(1):141-156.
- Cignoni, P., M. Callieri, M. Corsini, M. Dellepiane, F. Ganovelli, and G. Ranzuglia (2008). MeshLab: an Open-Source Mesh Processing Tool. *Sixth Eurographics Italian Chapter Conference*, pp. 129-136
- Charlin, Judith, Rolando González-José (2012). Size and Shape Variation in Later Holocene Projectile Points of Southern Patagonia: A Geometric Morphometric Study. *American Antiquity*, 77(2):221-242.

- Davis, Loren G., Samuel C. Willis, and Shane J. Macfarlan (2012). Lithic Technology, Cultural Transmission, and the Nature of the Far Western Paleoarchaic-Paleoindian Co-Tradition. In *Meetings at the Margins: Prehistoric Cultural Interactions in the Intermountain West*. Ed. David Rhode, University of Utah Press, Salt Lake City, 47–64.
- Davis, Loren G., Alex J. Nyers (2014). A Cryptocrystalline silicate provenance system for the lower Salmon River canyon of western Idaho. Pacific Slope Archaeological Laboratory, Oregon, 1-58.
- Davis, Loren G., Dan W. Bean, Alex J. Nyers, and David R. Brauner (2015). GLiMR: A GIS Based Method for the Geometric Morphometric Analysis of Artifacts. *Lithic Technology*, 40(3):199-217.
- Davis, Loren G., Dan W. Bean, Alex J. Nyers (2017). Morphometric and technical attributes of western stemmed tradition projectile points revealed in a second artifact cache from the cooper's ferry site, idaho. *American Antiquity*, 82(3):536-557.
- Dogandzic, Tamara, David R. Braun, Shannon P. McPherron (2015). Edge Length and Surface Area of a Blank: Experimental Assessment of Measures, Size Predictions and Utility. *PLoS: ONE*, 10(9):1-21.
- Flenniken, J. Jefferey, Anan W. Raymond (1986). Morphological Projectile Point Typology: Replication Experimentation and Technological Analysis. *American Antiquity*, 51(3):603-614.
- Frison, George C. (1968). A Functional Analysis of Certain Chipped Stone Tools. *American Antiquity*, 33(2):149-155.

- Iovita, Radu (2011). Shape Variation in Aterian Tanged Tools and the Origins of Projectile Technology: A Morphometric Perspective on Stone Tool Function. *PLoS: ONE*, 6(12):1-14.
- Knecht, Heidi (1997). Projectile Points of Bone, Antler, and Stone: Experimental Explorations of Manufacture and Use. *Projectile Technology: Interdisciplinary Contributions to Archaeology*. Ed. Heidi Knecht. Springer, Boston, 191-212.
- Kuhn, Steven L. (1990). A Geometric Index of Reduction for Unifacial Stone Tools. *Journal of Archaeological Science*, 7:583-593.
- Magne, Martin P. R. (2001). Debitage Analysis as a Scientific Tool for Archaeological Knowledge. *Lithic Debitage: Context, Form, Meaning*. Ed. W. Andrefsky Jr. University of Utah Press, Salt Lake City, 21-31.
- Marsh, Erik J., Jefferey R. Ferguson (2010). Introduction. *Designing Experimental Research in Archaeology: Examining Technology through Production and Use*. Ed. Jefferey R. Ferguson. University Press, Colorado, 1-12.
- Nance, J. D. (1971). Functional Interpretations from Microscopic Analysis. *American Antiquity*, 36(3):361-366.
- Reti, Jay S. (2016). Quantifying Oldowan Stone Tool Production at Olduvai Gorge, Tanzania. *PLoS: ONE*, 11(1):1-24.
- Serwatka, Kamil, Felix Riede (2016). 2D Geometric Morphometric Analysis Casts Doubt on the Validity of Large Tanged Points as Cultural Markers in the European Final Paleolithic. *Journal of Archaeological Science, Reports* 9:150-159.

- Shott, Michael J. (1996). An Exegesis of the Curation Concept. *Journal of Anthropological Research*, 52(3):259-280.
- Shott, Michael J., Jesse A. M. Ballenger (2007). Biface Reduction and the Measurement of Dalton Curation: A Southeastern United States Case Study. *American Antiquity*, 72(1):153-175.
- Shott, Michael J., Mark F. Seeman (2015). Curation and Recycling: Estimating Paleoindian Endscraper Curation Rates at Noble Pond, Ohio, USA. *Quaternary International*, 361:319-31.
- Smith, Geoffery M. (2015). Modeling the influences of raw material availability and functional efficiency on obsidian projectile point curation: A Great Basin Example. *Journal of Archaeological Science, Reports* 3:112-121.
- Skibo, James M. (1992). Ethnoarchaeology, Experimental Archaeology and Inference Building in Ceramic Research. *Archaeologia Polona*, 30:27-38.
- Skibo, James M. (1994). The Kalinga Cooking Pot: an Ethnoarchaeological and Experimental Study of Technological Change. *Kalinga Ethnoarchaeology: Expanding Archaeological Method and Theory*. Eds. W. A Longacre and J. M. Skibo. Smithsonian Institution Press, Washington D.C., 113-126.
- Thomas, David H. (1981). How to Classify the Projectile Points from Monitor Valley, Nevada. *Journal of California and Great Basin Archaeology*, 3(1):7-43.
- Towner, Ronald H., Miranda Warburton (1990). Projectile Point Rejuvenation: A Technological Analysis. *Journal of Field Archaeology*, 17(3):311-321.

Wachowiak, Melvin J., Basiliki V. Karas (2009). 3D Scanning and Replication for Museum and Cultural Heritage Applications. *Journal of the American Institute for Conservation*, 48:141-158.

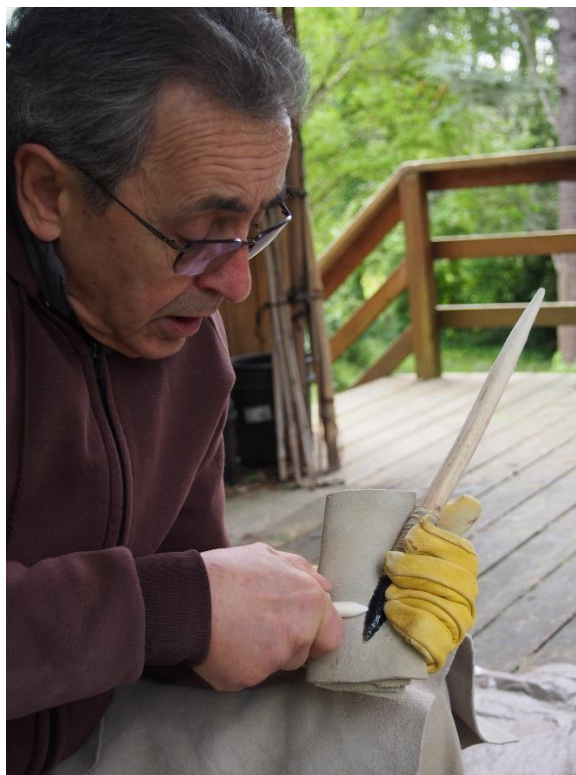
Appendix A



Figure A.1: Experimental prismatic blade core and blades used in the WST replication.



(a)



(b)



(c)



(d)

Figure A.2: Experimental resharpening process. (a) Hafting method, (b) primary resharpening direction, (c) dulling of the blade, and (d) pressure flaking method.

Appendix B

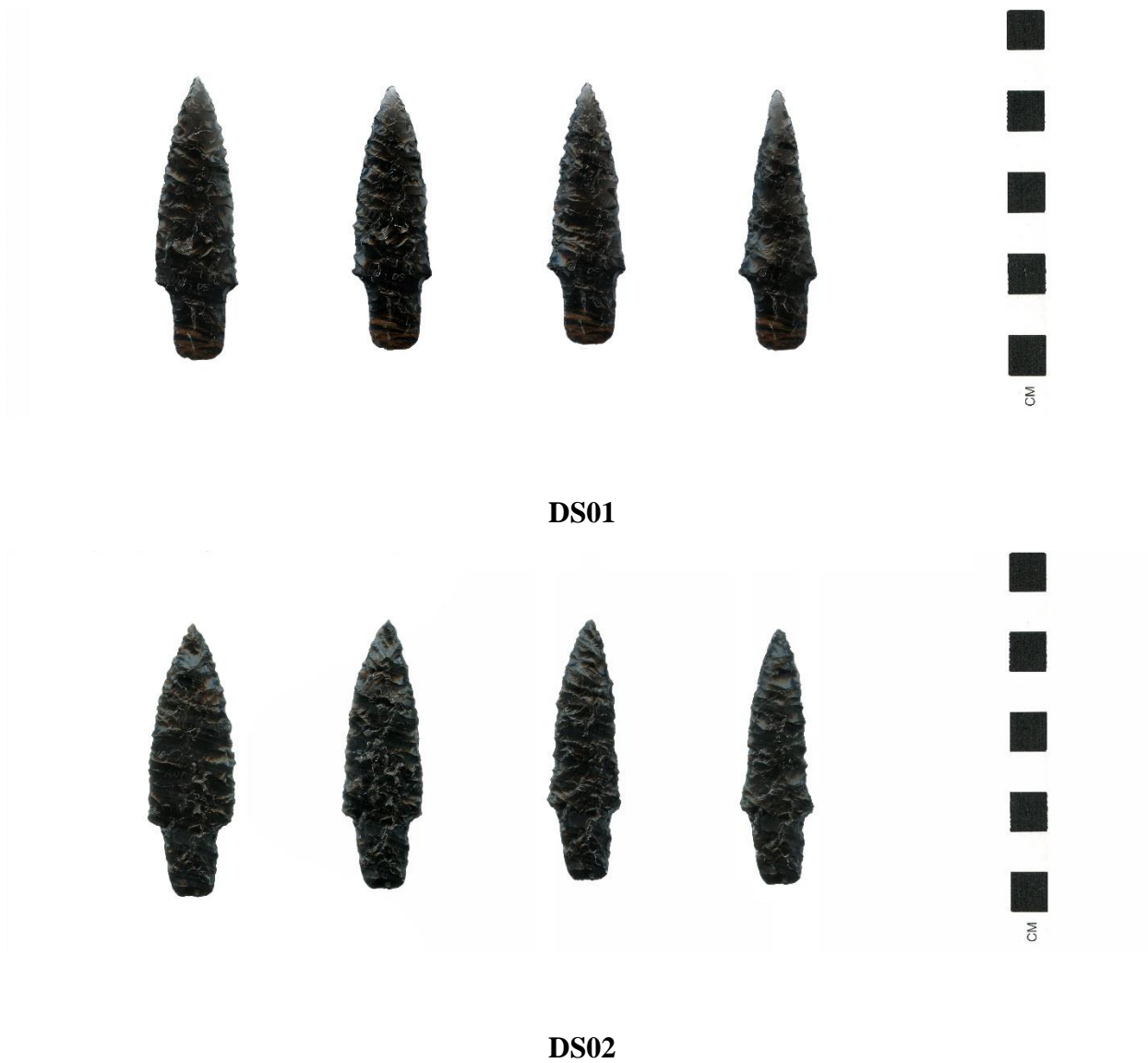


Figure B.1: Two-Dimensional scanned images of resharpening stages for each projectile point DS1-DS30.



DS03



DS04



DS05

Figure B.1: Continued...



DS06



DS07



DS08



Figure B.1: Continued...



DS09



DS10



DS11

Figure B.1: Continued...



DS12



DS13



DS14



Figure B.1: Continued...



DS15



DS16



DS17

Figure B.1: Continued...



DS18



DS19



DS20



Figure B.1: Continued...



DS21



DS22



DS23



Figure B.1: Continued...



DS24



DS25



DS26

Figure B.1: Continued...



DS27



DS28



DS29

Figure B.1: Continued...



DS30

Figure B.1: Continued...

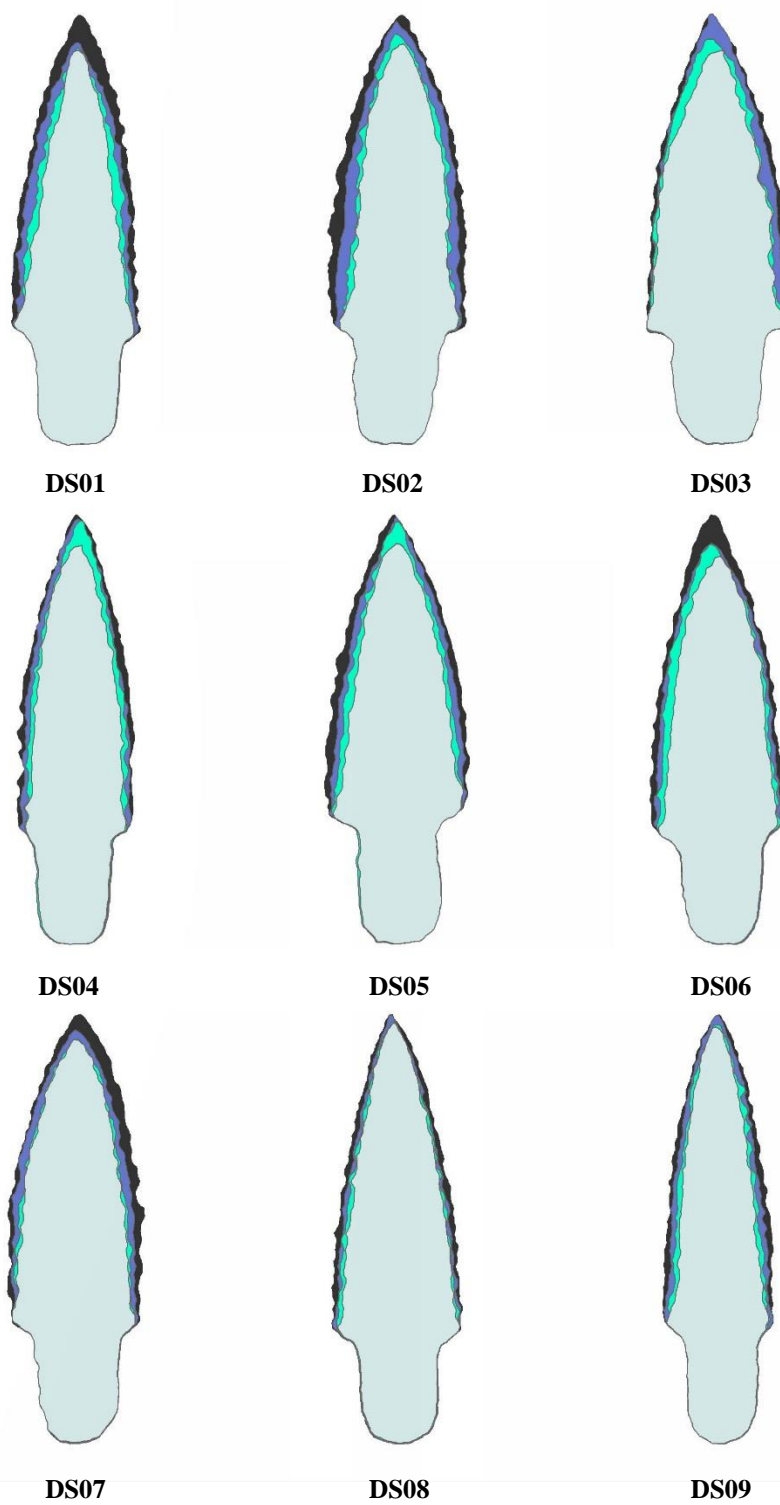


Figure B.2: Projectile point outline overlay of each stage of reshaping DS1-DS30.

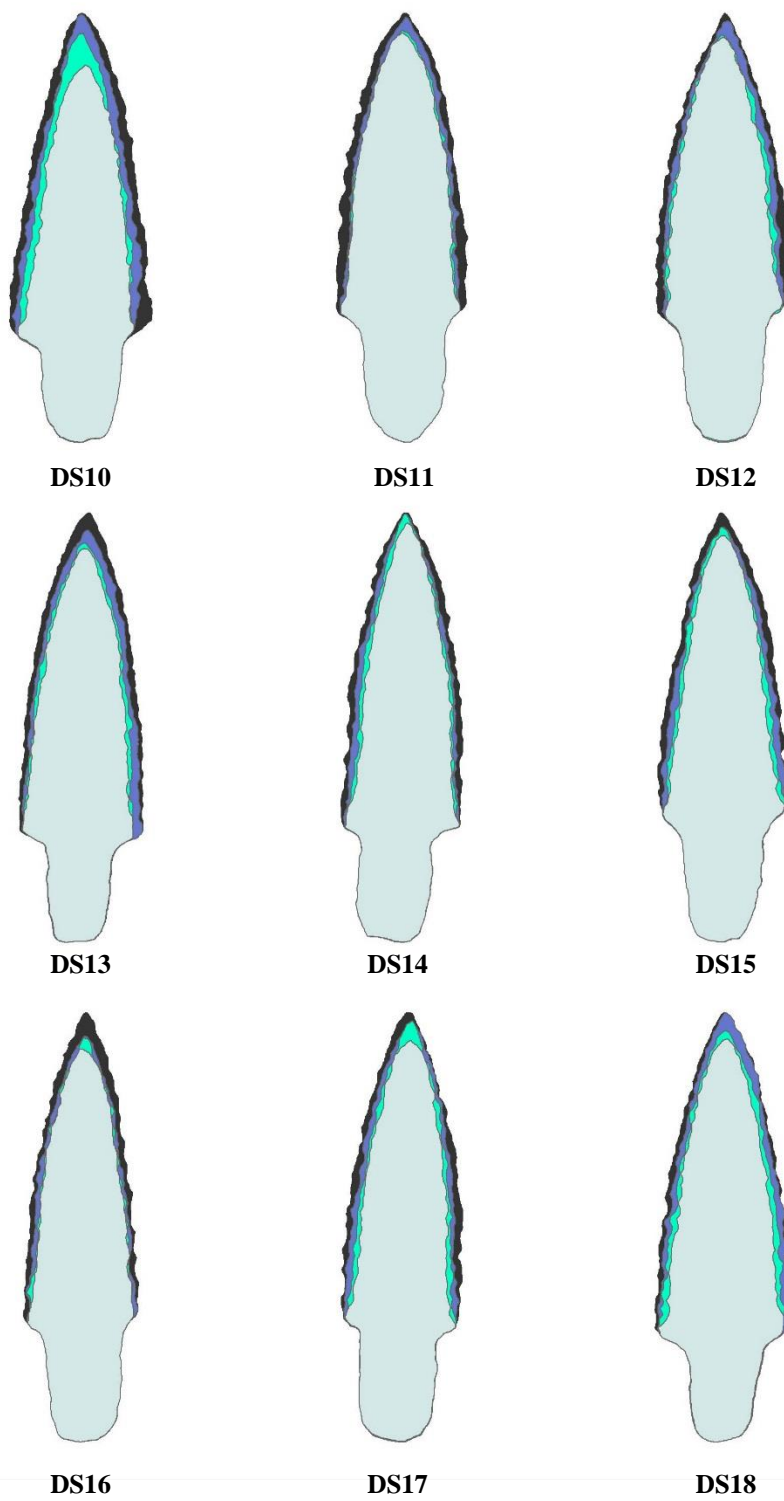


Figure B.2: Continued...

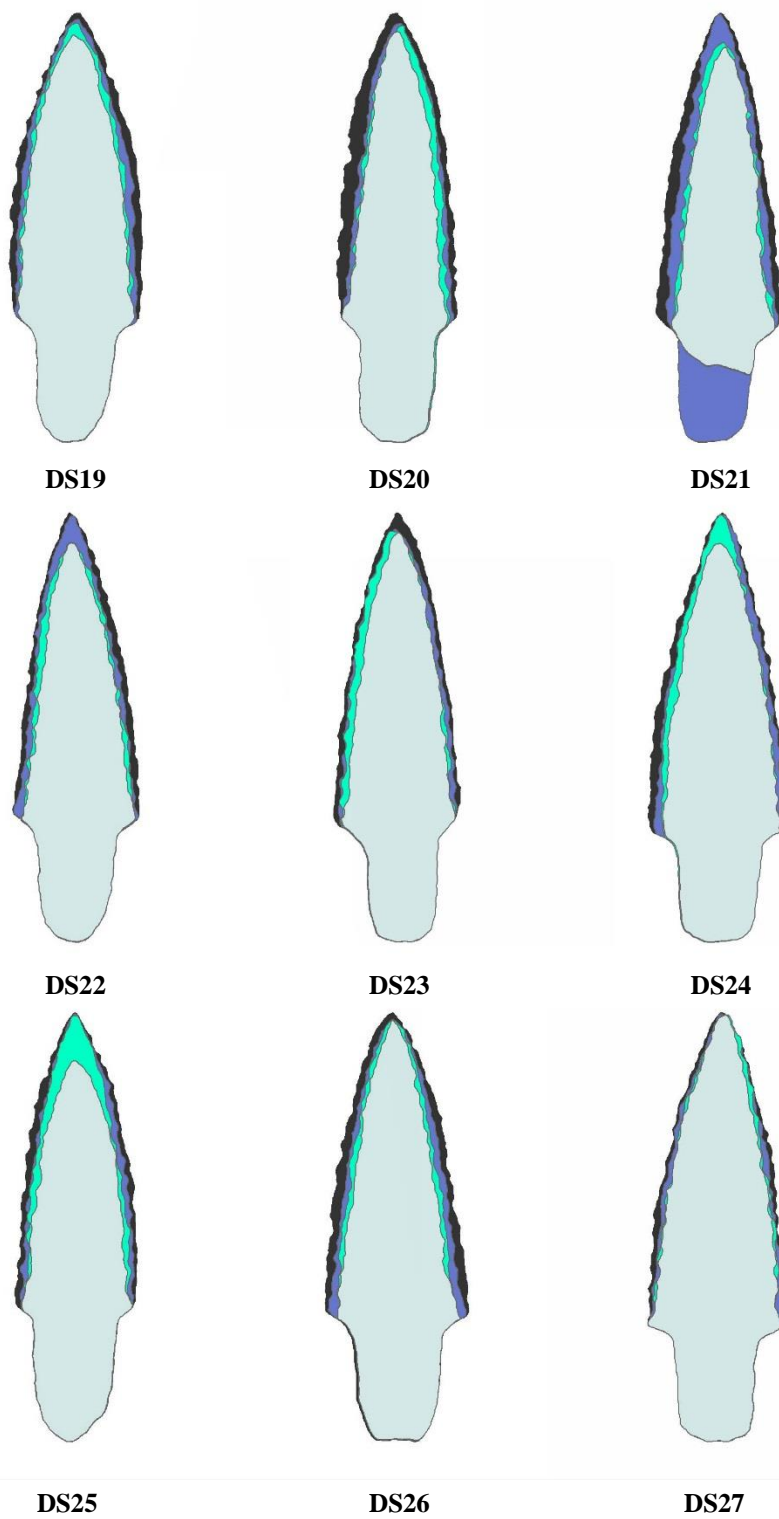


Figure B.2: Continued...

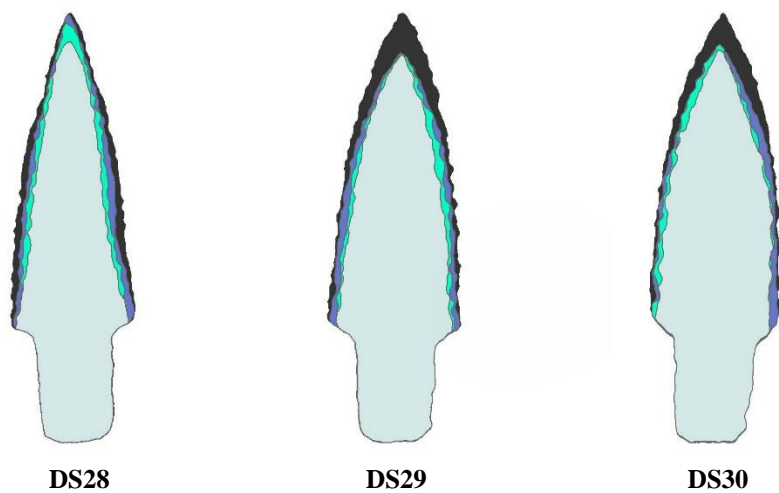


Figure B.2: Continued...

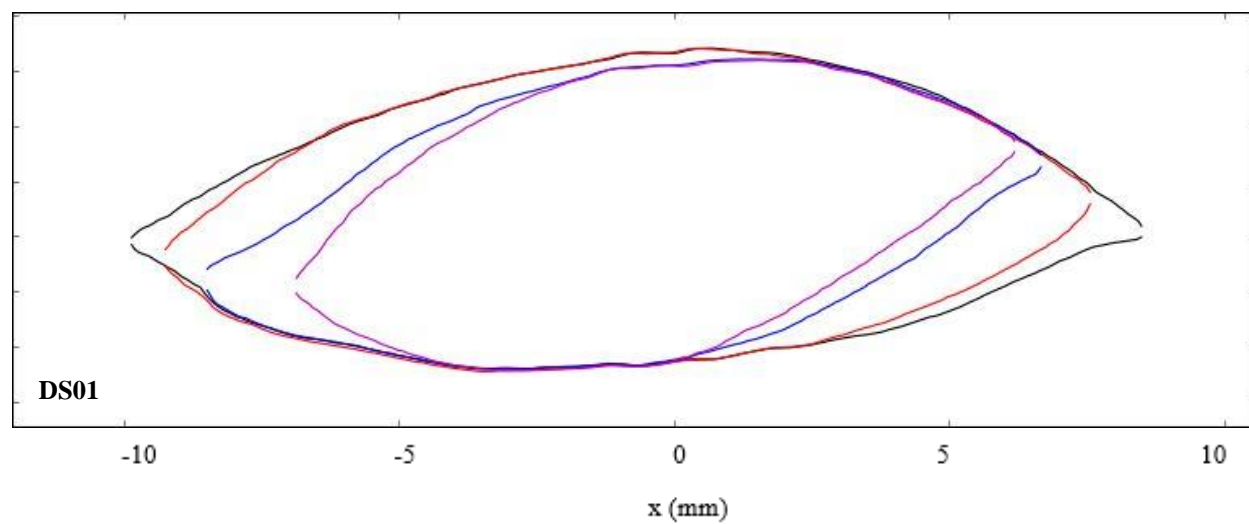


Figure B.3: Cross-section comparison for each resharpening event DS1-DS30.

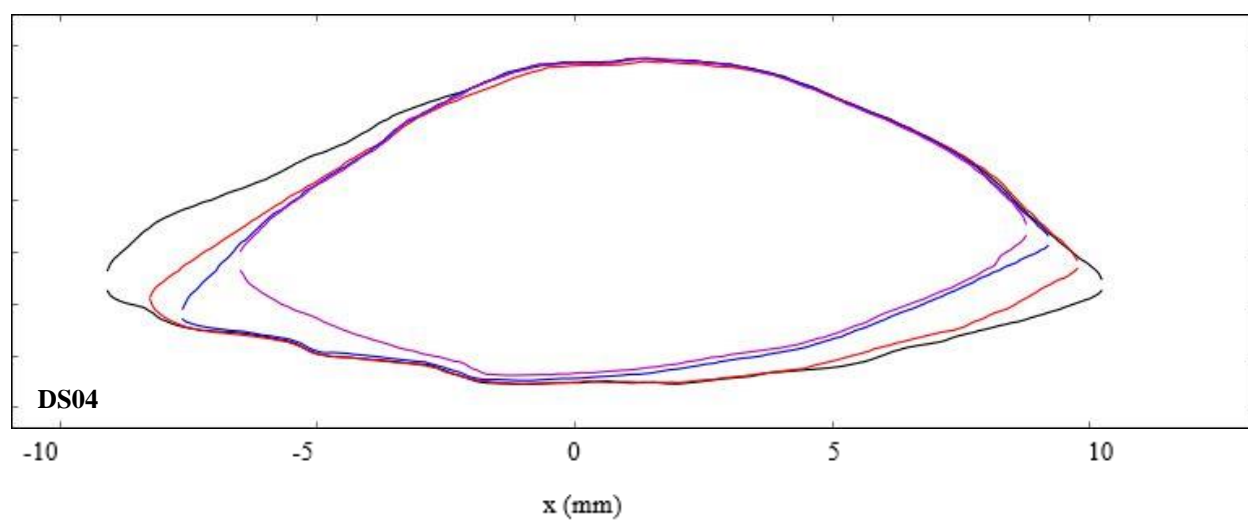
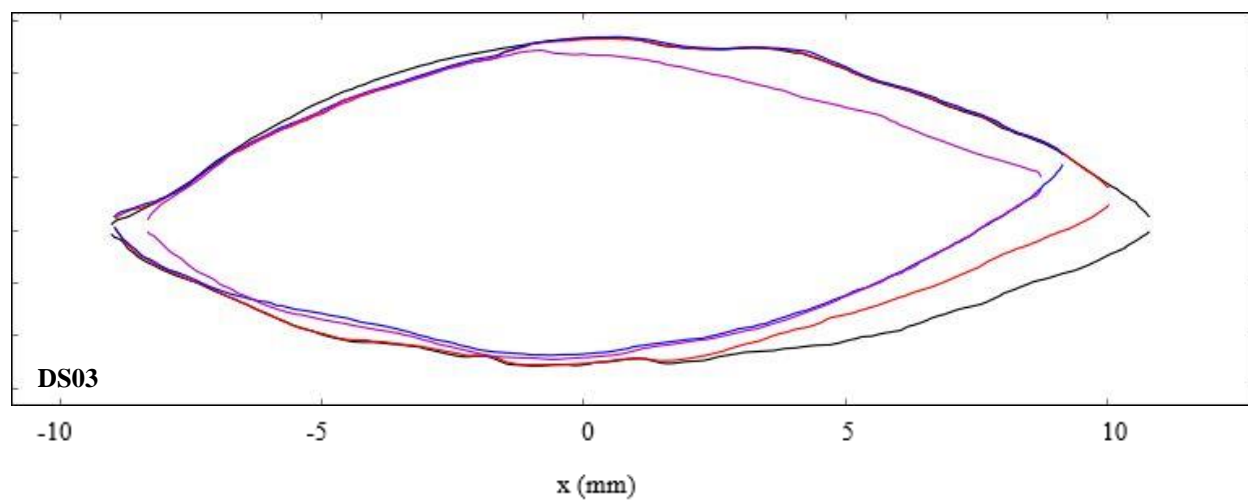
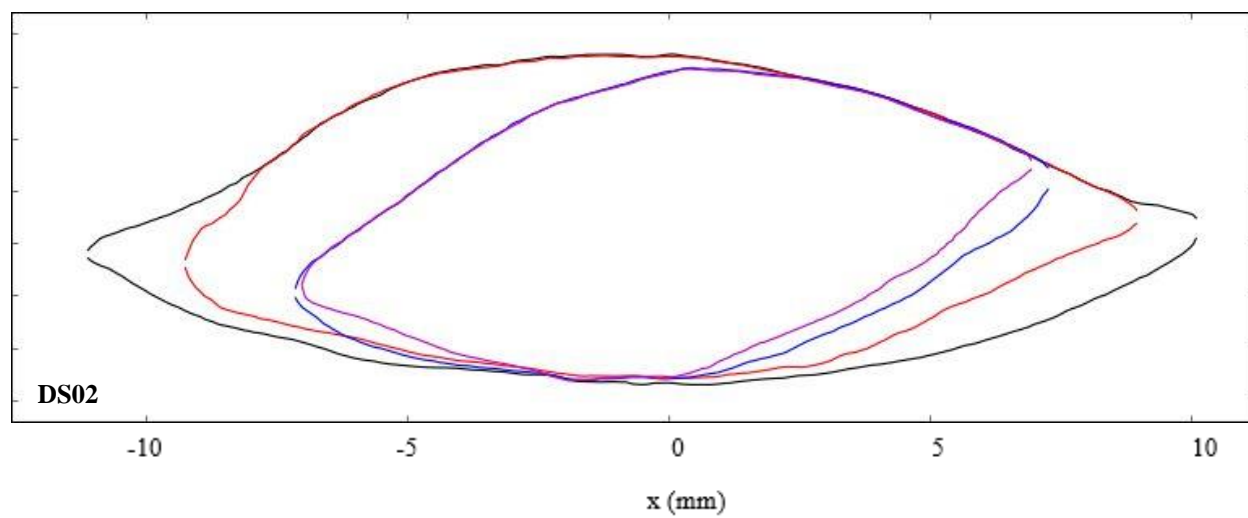


Figure B.3: Continued...

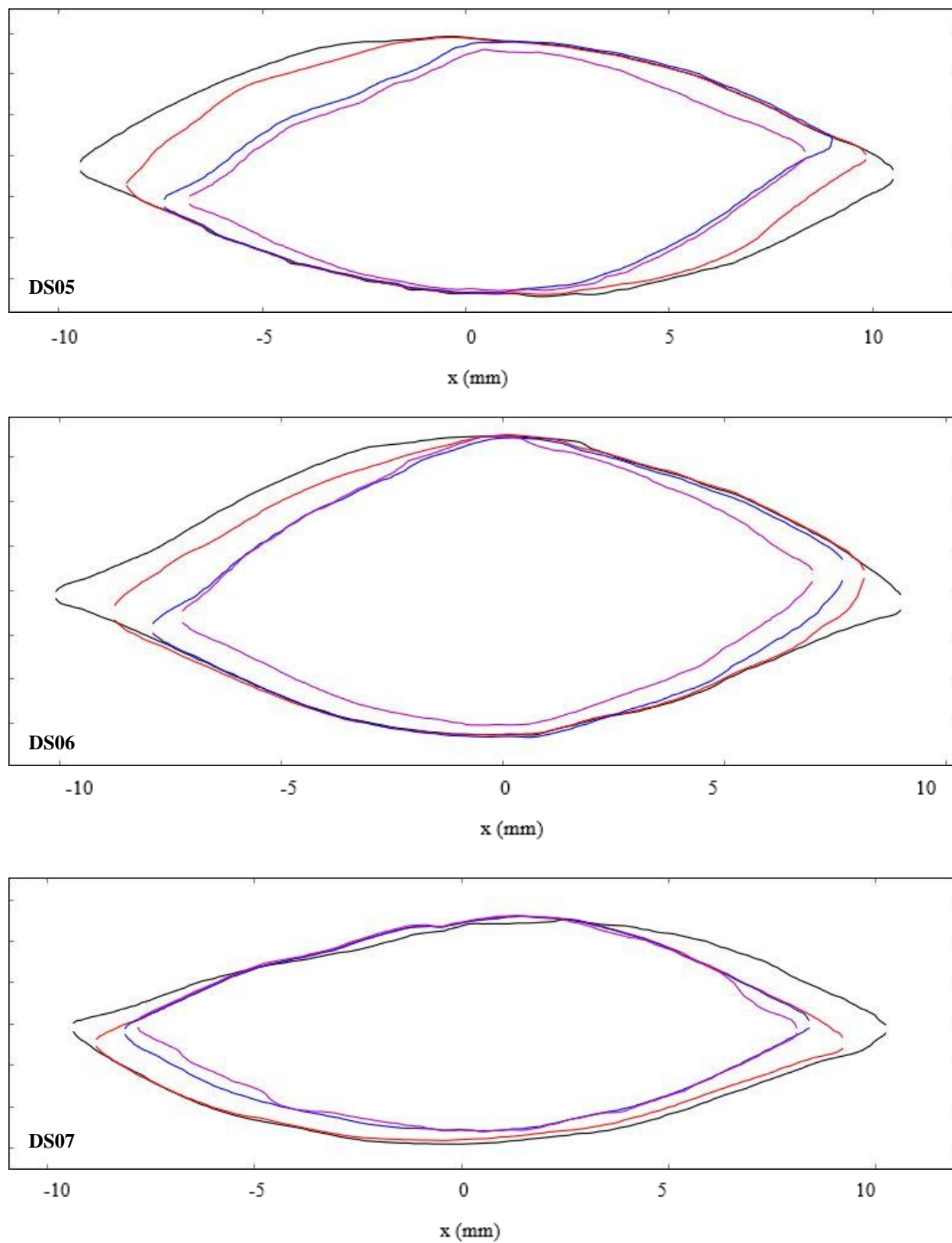


Figure B.3: Continued...

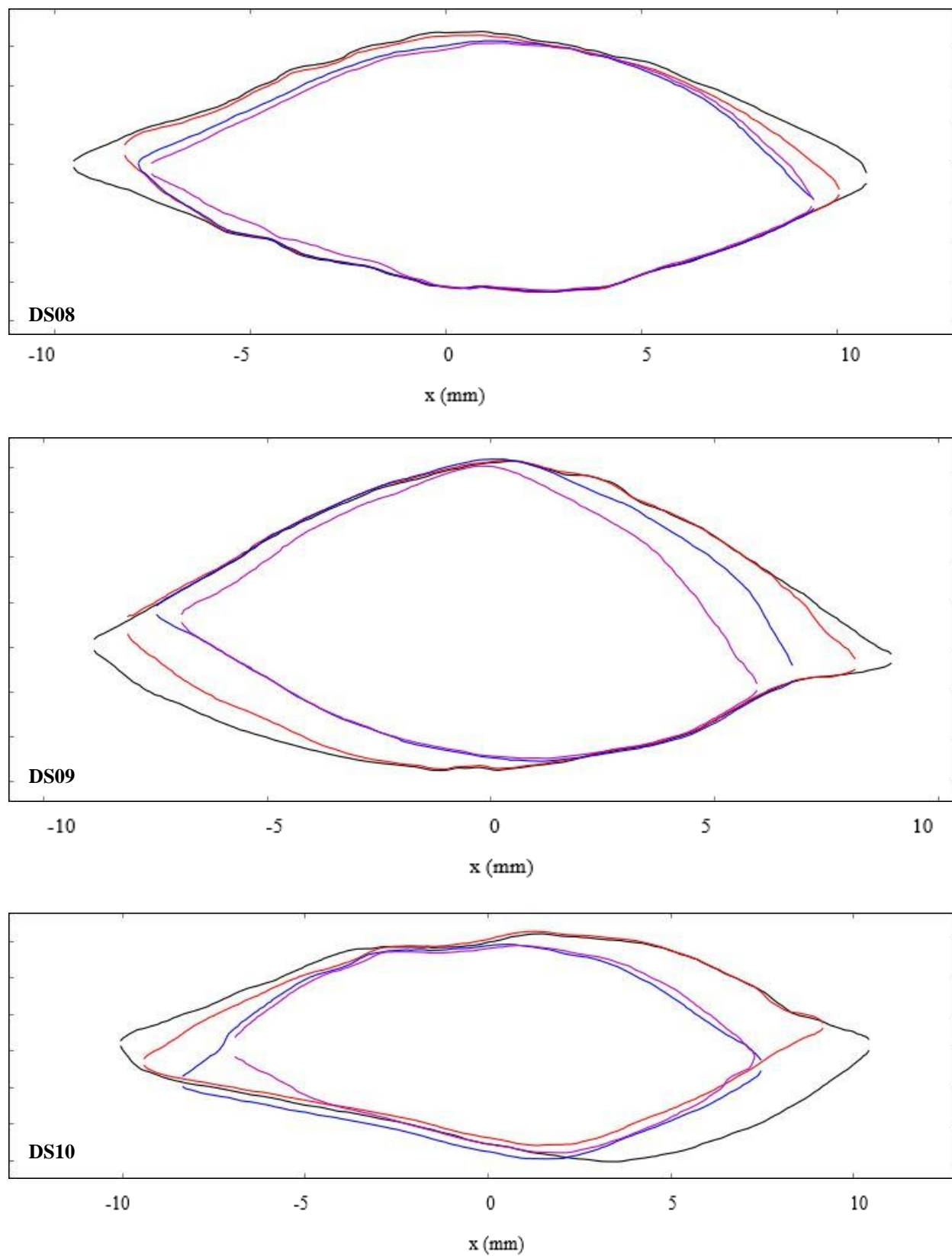


Figure B.3: Continued...

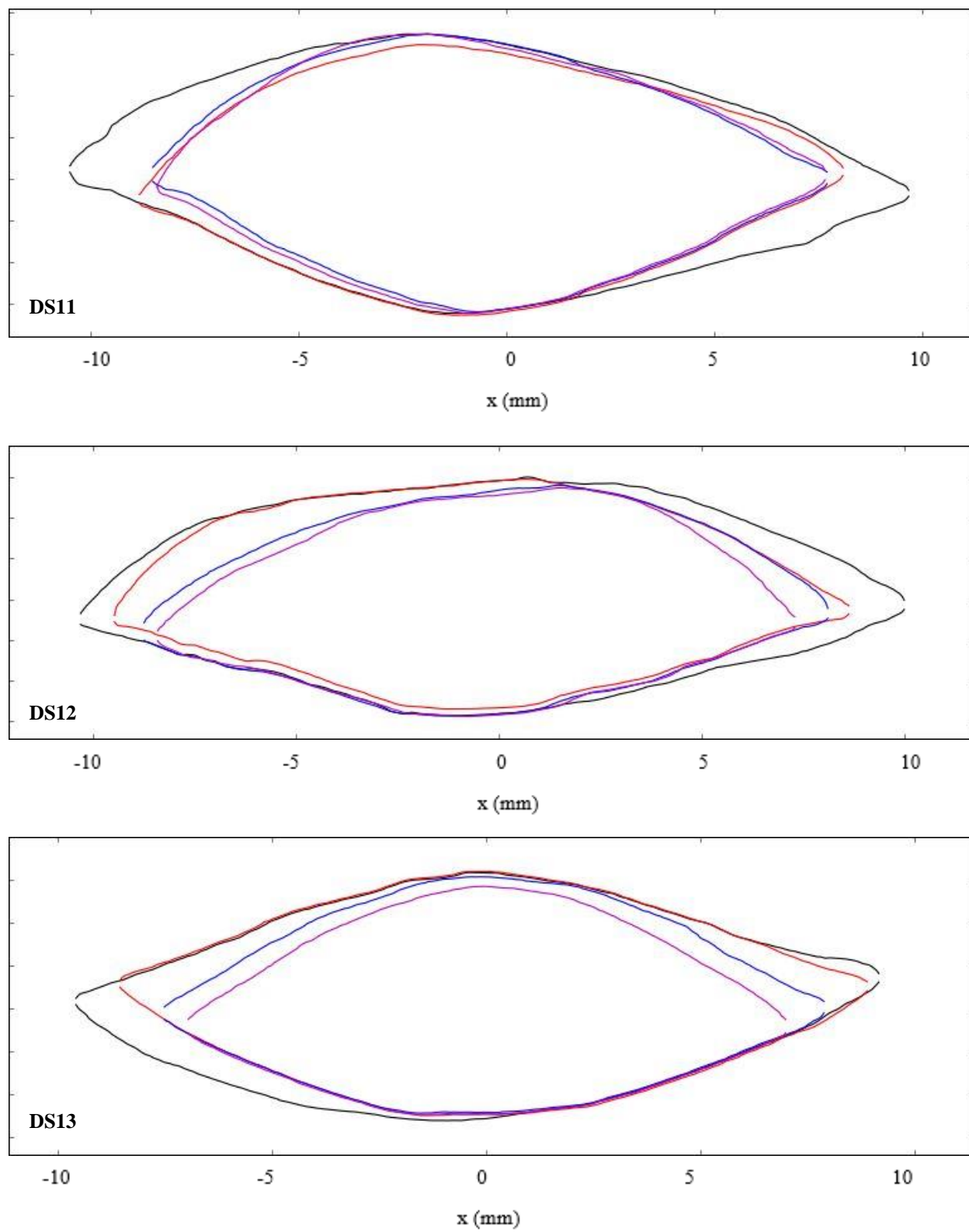


Figure B.3: Continued...

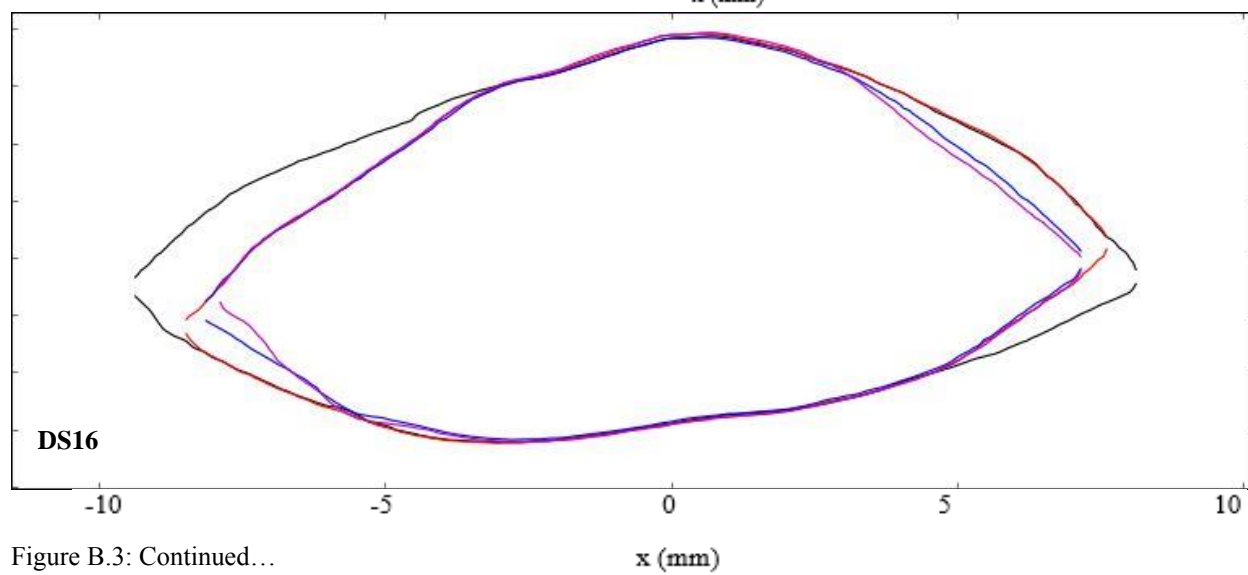
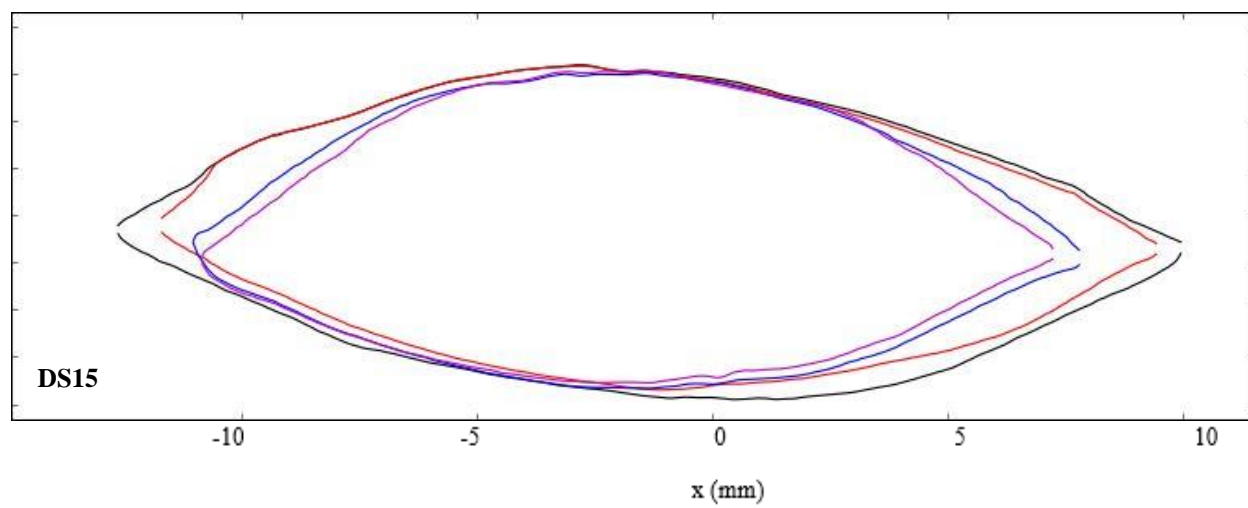
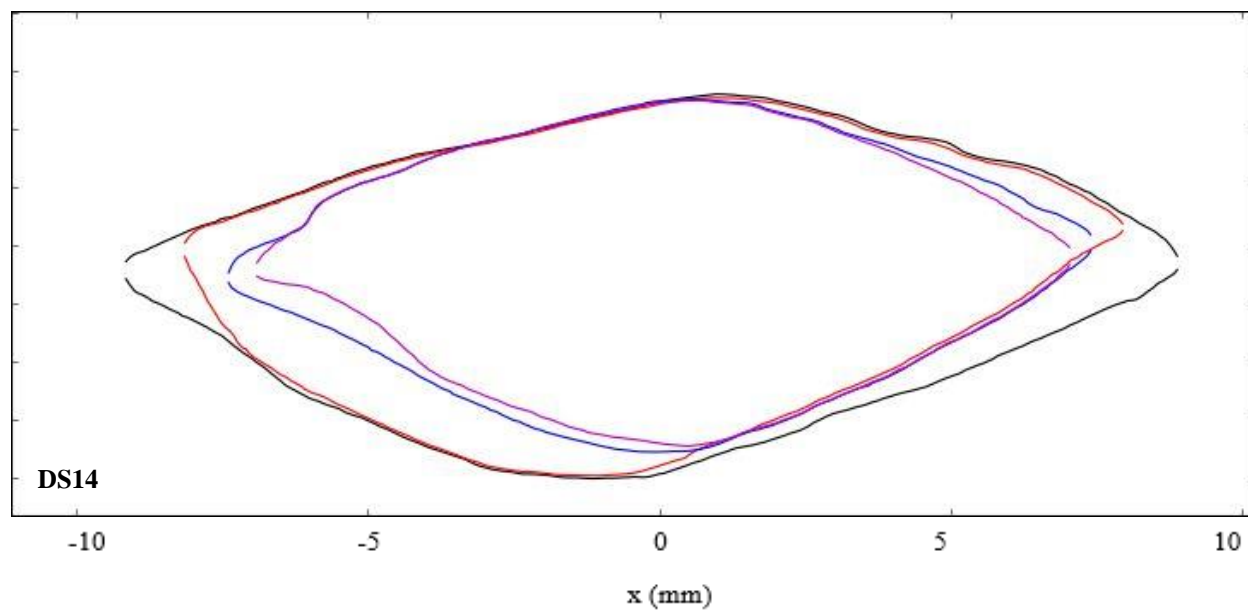


Figure B.3: Continued...

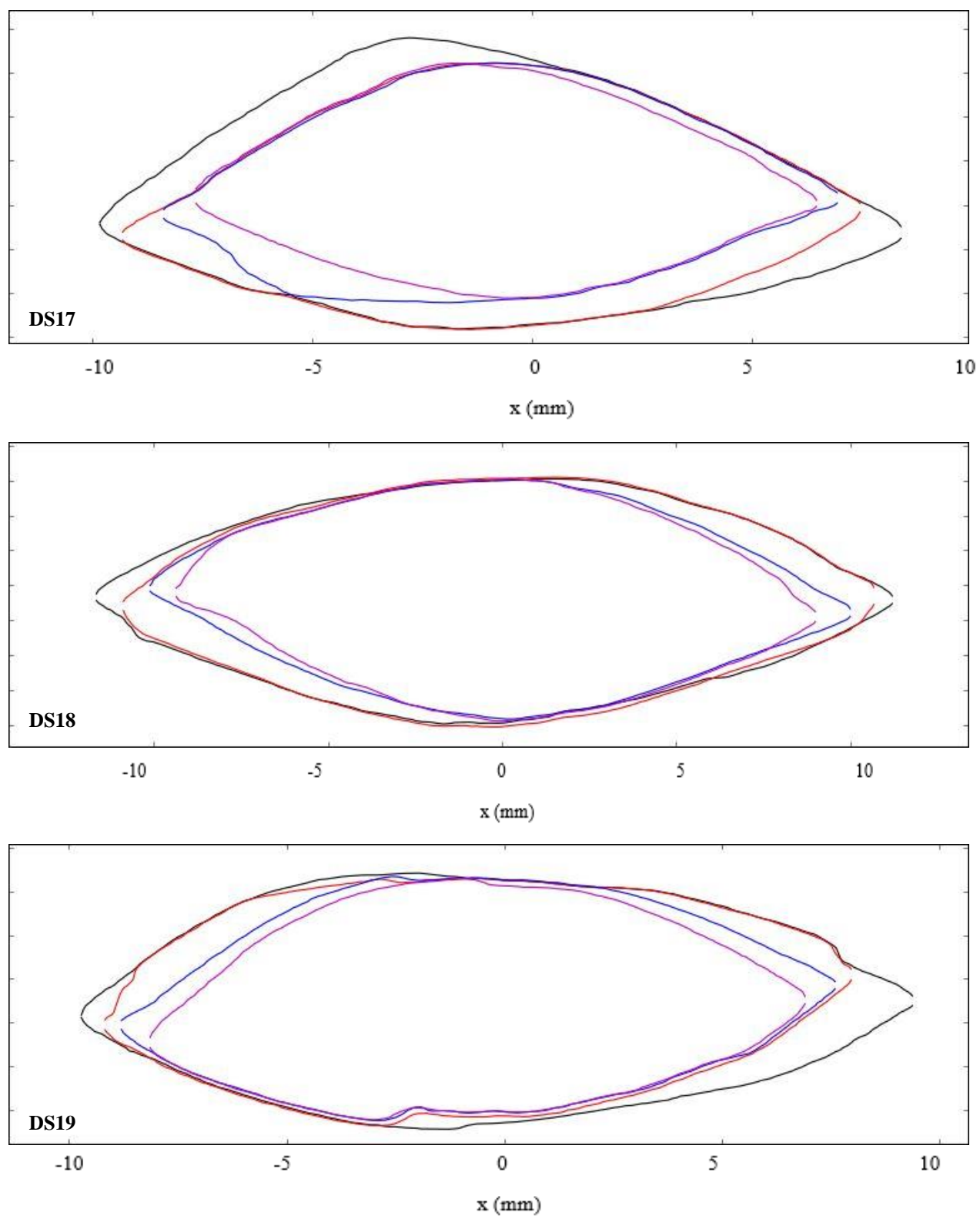


Figure B.3: Continued...

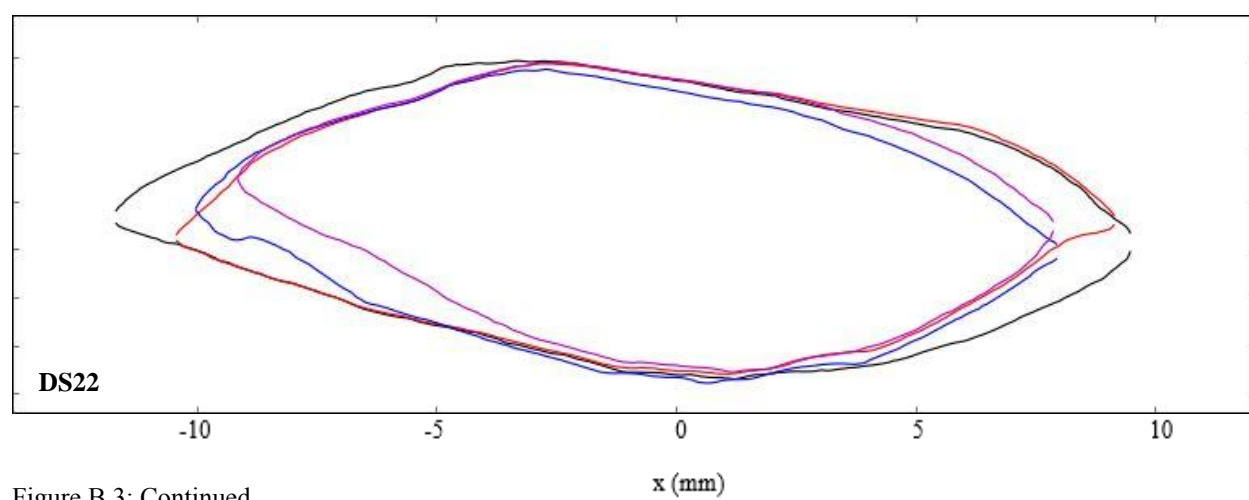
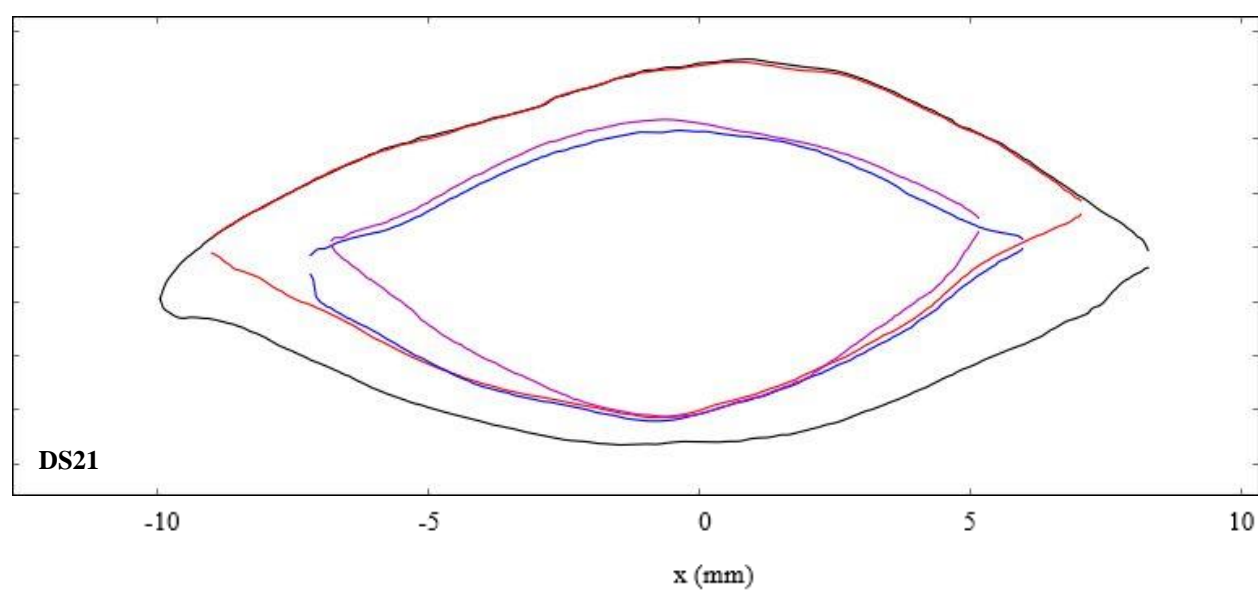
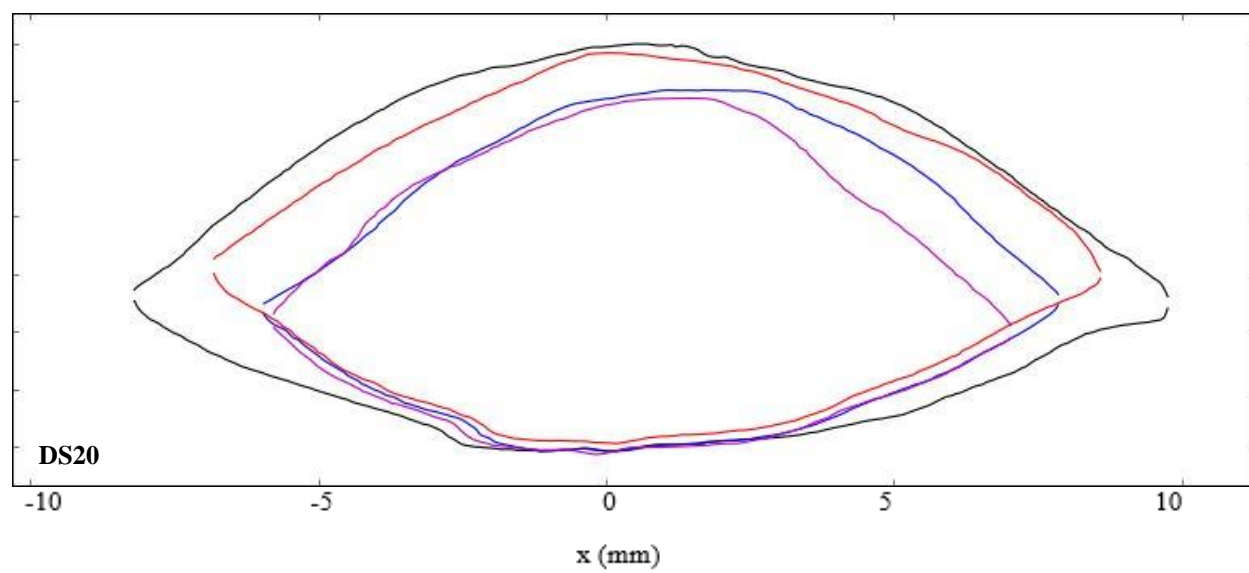


Figure B.3: Continued...

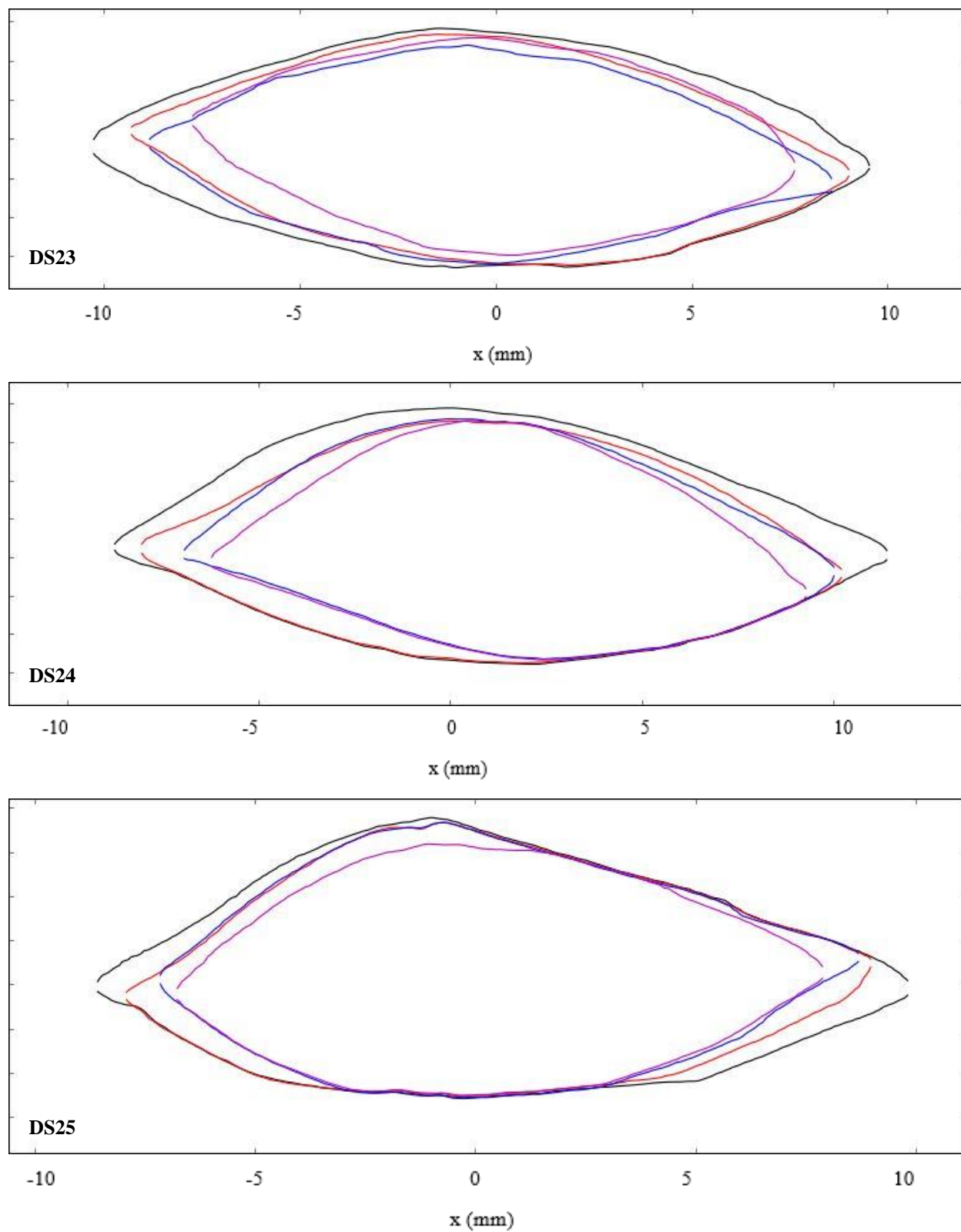


Figure B.3: Continued...

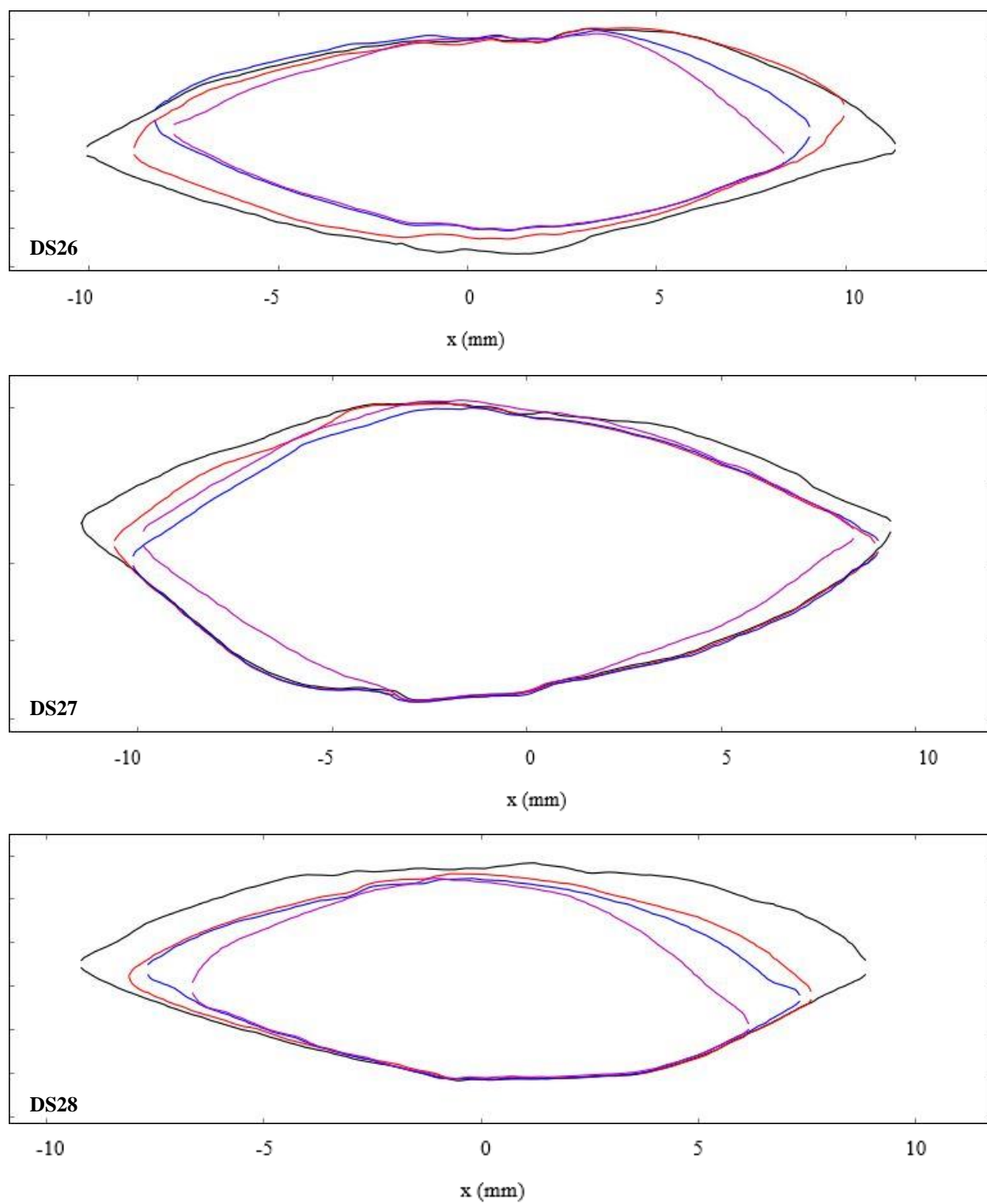


Figure B.3: Continued...

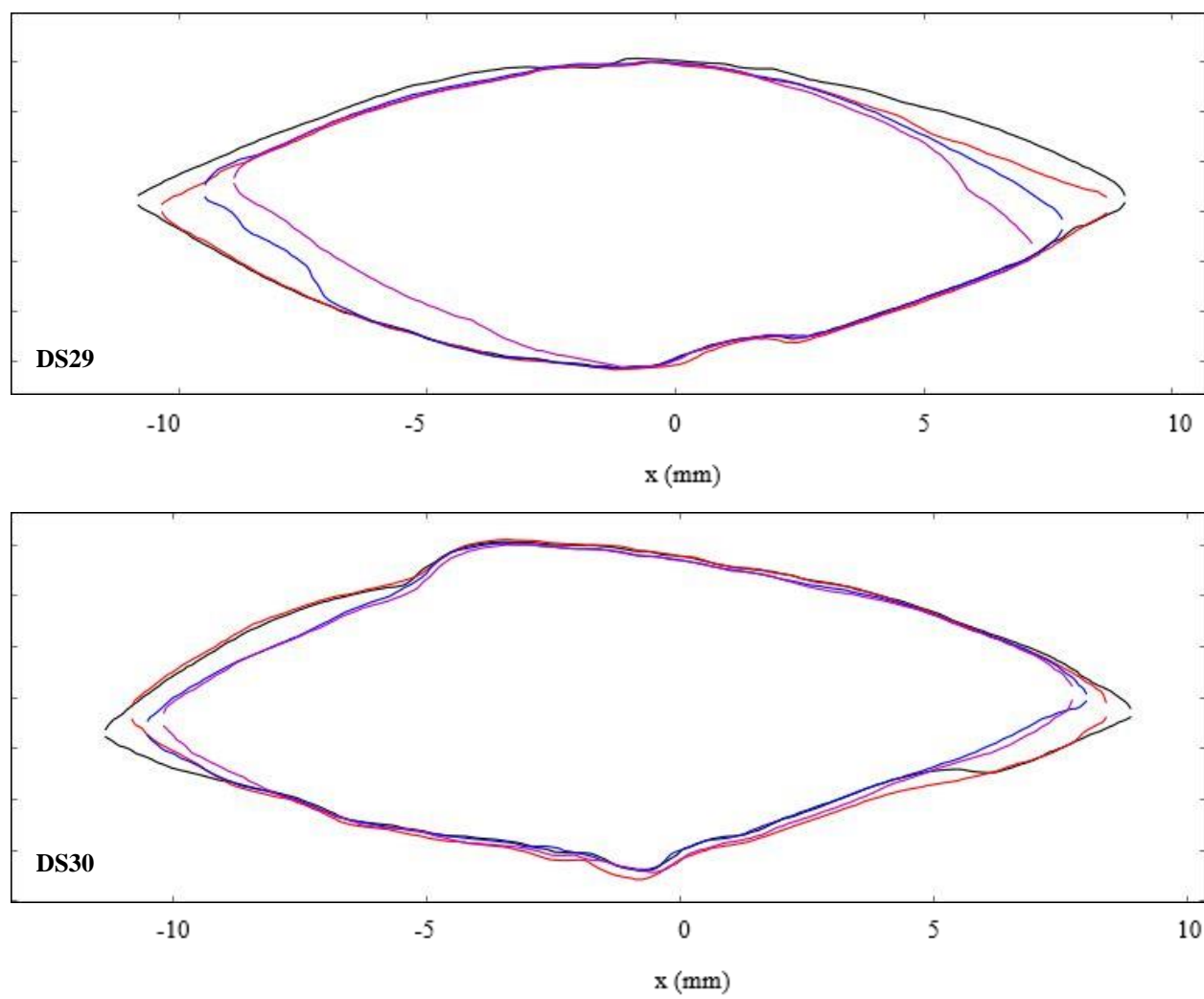
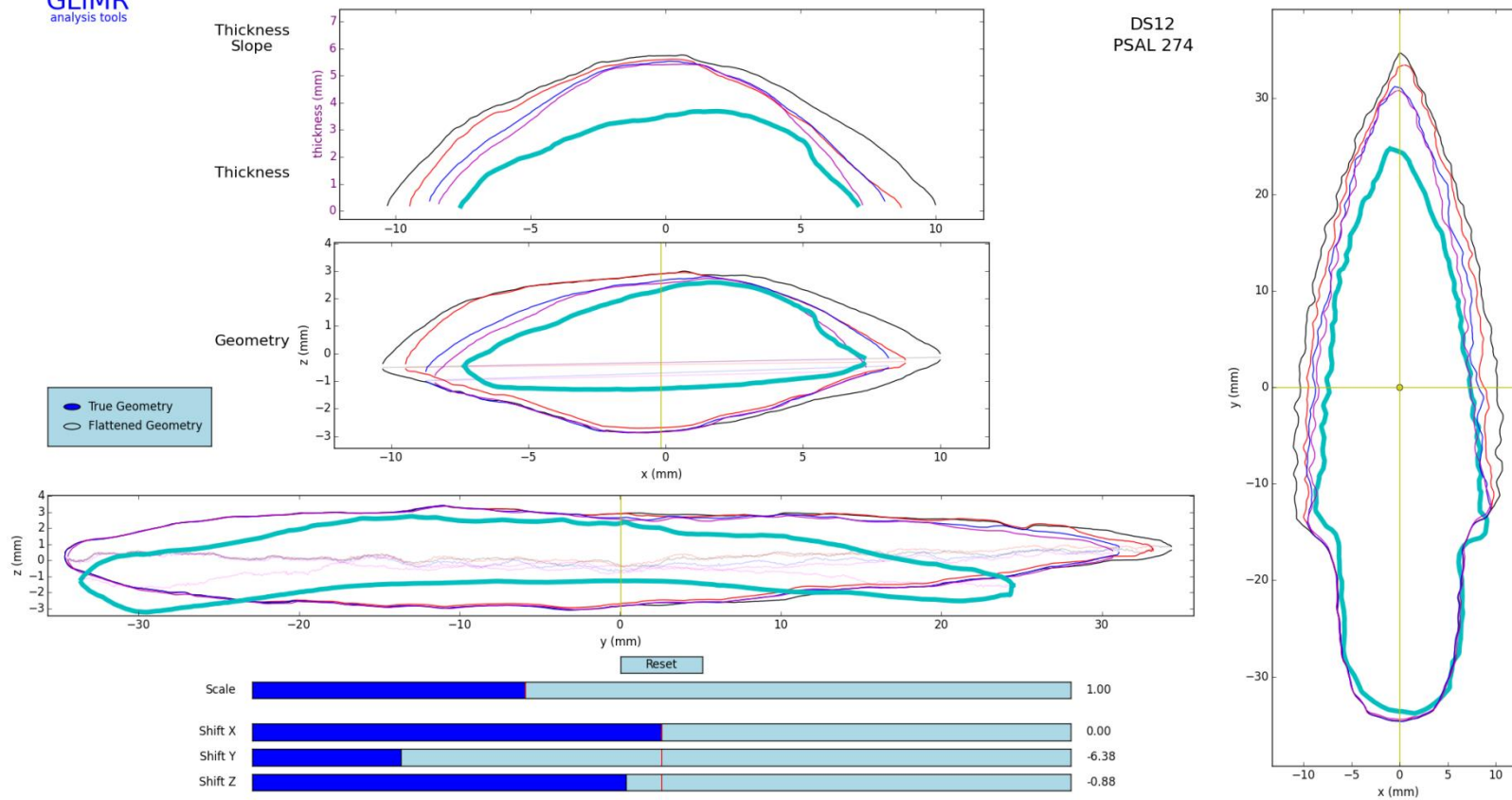


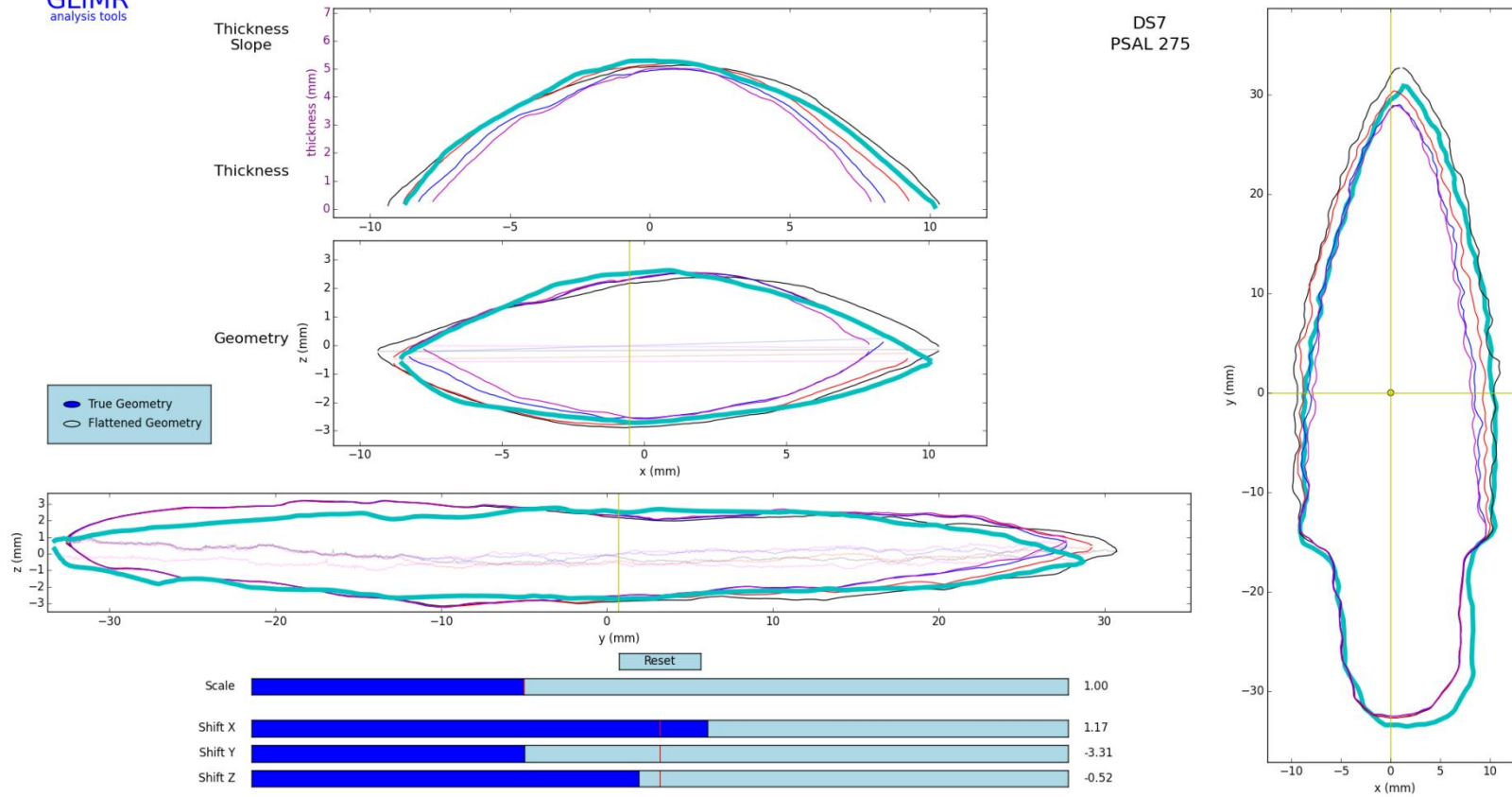
Figure B.3: Continued...

Appendix C



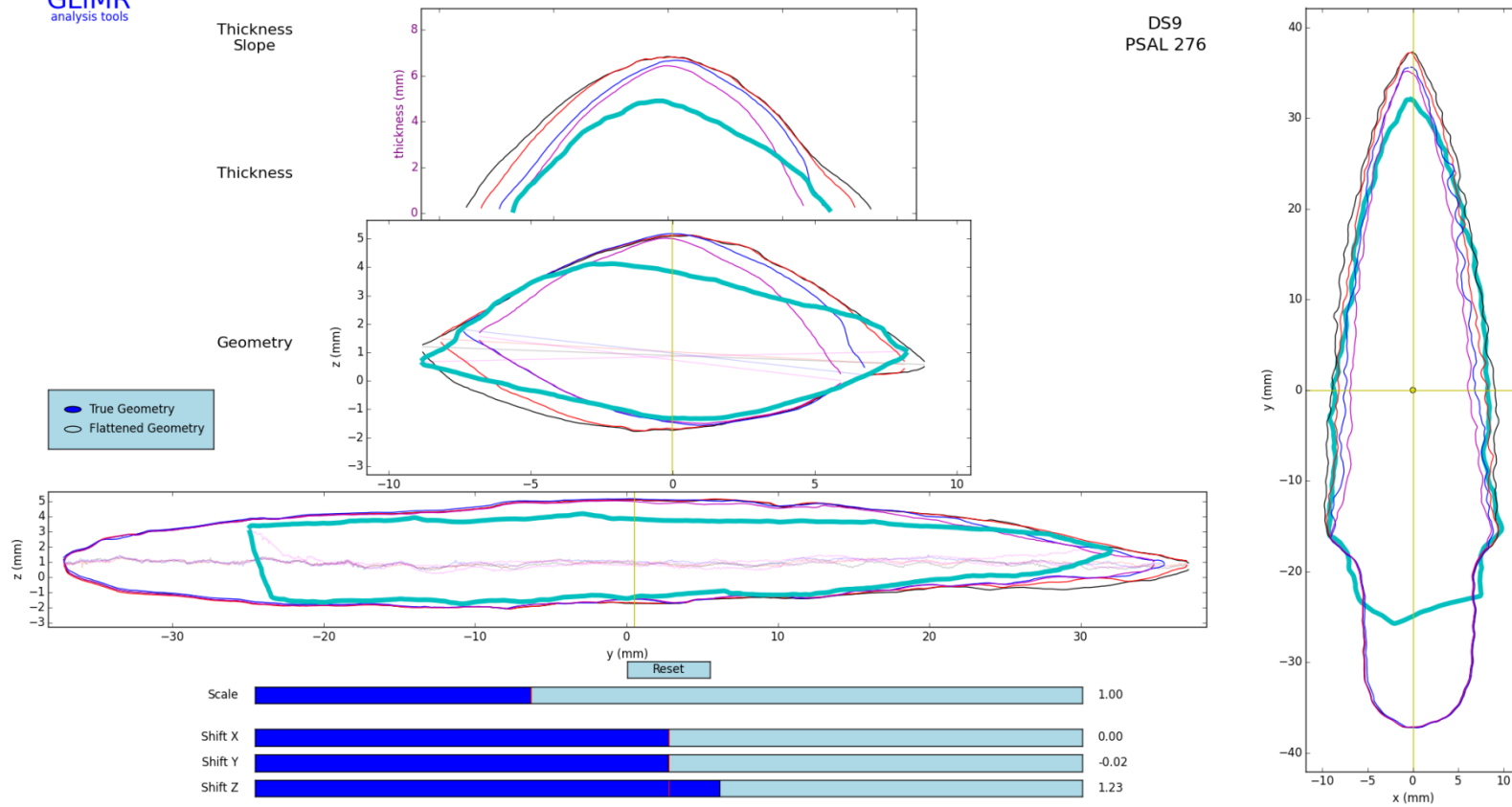
73-24940 vs DS12

Figure C.1: PFP1 projectile point cross section comparison with nearest similar DS number series.



73-24941 vs DS07

Figure C.1: Continued...

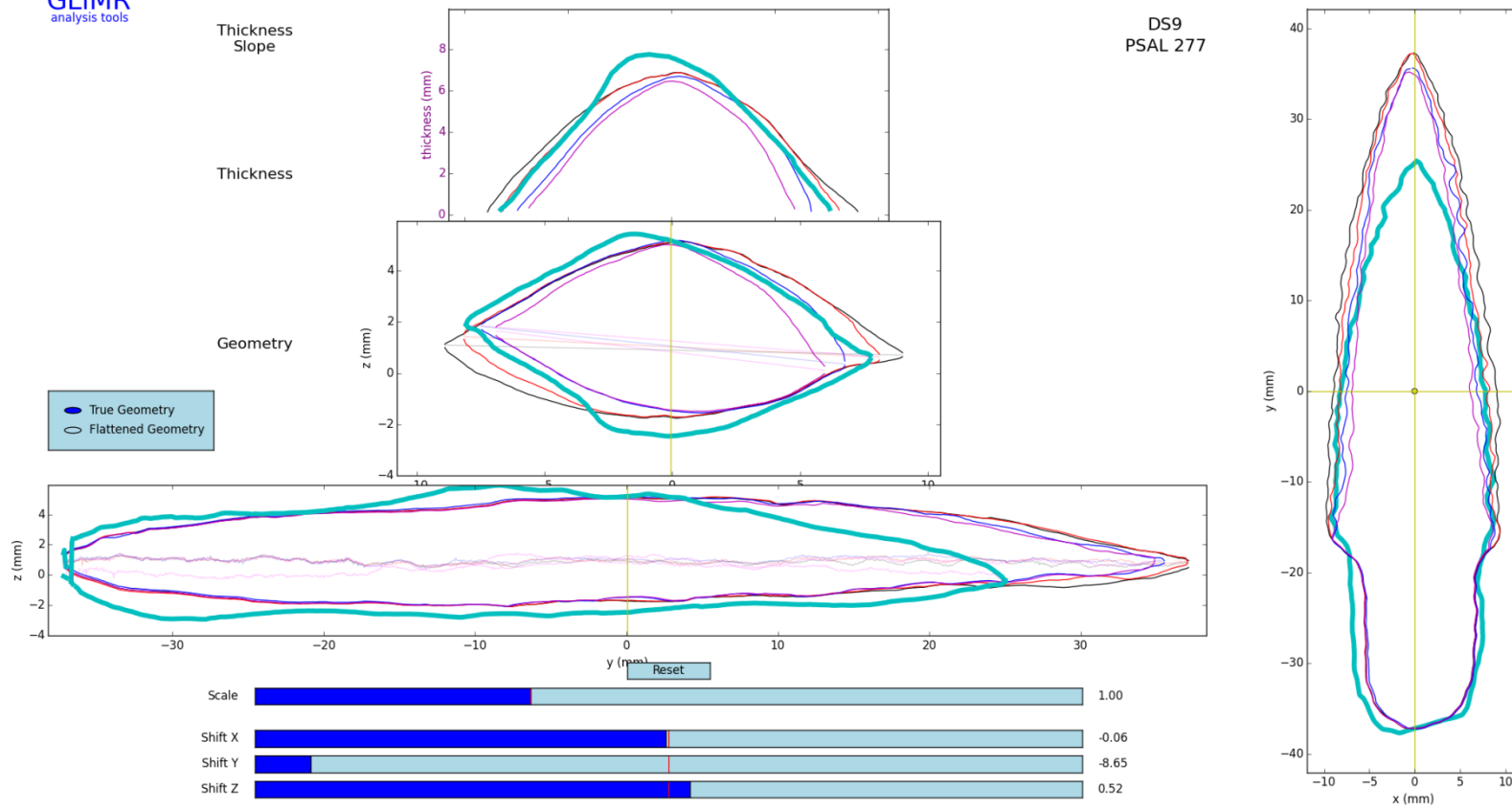


73-24942

vs

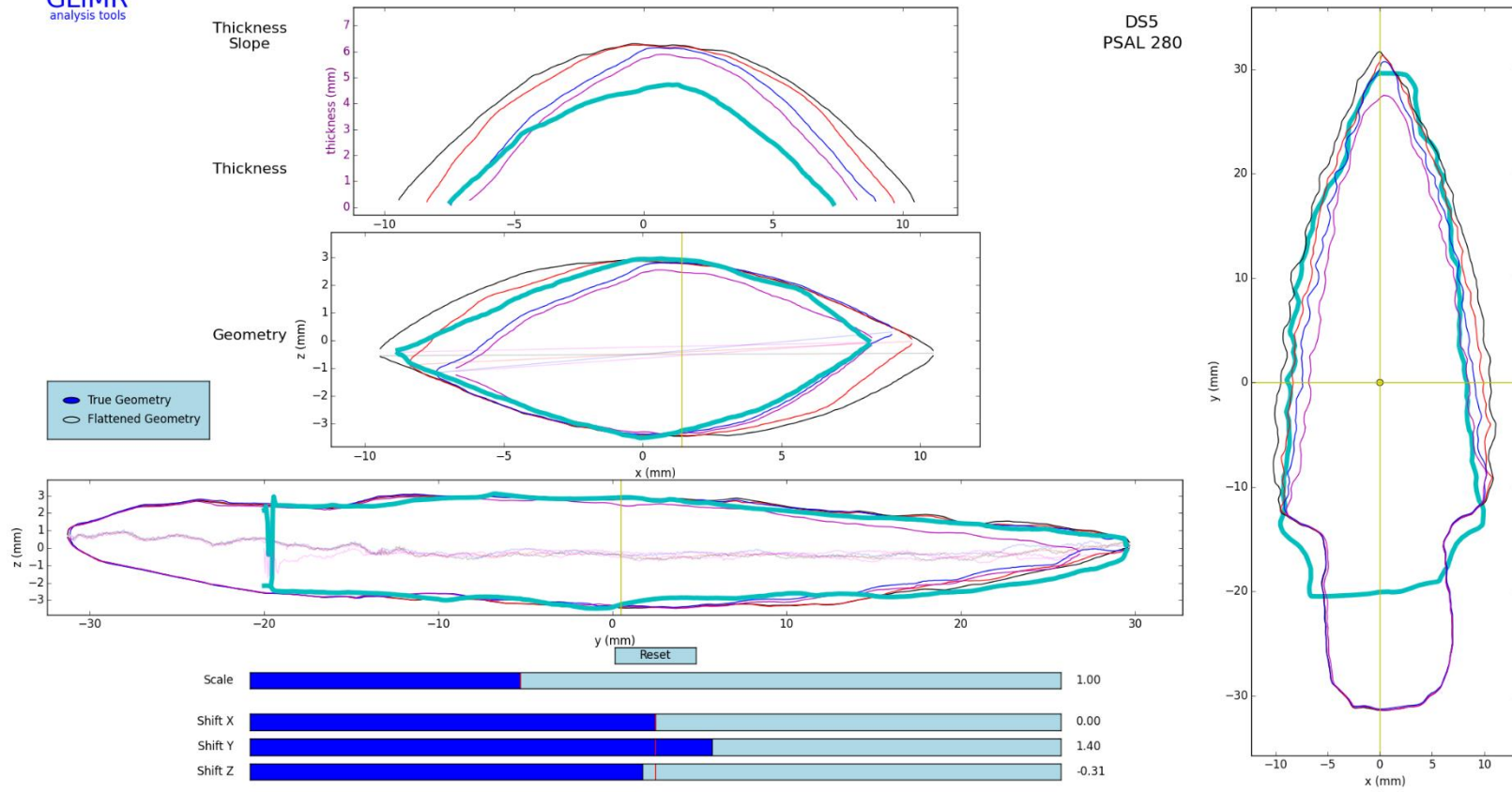
DS09

Figure C.1: Continued...



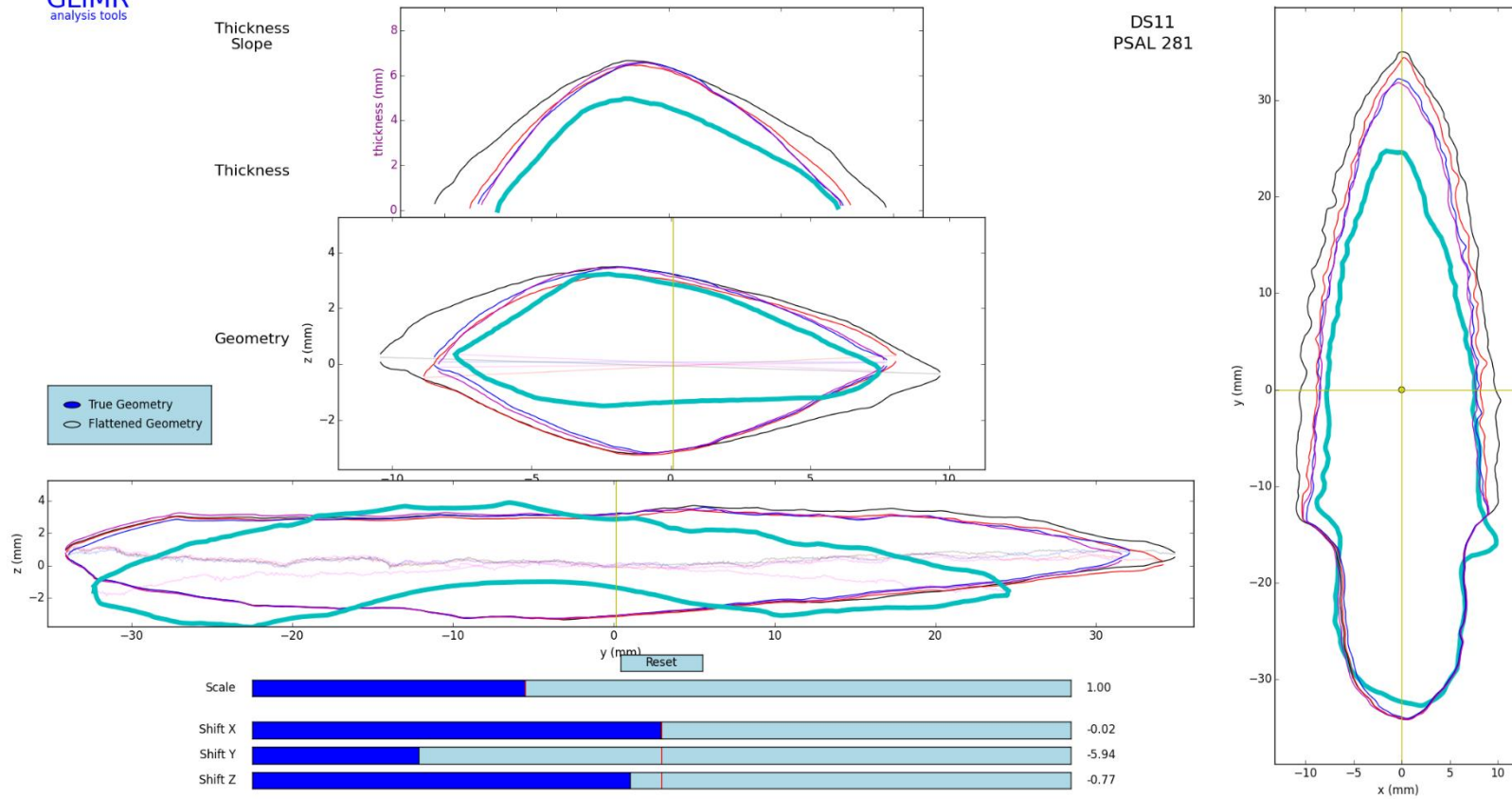
73-24943 vs DS09

Figure C.1: Continued...



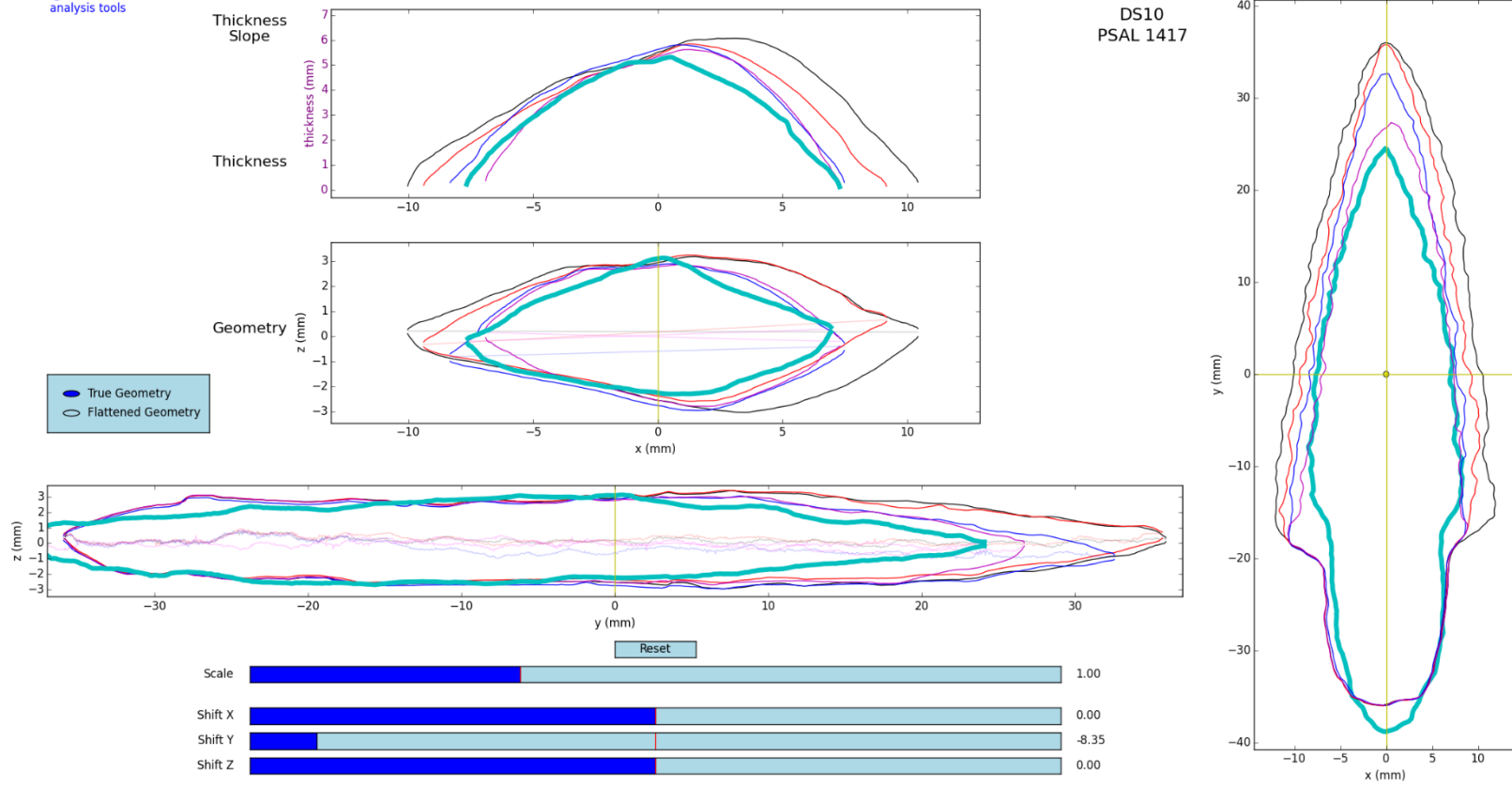
73-24948 vs DS05

Figure C.1: Continued...



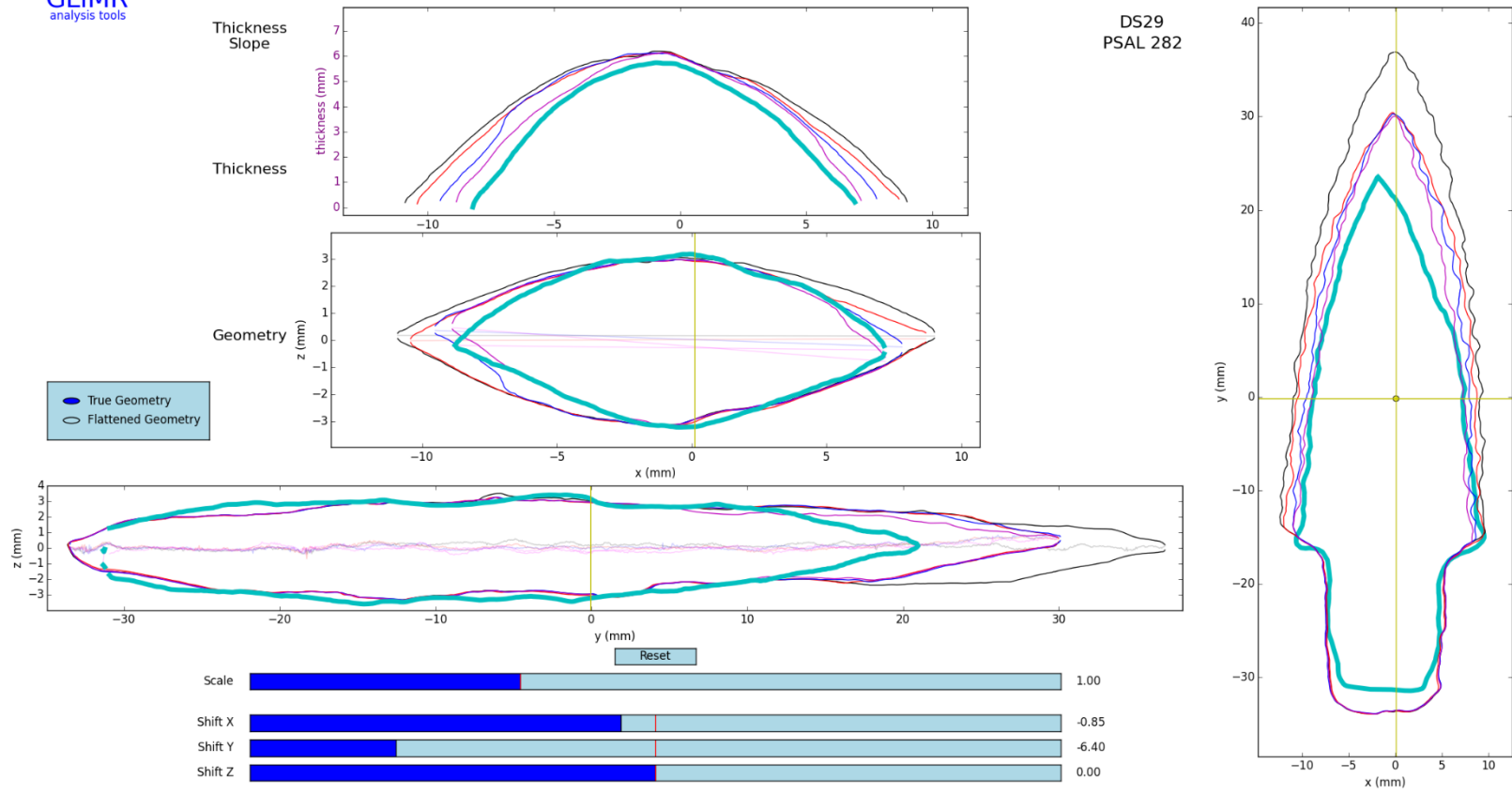
73-24949 vs DS11

Figure C.1: Continued...



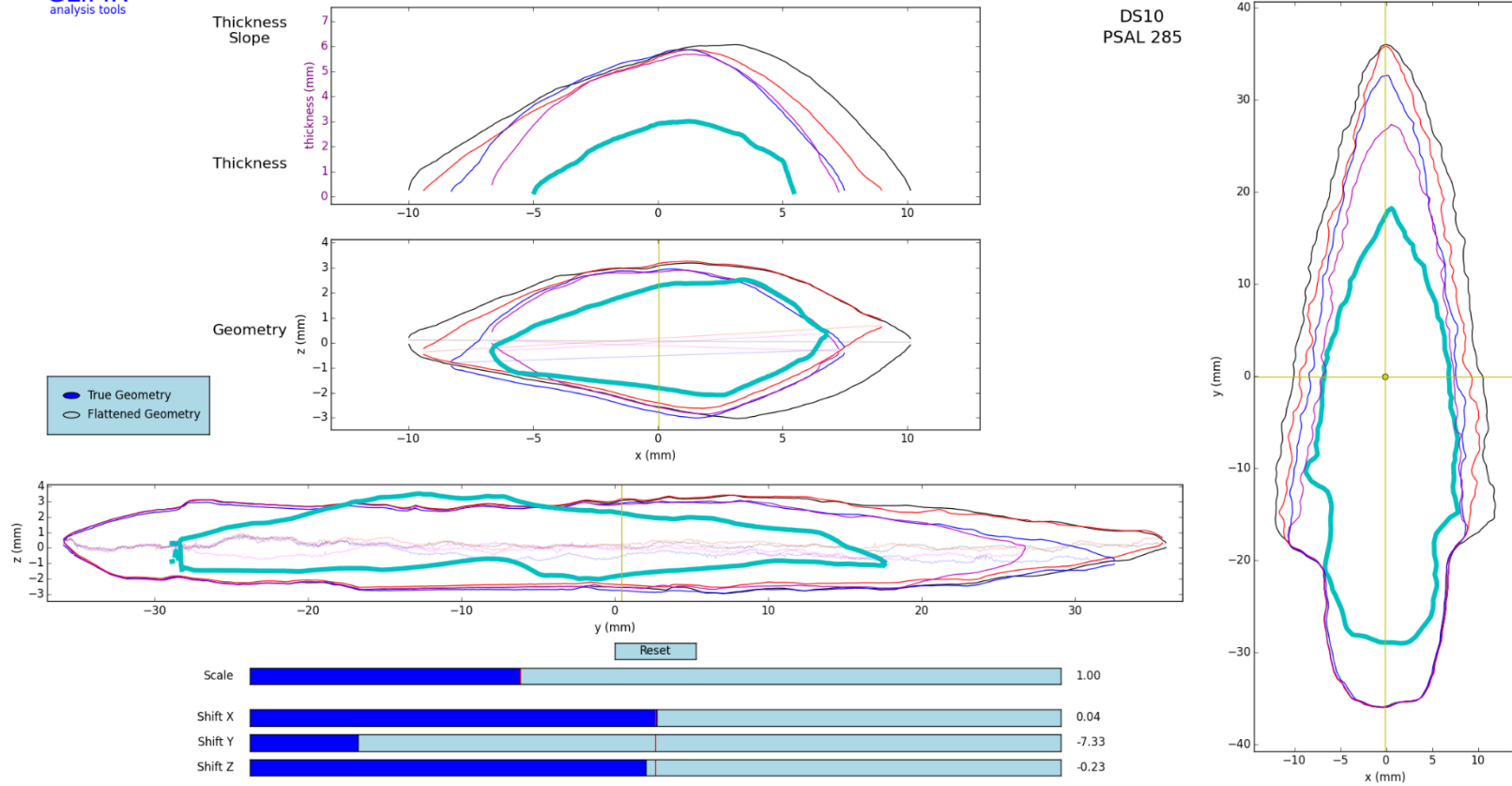
73-24950 vs DS10

Figure C.1: Continued...



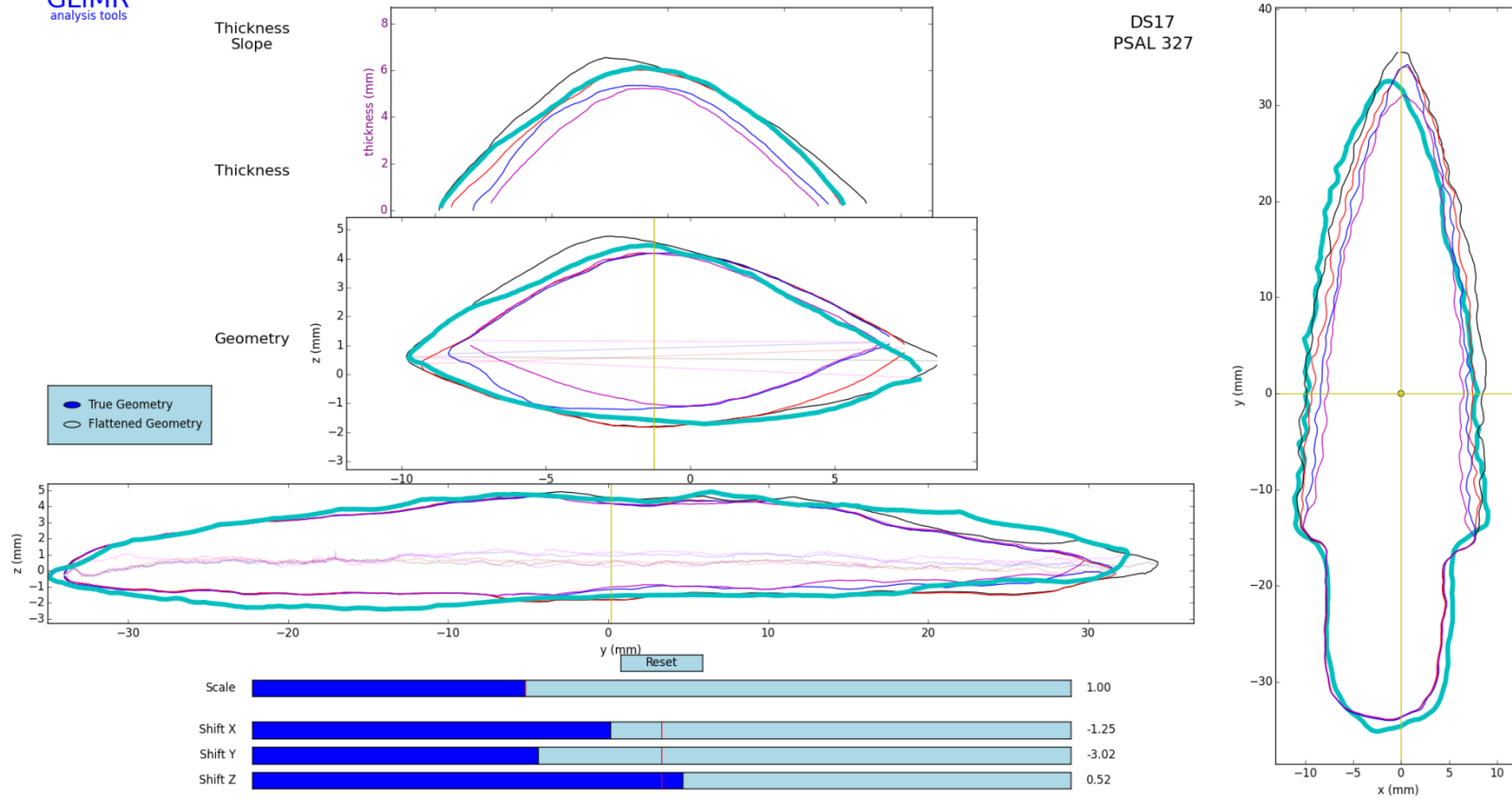
73-24951 vs DS29

Figure C.1: Continued...



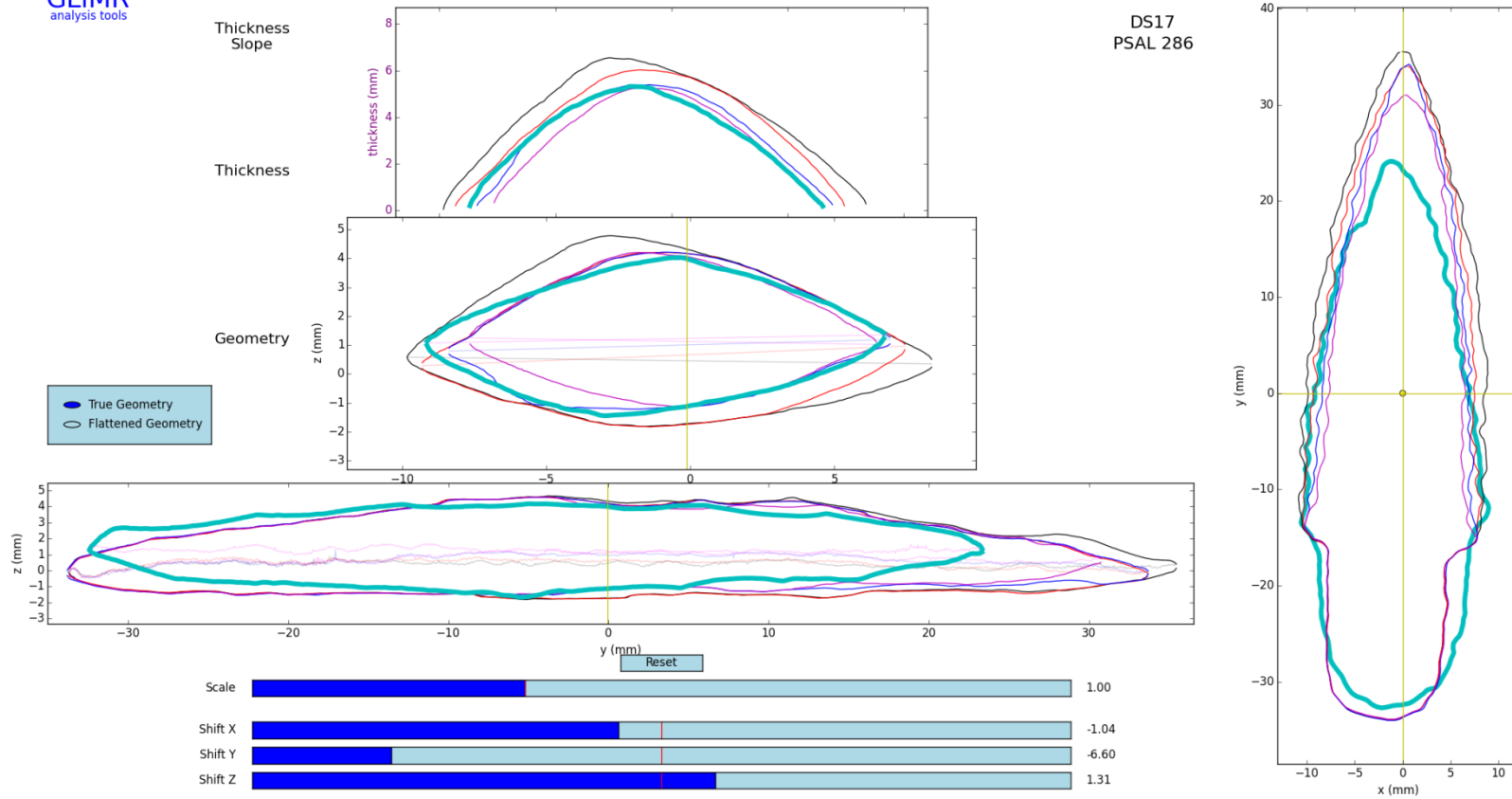
73-24957 vs DS10

Figure C.1: Continued...



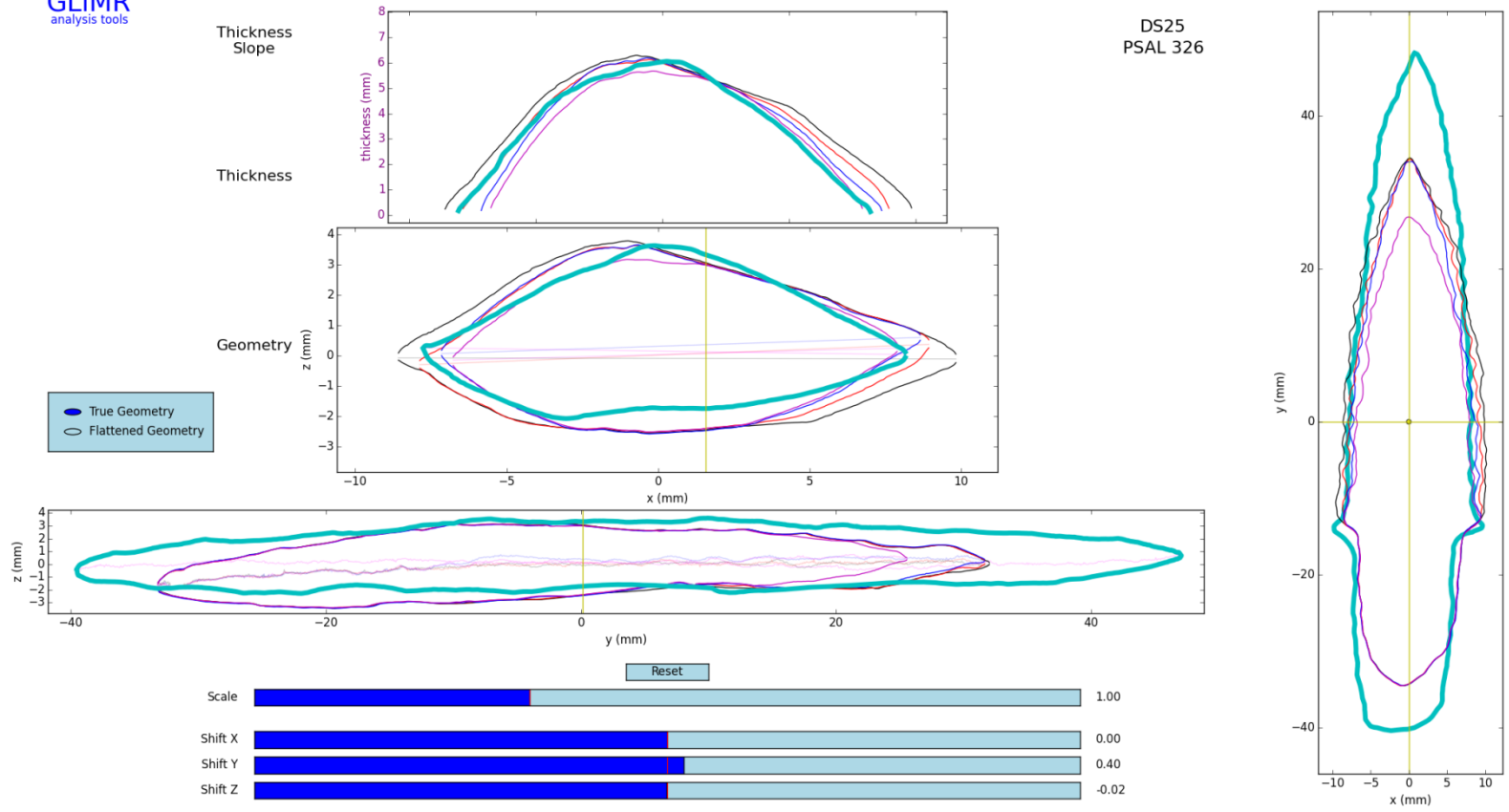
73-24958 vs DS17

Figure C.1: Continued...



73-24959 vs DS17

Figure C.1: Continued...



73-27087 vs DS25

Figure C.1: Continued...